6 P5

ONLINE MICROWAVE MEASUREMENT OF COMPLEX DIELECTRIC CONSTANT

Sean R. Mercer MSc(Eng.)

DECLARATION

I declare that this dissertation is my own unaided work. It is being submitted in fulfilment of the requirements for the degree of Doctor of Philosophy in Electrical Engineering at the University of Cape Town. This thesis has not been submitted before for any degree or examination at any other University.

Signature removed

(Signature of Candidate)

2nd day of August 1990

ABSTRACT

This dissertation examines the problem of on-line measurement of complex dielectric constant for the purpose of dielectric discrimination or product evaluation using microwave techniques. Various methods of signal/sample interaction were studied and consideration was given to the problem of sorting irregularly shaped discrete samples.

The use of microwave transmission and reflection measurements was evaluated. The signal reflection methods were deemed to be best suited to applications with constant geometry feed presentation (ie. a continuous, homogeneous product stream with little variation in surface geometry).

The previously unsolved problem of separating barren waste rock (gabbro) from dimendiferous kimberlite rock at Premier Diamond Mine was examined. A study of low power microwave signal attenuation through the rocks revealed a detectable difference in signal attenuation over a broad frequency spectrum. Dynamic tests with a specially designed microwave transmitter and receiver and a laboratory conveyor belt system showed that 93% of the kimberlite could be retained whilst rejecting 67% of the gabbro.

An investigation of microwave resonant structures was undertaken. Rectangular waveguide structures were shown to be more suitable than coaxial and stripline structures due to the constraints on the field distributions within the structures. A linearly polarised 500MHz waveguide cavity system was developed and tested. Problems with sample orientation dependence led to the examination of resonant structures with more than one plane of polarisation.

A TE_{11} cylindrical cavity was found to be unsuitable for analysis of irregular shaped samples as signal polarisation

twisting was found to occur in this structure. A TM_{011} cylindrical cavity was shown to offer an improvement over the linearly polarised rectangular waveguide due to its radially symmetric electric field distribution. This cavity offered orientation independence in two planes due to it's electric field distribution.

A linearly polarised resonant cube, simultaneously excited in three different planes, was investigated. The results were promising but problems with ambiguity were encountered due to the three very similar resonant frequencies.

A rectangular parallelopiped was used to eliminate the ambiguity problem. This was excited with three different planes of polarisation, each with a different resonant frequency. Sample mass and length were found to be directly proportional to resonant frequency shift in the cavity. Using this information, the square root of the sum of the squares of the single plane dielectric constant was plotted. The results indicated that the effect of the orientation of an irregularly shaped sample was significantly reduced. A structure had been developed to improve the accuracy of results by reducing the effect of sample orientation in the measuring cavity.

ACKNOWLEDGEMENTS

I would like to thank Professor B J Downing for his guidance, support and patience during this project.

I would like to thank De Beers Diamond Research Laboratories for their financial support, assistance and co-operation during this project. In particular, thanks are due to Dr J D Salter and other De Beers personnel, including Mr L Nordin, for their technical assistance and advice.

The financial assistance from the Council for Scientific and Industrial Research was gratefully appreciated.

CONTENTS **Page**

LIST OF FIGURES

FIGURE Page

CHAPTER 1

1.0 INTRODUCTION

This dissertation examines the problem of on-line measurement of complex dielectric constant for the purpose of dielectric discrimination or product evaluation using microwave techniques. Various methods of signal/sample interaction will be studied.

In the past, numerous techniques have been employed to determine the dielectric constant of many different materials. These techniques include methods based on a materials conductivity, capacitance/infrared reflection, microwave signal attenuation and/or phase shift, electron spin resonance (ESR) and nuclear magnetic resonance (NMR) [1-5].

The conductive and capacitive techniques require the sensor heads to be in contact with the dielectric material [3]. The bulk density of a sample often influences the measured parameter. This can be counteracted by combining a bulk density measurement, using gamma ray attenuation, with another measured parameter such as microwave signal attenuation [6]. The infrared reflection technique is commonly employed to monitor moisture in solids [2]. This technique, however, is adversely affected by surface phenomenon such as surface moisture and dust and the measured surface properties are often not a true representation of the properties of the whole material.

Expensive measuring techniques such as ESR and NMR can yield extremely accurate results. Whilst ESR has been employed to determine the carbon content of coal conveyed as an air suspension [4], the development of on-line applications of

ESR and NMR has been inhibited by high cost and system complexity.

One of the most obvious criteria for an on-line measurement system is the question of sensor attrition and abrasion. To this end, non contact measurements are preferred. This is of particular importance when the dielectric material is either easily damaged or is potentially damaging to the sensors.

Microwave irradiation techniques offer the possibility of accurate non contact measurements. Microwave signal attenuation and phase shift have been used on-line, mainly in the determination of the moisture content of solids [1, 6-8]. Microwave signal reflection techniques suffer similar problems to the infrared technique in that only the surface properties of the sample are monitored. Microwave transmission measurements, however, allow the properties of the whole material to be determined. A variety of microwave techniques will be examined with a view to on-line application.

A brief chapter by chapter breakdown of the thesis structure is given below. A review of conduction in dielectric materials is presented in chapter two. The phenomenon of dielectric polarisation and anisotropy are considered.

Microwave measurement options for on-line use are given in chapter three. Particular attention is given to attenuation measurements. The development of a microwave ore sorting system is presented in chapter four. Signal propagation through different samples is investigated.

The design of a microwave transmitter and receiver is described in chapter five. Static and dynamic tests results obtained using this equipment are presented in chapter six.

A laboratory scale system using a conveyor belt demonstrated the viability of the ore sorting system. This work led to publications [10, 11] and the filing of a patent [12].

Microwave resonant structures are investigated in chapters seven and eight [13-19]. In chapter seven, waveguide, coaxial and stripline structures are examined. Waveguide resonant structures were shown to be most suitable for dielectric measurements. The construction of a 500MHz waveguide cavity system is described and test results using this linearly polarised cavity are presented. Problems with sample orientation dependence led to the examination of resonant structures with more than one plane of polarisation.

Resonant structures with two and three planes of polarisation are examined in chapter eight. A TE_{111} and a TM_{011} cylindrical cavity were studied to try and identify a resonant structure that would not be adversely affected by sample orientation. Spherical resonant structures were found to be unsuitable due to their inherent field properties. A rectangular parallelopiped cavity was extensively investigated. This structure was linearly polarised but simultaneously excited in three different planes. It was found that the effect of sample orientation could be greatly reduced using this structure.

Concluding remarks are given in chapter nine.

1.1 LIST OF REFERENCES

[1] KRAZEWSKI, A., "Microwave Aquametry - A Bibliography 1955-1979", J. Microwave Power, vol. 15, no. 4, 1980, pp 298-310.

[2] KLEIN, A., "Comparison of rapid moisture meters",Aufbereitungs-Technik, no. 1, 1987, pp 10-16.

[3] HALL, D.A., MORRIS, G.F., SCOTT, C., "The continuous determination of moisture in coal - The use of a capacitance method", Mining and Minerals Engineering, vol. 5, no. 10, 1969, pp 30-40.

[4] CARR-BRION, K., "Radio and Microwave frequency techniques for On-line analysis", Trans. Inst. MC, vol.9, no.1, Jan-Mar. 1987, pp 3-7.

[5] CARR-BRION, K.G., "The On-line determination of moisture in bulk solids - an Overview", I Mech E Seminar-On-line Moisture Measurement of Bulk Solids for Process Control, 17th March 1988, pp 1-3.

[6] ZEHNDER, C.B., "Application of the Combination Microwave-Gamma ray gauge to wood chip weight and moisture measurement", Pulp and Paper magazine of Canada, 1967, vol. 10, pp T678-688.

[7] JACOBSEN, R., MEYER, W., SCHRAGE, B., "Density independent moisture meter at X-band", 10th European Microwave Conference 1980, pp 216-220.

[8] KALINSKI, J., "Self-adjustable microwave homodyne circuit for on-line simultaneous attenuation and phase measurements", 7th European Microwave Conference 1977. pp 267-272.

[9] KLEIN, A., "On-line Microwave Meter for determining the moisture content of bulk materials on Conveyor belts", I Mech E Seminar-On-line moisture measurement of Bulk Solids for Process Control, 17th March, 1988, pp 37-42.

[10] MERCER, S.R., DOWNING, B.J., SALTER, J.D., NORDIN, L., "Microwave discrimination techniques for rock sorting", SAIEE 2nd Joint Symposium on Antennas and Propagation and Microwave Theory and Techniques, August 1988.

[11] MERCER, S.R., DOWNING, B.J., SALTER, J.D., NORDIN, L., "Microwave discrimination techniques for rock sorting", Elektron, Nov/Dec 1988, pp 19-20.

[12] NORDIN, L., SALTER, J.D., DOWNING, B.J., "Sorting Method and Apparatus", SA Patent 87/8309, Filed 28 November 1988.

[13] DE WAAL, A., MERCER, S.R., DOWNING, B.J., "On-line fruit weighing using a 500MHz waveguide cavity", Electronics Letters, 18th Feb. 1988, vol. 24, no. 4, pp 212-213.

[14] DOWNING. B.J., MERCER, S.R., SALTER, J.D., NORDIN, L., "Sorting particulate material on the basis of size or composition", SA Patent 88/7740, filed 17th October 1988.

[15] DOWNING, B.J., MERCER, S.R., SALTER, J.D., NORDIN, L., "Sorting particulate material on the basis of size or composition", Australian Patent AU 2404088.

[16] DOWNING, B.J., MERCER, S.R., SALTER, J.D., NORDIN, L., "Sorting particulate material on the basis of size or composition", Brazilian Patent BR 18805383.

[17] DOWNING, B.J., MERCER, S.R., SALTER, J.D., NORDIN, L., "Sorting particulate material on the basis of size or composition", Canadian Patent Ca 5804281.

[18] DOWNING, B.J., MERCER, S.R., SALTER, J.D., NORDIN, L., "Sorting particulate material on the basis of size or composition", United Kingdom Patent UK 88244447.

[19] DOWNING, B.J., MERCER, S.R., SALTER, J.D., NORDIN,L., "Sorting particulate material on the basis of size or composition", U.S.A. Patent U.S. 07259843.

CHAPTER 2

2.0 DIELECTRIC MATERIALS AND ELECTROMAGNETIC RADIATION

All materials can be divided into three main groups depending on their conductivity. These groups are conductors, semiconductors and insulators or dielectrics. The term dielectric originates from the Greek dia + electric, where dia means through [1]. Dielectric materials are those in which a steady electric field can be established without causing an appreciable current flow.

The distinction between the three categories is often vague and is dependent on the conduction mechanism within the material. The microscopic effects of a perturbing field on a dielectric are described by means of various polarisation mechanisms. The permittivity and permeability of a dielectric are a macroscopic representation of the field/dielectric interaction.

2.1. POLARISATION IN DIELECTRICS

The dielectrics constant or permittivity of a material is not an absolute constant but can vary with frequency, temperature, bonding, crystal structure, phase constitution and structural defects of the dielectrics.

The relative permittivity ϵ_r of a dielectric is defined [2] as

$$\epsilon_r \equiv \epsilon/\epsilon_o \qquad (2.1)$$

where ϵ = dielectric permittivity

ϵ_o = permittivity of free space

ϵ_r may be complex to allow for energy losses within the dielectric.

In dielectrics there are no free charges to allow dc conduction. An applied electric field can cause

displacement currents in the dielectric as a result of the movement of bound charges. If an electrically neutral dielectric is placed in an electric field it is possible for the electron cloud around each atomic nucleus to distort in accordance with the field. This displacement of bound charge is known as polarisation.

The relative displacement of charge in the dielectric results in each atom acquiring a dipole moment p in the direction of the applied field. It is useful to define the total polarisation P such that

$$P = Np \qquad (2.2)$$

where N = total number of atoms per molecule.

The polarisation P is proportional to the applied electric field E. The constant of proportionality is dependent on the ease of polarisability of the material [3].

$$P = \chi \epsilon_o E \qquad (2.3)$$

where χ = dielectric susceptibility of material.

In classical electromagnetic theory the effect of a dielectric material is treated by considering the electric displacement vector D, as two terms, the second of which caters for the effect of the dielectric [4]:

$$D = \epsilon_o E + P \qquad (2.4)$$

Substituting equation (2.2) in (2.3) gives:

$$D = \epsilon_o (1 + \chi) E$$

$$D = \epsilon_o \epsilon_r E \qquad (2.5)$$

Equation 2.11 indicates the effect of a dielectric when placed in an electric field but a study of polarisation mechanisms in dielectrics is necessary to establish the frequency and temperature dependence of the dielectric permittivity.

2.1.1. Electronic Polarisation

Electronic polarisation occurs in all dielectrics. Figure 2.1 shows the induced displacement of the electron cloud around an atomic nucleus due to the presence of an external field [5].

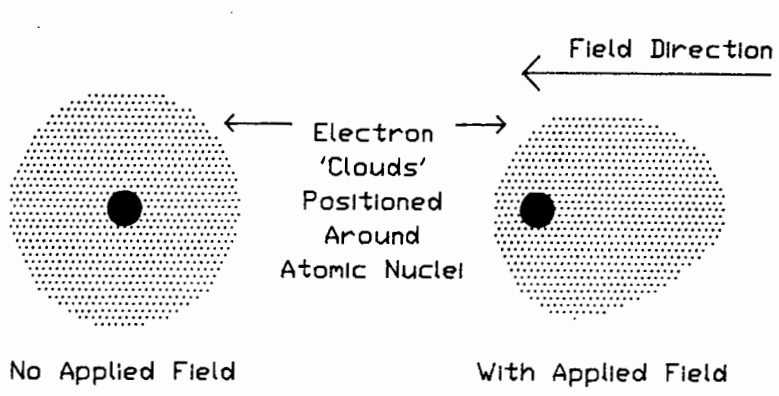

Figure 2.1 Electronic Polarisation

Consider a low density substance with no molecular interaction for simplicity. The motion of an electron in a time varying field is given by:

$$m_e * \delta^2 x/\delta t^2 + \gamma m_e * \delta x/\delta t + m_e w_o^2 x = qE \qquad (2.6)$$

where x = electron displacement

m_e = electron mass

The first term is the force due to the electron inertia. The second term is a resistive or dissipative force opposing the motion. The third term is a restoring force. The term on the right of equation 2.6 is the driving force of the electric field. The constant w_o is the resonant frequency of the molecule.

This is the equation for a damped harmonic oscillator [6] If $E = E_o e^{jwt}$ then

$$x = qE / m_e * (j\gamma w + w_o^2 - w^2) \qquad (2.7)$$

The induced dipole moment is therefore

$$p = q^2E/m_e(j\gamma w + w_o^2 - w^2)$$

$$p = \alpha\epsilon_o E \qquad (2.8)$$

where α = atomic polarisability of the atom.

It can be seen from equation 2.8 that ϵ and α exhibit frequency dependence. The above approach is crude in that it assumes that the atom has only one resonant frequency. Quantum mechanics predicts many resonant frequencies, usually in the optical and low infra-red regions. Electronic polarisation is strongest in the optical frequency range and has only a weak effect at microwave frequencies.

When a high density substance is examined, molecular interaction must be considered. Here the field acting on an individual molecule will be affected by the polarisation of adjacent atoms. The Clausius-Mossotti equation [7] is used to indicate the increase in polarisation due to the effect of neighbouring molecules. The electronic polarisability of a dielectric is related to it's dielectric constant by means of this relation [8,9]. The Clausius-Mossotti relation is only valid for non-polar or very weakly polarisable dielectrics [10].

2.1.2. Orientation Polarisation

Orientation polarisation occurs in liquids and solids which have asymmetric molecules whose permanent dipole moments can be aligned by the electric field. Thus orientation polarisation is specific to polar molecules [11]. The magnitude of orientation polarisation is usually far greater than electronic polarisation. Dielectrics exhibiting orientation polarisation usually have large permittivities.

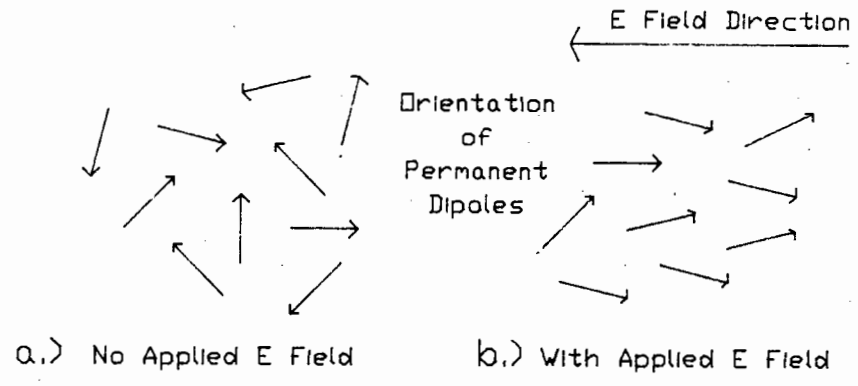

Figure 2.2 Orientation Polarisation

Figure 2.2a shows the random orientation of the permanent dipoles in the absence of an applied field. In this state the randomly orientated dipole moments cancel and the dielectric has zero nett polarisation. The effect of an applied static field is shown in figure 2.2b. The dipoles tend to align in accordance with the applied field. The effect of random thermal motion is to prevent the dipoles from lining up perfectly [12]. Polarisation by this mechanism is therefore highly temperature dependent. The polarisation is weakened with increasing temperature.

The Currie Law [13] exemplifies this thermal effect whereby the dielectric polarisability is inversely proportional to temperature.

Consider the case of a time varying electric field applied to a dielectric exhibiting orientation polarisation. The polar molecules are unable to accurately follow rapid variation in the field due to their moments of inertia. This results in the total polarisation P lagging in phase with respect to the

electric field E. The phase difference is frequency dependent, resulting in a complex permittivity $\epsilon_r = \epsilon' - j\epsilon''$.

The Debye formula [14] is used to describe the variation of permittivity, versus frequency for low density polar dielectrics. An Argand diagram of ϵ'' versus ϵ' using frequency as a parameter is often used in categorising dielectrics. It can then be shown that the effect of orientation polarisation reduces with increasing frequency.

2.1.3. Ionic Polarisation

Ionic polarisation occurs in dielectrics with ionic lattice structures. Figure 2.3(a) shows an ionic lattice in the absence of an external field.

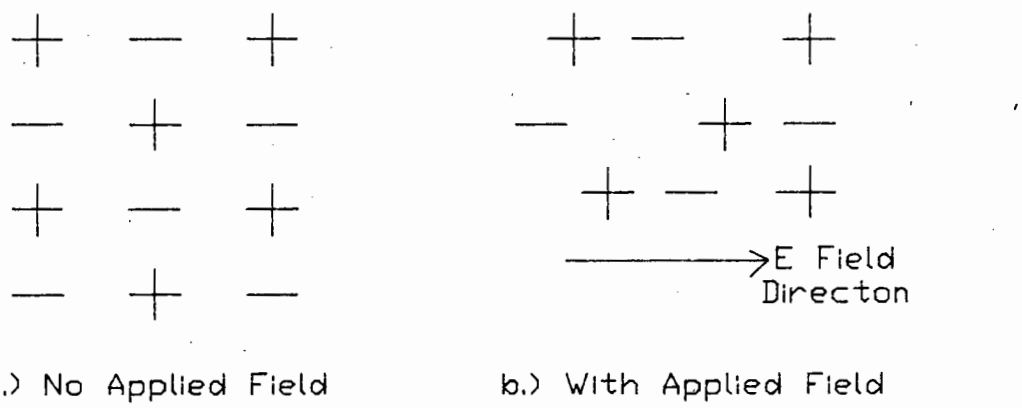

Figure 2.3 Ionic Polarisation

When an external field is applied as shown in figure 2.3(b), the oppositely charged ions are displaced from their relative positions in the crystal lattice. This ionic displacement gives rise to dipole formation and hence polarisation [11,15].

Ionic polarisation only occurs in crystal lattices with weakly bonded ions. Due to the ions' moments of inertia, the ionic polarisability decreases with increasing frequency. The effect of random thermal energy also reduces the ionic polarisation with increasing temperature.

2.1.4. Space Charge Polarisation

Space charge polarisation occurs in multiphase dielectrics. There is an accumulation of charges at phase interfaces in these dielectrics. Space charge polarisation is possible when one of the phases present has a much higher resistivity than the others [15].

Charge carriers usually exist that can migrate through the dielectric material. These charge carriers can become trapped in the material or at the phase interfaces. This results in a space charge and a macroscopic field distortion. This phenomenon is generally only found in multiphase insulators at elevated temperatures.

2.2 FREQUENCY DEPENDENCE OF DIELECTRIC CONSTANT

The time taken for a polarisation process to reach equilibrium orientation is known as its relaxation time. The relaxation frequency is given as 1/relaxation time. If the frequency of the applied electric field exceeds the relaxation frequency of a particular polarisation mechanism then the dipoles cannot reorient themselves quickly enough and that polarisation mechanism ceases to function [16].

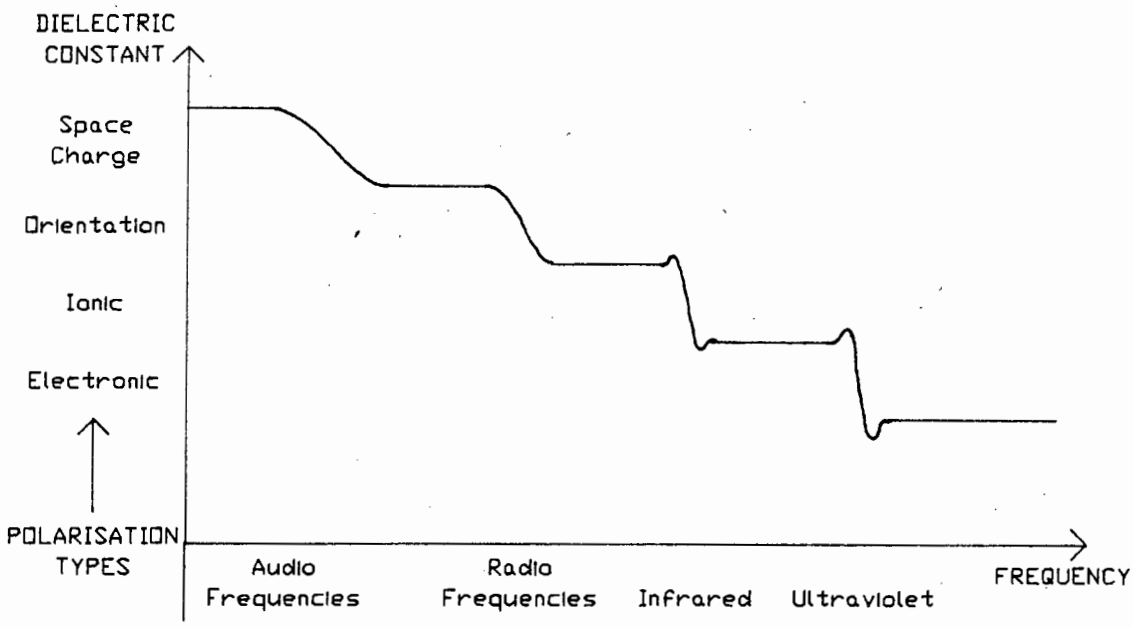

Figure 2.4 Polarisation Frequency Dependence

Figure 2.4 demonstrates the frequency dependence of the total polarisability of a materials dielectric constant [17]. It can be seen that the relaxation frequencies of all four processes differ widely.

2.3. DIELECTRIC ANISOTROPY AND ANOMALY

It is possible for a substance to display a dielectric constant that is anisotropic [18]. This is often due to an assymetrical crystal structure. Materials that have crystalline grains in preferred orientations often exhibit dielectric anisotropy.

In such substances the polarisation P may no longer be in the direction of the applied electric field. The dielectric's orientation in the field will affect the magnitude of the permittivity and also the angle between the polarisation and the applied field. The mathematics concerning anisotropic media are well presented by Jones [19].

The situation is further complicated when multiphase dielectrics are considered. These can be treated either as a mixture, an unordered composition of the constituents, or as a matrix where evenly distributed inclusions are present in a host material. There are a variety of approximate formulae available for calculation of dielectric permittivity in two phase mixtures [20]. These formulae assume that no interactions occur between the constituents.

This is often not the case and interaction can occur between the polarisations of the different molecules present. The result can be a substance where the permittivity of the substance is greater than the permittivity of all the constituents.

In the case of a material made up of a layer of insulating material covered by a layer of conducting material where the concentration of the insulating region is small, the low-frequency dielectric constant can be extremely large [21,22]. This is known as the Maxwell-Wagner effect.

It can be seen that the interactions in multiphase materials are extremely complex and the resultant dielectric permittivity is very difficult to predict. The situation becomes increasingly more complex as the number of constituent components increases.

2.4. PERMITTIVITY AND PERMEABILITY

The interaction of dielectrics and the electric field vector is quantified by the complex permittivity of the dielectric [23]. The complex permittivity of a material is used to model the loss in a dielectric without considering the mechanism of loss.

$$\epsilon = \epsilon' - j\epsilon'' \qquad (2.9)$$

ϵ' = dielectric constant

ϵ'' = loss factor = $\sigma/w\epsilon_o$

The dielectric constant is a measure of the ability to store E field energy. The loss factor describes energy dissipation in the material.

The permeability of a dielectric describes its interaction with the H field vector [24].

$$\mu = \mu' - j\mu'' \qquad (2.10)$$

μ' is a measure of the ability to store the H field energy whilst μ'' is a measure of the H field dissipation in the material. Most dielectrics have a permeability equal to that of free space (μ_o). The permittivity and permeability are tensors, except, for time invariant, linear and isotropic media. In this case, the permittivity and permeability are scalar quantities.

2.5. MAXWELLS EQUATIONS

Maxwell's equations describe the interaction of electromagnetic radiation with matter. The microwave spectrum, from 300MHz to 300GHz, is a subset of the electromagnetic spectrum. Here the signal wavelengths are much greater than the dimensions of atomic or molecular structures but are often comparable to the dimensions of many dielectric bodies.

James Clark Maxwell formulated the following four electromagnetic equations during the late 1800's.

$$\nabla \wedge H = \dot{D} + J \qquad (2.11)$$

$$\nabla \wedge E = -\dot{B} \qquad (2.12)$$

$$\nabla . D = \rho \qquad (2.13)$$

$$\nabla . B = 0 \qquad (2.14)$$

where

$$\nabla . J = -\dot{\rho} = \sigma E \qquad (2.15)$$

$$D = \epsilon E \qquad (2.16)$$

$$B = \mu H \qquad (2.17)$$

here
- E = Electric field strength
- D = Displacement current density
- H = Magnetic field strength
- B = Magnetic flux density
- J = Current density
- ρ = charge density

Maxwell's equations can be manipulated to provide an expression for the complex propagation constant, γ , for a medium [25].

$$\gamma = \alpha + j\beta \qquad (2.18)$$

- α = Attenuation constant in N/m
- β = phase constant in rad/m

The attenuation and phase constants can be expressed in terms of α, ϵ and μ as shown below [26].

$$\alpha = w\left[\mu\epsilon/2 \left(\sqrt{1 + \sigma^2/w^2\epsilon^2} - 1 \right) \right] \qquad (2.19)$$

$$\beta = w\left[\mu\epsilon/2 \left(\sqrt{1 + \sigma^2/w^2\epsilon^2} + 1 \right) \right] \qquad (2.20)$$

For a linear, homogeneous, source free and infinite medium, a plane wave representation of the wave equation [27], derived from Maxwells equations, is possible. This is obtained by assuming that the E and H field vectors only depend on z and t in Cartesian co-ordinates. The Cartesian co-ordinates system is shown in figure 2.5

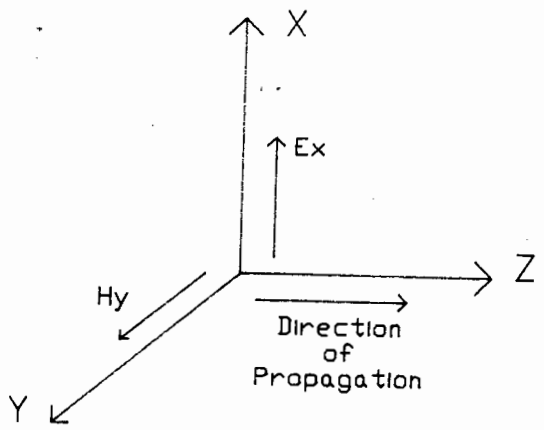

Figure 2.5 Plane Wave Representation in Cartestian Co-ordinates

The solution to the wave equation can then be written as [28]:

$$E = E_o e^{-\alpha z} e^{-j(wt-\beta z)} \qquad (2.21)$$

$$H = H_o e^{-\alpha z} e^{-j(wt-\beta z)} \qquad (2.22)$$

A study of equations 2.21 and 2.22 reveals that as the wave progresses through the medium in the z direction, the amplitude decreases exponentially in accordance with the attenuation constant whilst the phase constant β indicates phase variations in the medium. A graphic representation of this is presented in figure 2.6

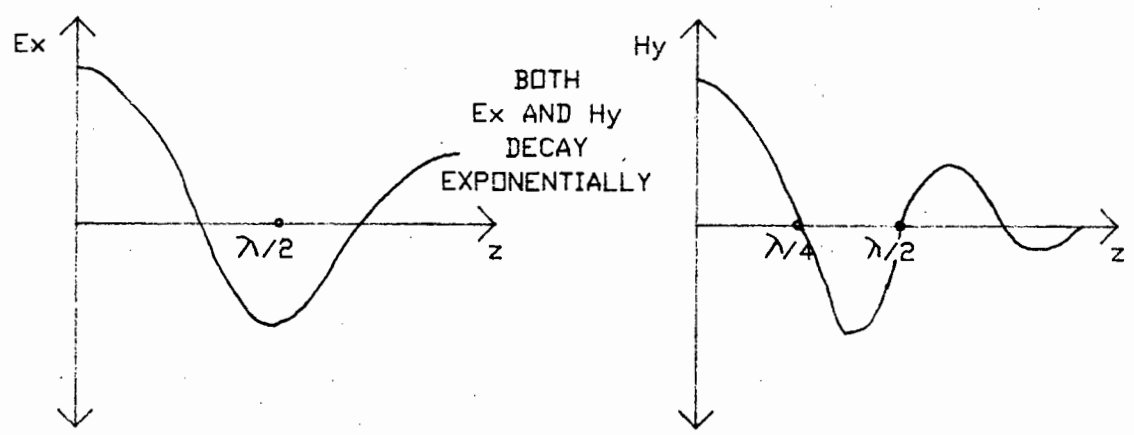

Figure 2.6 Plane Wave Propagation in Lossy Dielectric

2.6 ENERGY LOSSES IN DIELECTRICS

Energy losses can occur in dielectrics due to dipole relaxation and dc conductivity. First consider losses due to dipole relaxation. As mentioned in section 2.1.2. for a periodic electric field $E = E_o * \cos wt$, the polarisation may not be in phase with the field. There is a frequency dependent phase lag, ϕ , between the field E and the electric displacement vector D. Substituting into equation 2.5:

$$D = \epsilon E * \cos(wt - \phi) \qquad \text{where } \phi > 0$$

$$\text{or} \quad D = \epsilon e^{-j\phi} E * \cos wt \qquad (2.23)$$

where $\epsilon e^{-j\phi}$ is complex permittivity allowing for the phase difference between D and E.

A finite, non zero conductivity will also produce a loss in the dielectric. Substituting into equation (2.14) we get:

$$\text{curl } H = jw\epsilon E + \sigma E$$

$$= jw\epsilon_o [\, \epsilon' - j\epsilon'' - j(\sigma / w\epsilon_o) \,] * E \qquad (2.24)$$

It can be seen from equation 2.33 that the loss factor is composed of the old loss factor due to polarisation and the new term $\sigma/w\epsilon_o$ due to the resistive loss. As far as external effects relating to energy loss are concerned, these two terms can be combined to form the loss factor, irrespective of loss mechanism.

Energy dissipation in a dielectric can be quantified by means of the Poynting theorem which states that the vector product $P = E \wedge H$ at any point is a measure of the rate of energy flow/unit area at that point [29]. The direction of energy flow is perpendicular to E and H and in the direction of $E \wedge H$.

It can be shown by means of the Poynting theorem that for a unit volume and constant E field in the region [30]:

$$\text{Power dissipated} = \tfrac{1}{2}\sigma|E|^2 = \tfrac{1}{2}w\epsilon_o\epsilon_r''|E|^2 \qquad (2.25)$$

2.7. SIGNAL TRANSMISSION AND REFLECTION AT BOUNDARIES

Maxwell's equations have to be satisfied in any dielectric and at boundaries between different dielectrics. At any such boundary between two media, the following boundary conditions, implied by Maxwell's equations, must be satisfied:

1. The tangential components of the electric field must be continuous across the boundary
2. The tangential components of the magnetic field must be discontinuous across the boundary by an amount equal to the surface current density on the boundary
3. The normal component of B is continuous across the boundary
4. The normal component of D is discontinuous at the boundary by an amount equal to the surface charge

density on the boundary.

These boundary conditions are independent of interfacial geometry.

For a time varying wave normally incident on an air/perfect conductor ($\sigma=\infty$) interface, there is total signal reflection from the surface. Standing waves are formed between the incident and reflected waves in such a way that the boundary conditions are satisfied.

A dielectric boundary with a normal incident wave is shown in figure 2.7.

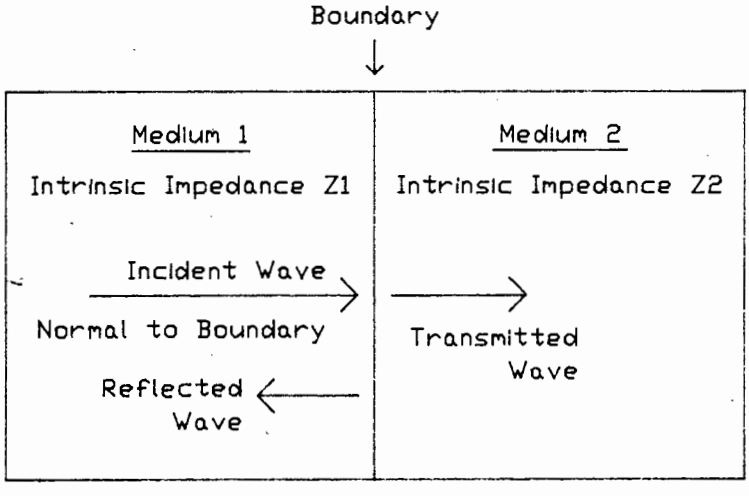

Figure 2.7 Normal Incidence at a Dielectric Interface

In this case the media have finite conductivities and there is a wave reflected from the boundary and a wave transmitted into the second medium. The reflection coefficient is given by [31].

$$\Gamma = (Z_1 - Z_2)/(Z_2 + Z_1) \qquad (2.26)$$
$$= (\sqrt{\epsilon_1} - \sqrt{\epsilon_2})/(\sqrt{\epsilon_1} + \sqrt{\epsilon_2}) \quad \text{for media where:}$$

$$\mu_1 = \mu_2 = \mu$$

Where signals are obliquely incident on a dielectric slab, Snell's law of refraction is used to describe the direction of the transmitted waves [32]. This situation is greatly complicated in the case of an irregular surface where signal scattering occurs.

2.8. LIST OF REFERENCES

[1] KIP, A.F., "Fundamentals of Electricity and Magnetism", McGraw-Hill, 1981, p 124.

[2] ROSE, R.M., SHEPARD, L.A., WULF, J., "The Structure and Properties of Materials, vol. 4, Electronic Properties", J. Wiley & Sons Inc, 1966, p 251.

[3] KITTEL, C., "Introduction to Solid State Physics", J. Wiley, New York, 1960, p 469.

[4] LOVELL, M.C., AVERY, A.J., VERNON, M.W., "Physical Properties of Materials", Van Nostrand Reinhold Company Ltd, 1976, p 155.

[5] ROSE, R.M., SHEPARD, L.A., WULF, J., "The Structure and Properties of Materials, volume 4, Electronic Properties", J. Wiley & Sons Inc, 1966, p 257.

[6] RAINVILLE, E.D., BEDIENT, P.E., "Elementary Differential Equations", 6th edition, Macmillan Publishing Co. Ltd., 1981, p 156.

[7] DEKKER, A.J., "Solid State Physics", Macmillan & Co., 1958, p 144.

[8] KITTEL, C., "Introduction to Solid State Physics", J. Wiley, New York, 1960, p 410.

[9] LOVELL, M.C., AVERY, A.J., VERNON, M.W., "Physical Properties of Materials", Van Nostrand Reinhold Co. Ltd., 1976, p 161.

[10] PARKHOMENKO, E.I., "Electrical Properties of Rocks", Plenum Press, New York, 1967, p 15.

[11] KIP, A.F., "Fundamentals of Electricity and Magnetism", McGraw-Hill, 1981, p 154.

[12] ROSE, R.M., SHEPARD, L.A., WULF, J., "The Structure and Properties of Materials, volume 4, Electronic Properties", J. Wiley & Cons, Inc., 1966, p 257.

[13] KIP, A.F., "Fundamentals of Electricity and Magnetism", McGraw-Hill, 1981, p 351.

[14] DEKKER, A.J., "Solid State Physics", Macmillan & Co., 1958, p 151.

[15] STUCHLY, M.A., "Fundamentals of the interaction of radio-frequency and microwave energies with matter", Radiation Protection Bureau, Health and Welfare Canada, Ottawa, Ontario K1A 0L2, pp 88-89.

[16] JORDAN, E.C., BALMAIN, K.G., "Electromagnetic Waves and Radiating Systems", Prentice-Hall Inc., 1968, p 306.

[17] PUGH, E.M., "Principles of Electricity and Magnetism", Addison-Wesley Publishing Co.Inc., 1970, p 142.

[18] PUGH, E.M., "Principles of Electricity and Magnetism", Addison-Wesley Publishing Co. Inc., 1970, p 147.

[19] JONES, D.S., "The Theory of Electromagnetism", Pergamon Press, 1964, pp 329.

[20] PARKHOMENKO, E.I., "Electrical Properties of Rocks", Plenum Press, New York, 1967, p 20.

[21] SEN, P.N., "Dielectric anomaly in inhomogeneous materials with an application to sedimentary rocks", Appl. Phys. Lett., vol. 39, no 8, pp 667-688.

[22] SEN, P.N., CHEW, W.C., "The Frequency Dependent Dielectric and Conductivity Response of Sedimentary Rocks", Journal of Microwave Power, 1983, vol. 18, no 1, pp 95-105.

[23] JORDAN, E.C., BALMAIN, K.G., "Electromagnetic Waves and Radiating Systems", Prentice-Hall Inc., 1968, p 301.

[24] JORDAN, E.C., BALMAIN, K.G., "Electromagnetic Waves and Radiating Systems", Prentice-Hall Inc., 196, p 305.

[25] MARCUVITZ, N., "Waveguide Handbook", MIT Radiation Laboratory Series, vol. 10, p 18.

[26] JORDAN, E.C., BALMAIN, K.G., "Electromagnetic Waves and Radiating Systems", Prentice-Hall Inc., 1968, p 125.

[27] JORDAN, E.C., BALMAIN, K.G., "Electromagnetic Waves and Radiating Systems", Prentice-Hall Inc., 1968, p 114.

[28] KIP, A.F., "Fundamentals of Electricity and Magnetism", McGraw-Hill, 1981, p 453.

[29] KIP, A.F., "Fundamentals of Electricity and Magnetism", McGraw-Hill, 1981, p 459.

[30] LIAO, S.Y., "Microwave Devices and Circuits", Prentice-Hall Inc, 1980, p 22.

[31] JORDAN, E.C., BALMAIN, K.G., "Electromagnetic Waves and Radiating Systems", Prentice-Hall Inc, 1968, Section 5.13.

[32] SILVER, S., "Microwave Antenna Theory and Design", MIT Radiation Laboratory Series, vol. 12, p 123.

CHAPTER 3

3.0 MICROWAVE MEASUREMENT OPTIONS

The microwave measurements applicable to on-line discrimination processes can be grouped into two main categories, transmission measurements and reflection measurements. Signal reflection measurements are performed by monitoring the reflected signal level from the surface of a product. A number of different transmission measurements can be performed. The attenuation or phase shift of a signal can be monitored. These parameters can be monitored separately or combined in a single system. Resonant structures can also be used to grade or evaluate a product.

3.1. ATTENUATION

It was shown in equations 2.21 and 2.22 that the exponential decay of the amplitude of an electromagnetic wave through a medium is dependent on the attenuation constant for the medium. The attenuation constant, α, is defined in equation 2.19.

The attenuation constant influences the rate of signal decay through the medium. It can be seen from equation 2.19 that the attenuation constant depends on the dielectric constant for the medium. If two media have different dielectric constants then their attenuation constants will differ and the two media will exhibit different amounts of signal attenuation. It can also be seen that two media with different conductivities, σ, will exhibit different amounts of signal attenuation even if they have the same dielectric constant.

This can be used as a basis for a microwave attenuation method for sorting two different products, assuming that

there are suitable differences in their dielectric properties. Variations in signal attenuation due to changes in moisture content, which cause changes in dielectric properties, have led to the attenuation techniques being exploited as a moisture meter [1,2]. In this method small variations in dielectric constant due to changing moisture content are noted in a relatively microwave transparent host material.

3.2. PHASE SHIFT

The propagation constant of a medium is also affected by the phase constant described by equation 2.20. It can be seen from this equation that the signal phase delay is dependent on the dielectric constant of the material through which it passes.

Signal phase changes through a product are usually monitored by means of a two channel system. Signal phase delays encountered in the system's test channel are measured by comparison to the phase of the signal in a bypass or test channel. This method is mainly used in moisture metering applications and is nearly always used in combination with attenuation measurements.

The phase shift method is complex and expensive in comparison to the attenuation method. Requirements such as a quartz controlled phase locked loop for two Gunn oscillators [3] are common.

3.3 COMBINED ATTENUATION AND PHASE MEASUREMENT

This type of system arose chiefly from moisture metering applications. Attenuation measurements are dependent on the bulk density of the sample. This meant that a method was required to remove the density dependence in order to

accurately monitor the samples moisture levels. The most common solution was to use the microwave system in conjunction with a gamma ray system [4].

The gamma ray system was used to provide a density measurement that was used as a correcting signal for the microwave units. The use of this correcting signal removed the density dependence of the attenuation measurements.

The use of a gamma ray system was often not preferred due to the high cost of the units and the regulations controlling them. Other methods of compensating for density dependence such as sample weighing are often not possible to use on-line. The use of combined attenuation and phase measurements was proposed by Krazewski [5] and Kalinsky [6]. This approach was also adopted by many other researchers [7-14].

Attenuation measurements and phase measurements are both density dependent. These measurements can be related to both density and moisture content by means of simultaneous equations. This means that density or layer thickness can be eliminated as an interfering quantity. Combined attenuation and phase measurements were first used for moisture monitoring in various products such as fish meal, milk and coffee powders and tobacco [8,11].

3.4. RESONANT STRUCTURES

The various properties of resonant structures such as cavities, stripline structure [15] and loop gap resonators [16] can be exploited to obtain information about the dielectric properties of different samples.

These methods and techniques are examined in detail in chapters seven and eight.

3.5. MICROWAVE ATTENUATION MEASUREMENT TECHNIQUES

3.5.1. Microwave Heating

Energy losses in dielectrics have been discussed in section 2.6. The history of microwave heating applications has been well documented in the literature [17]. There have also been microwave sensor applications in heat related areas [18, 19].

Applications of the microwave heating method exist in the minerals industry [20-28]. These applications are devoted to the laboratory analysis of small samples. Microwave heating has been used on-line for the drying and desulphurising of coal [26-27]. On-line applications of microwave heating are found in the preparation and processing of foodstuffs.

The heating method, however, has limited potential for sample discrimination purposes. The method cannot be applied to samples that can be damaged by heating. The microwave power requirements are also a limiting factor. The separation of different ore types is one potential non-damaging application of this method. Appendix A demonstrates the impractical power requirements for such an application.

3.5.2. Attenuation in Waveguide Structures

One possible method of measuring the microwave signal attenuation of a sample is to pass the sample through a non-radiating slot in a waveguide. The slot should be non-radiating to ensure maximum signal transmission through the waveguide structure.

The dimensions of most fundamental mode waveguides in the microwave frequency range are too small to allow many samples to be passed through them. The physical size increases as the signal frequency decreases. The signal attenuation for most dielectrics decreases with decreasing frequency. The frequency dependence of the dielectric constant for many materials is discussed in section 2.2.

Overmoded waveguide structures were considered as these could be constructed of suitable physical dimensions, without the operating frequency dropping too low for practical attenuation measurement. An operating frequency of 3GHz was chosen and fundamental mode (TE_{10}) and three times overmoded (TE_{30}) waveguides were constructed. The E field distribution across the end of the waveguides are shown in figure 3.1.

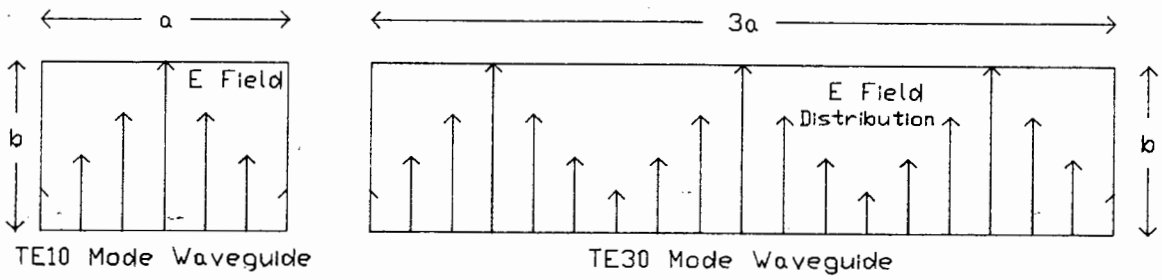

Figure 3.1 E field distribution in TE_{10} and TE_{30} waveguide.

The construction of the TE_{10} waveguide is shown in figure 3.2. The non radiating slots cut in the centre of the broad walls were chosen for maximum radiation with the resonant dimensions of 10cm long and 0.5cm wide.

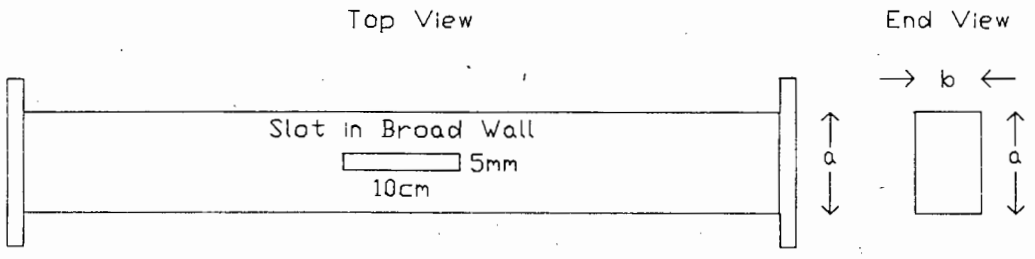

Figure 3.2 TE_{10} Waveguide

The construction of the TE_{30} waveguide is shown in figure 3.3. The non-radiating slots in centre of the broad walls were 10cm long and 7cm wide. This would allow larger samples to pass through this structure than through the fundamental mode waveguide.

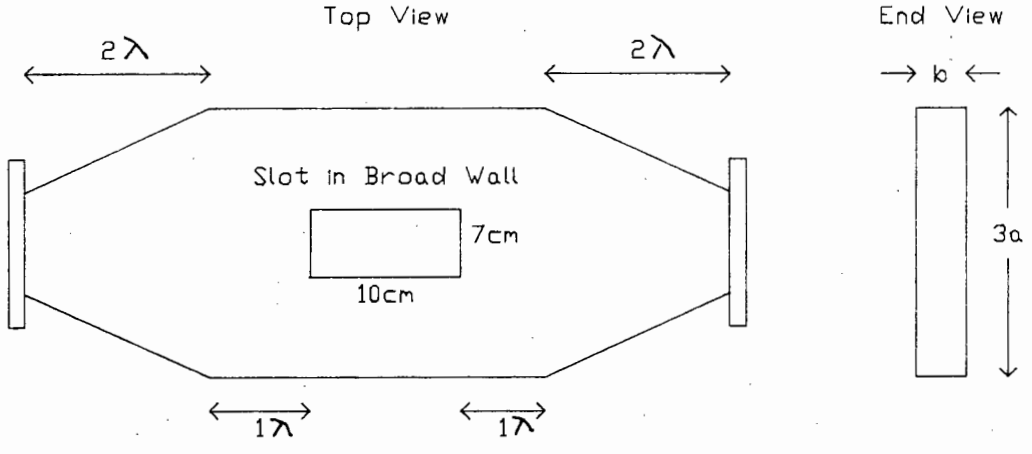

Figure 3.3. TE_{30} Waveguide

Coaxial cable to rectangular waveguide transformers were used to couple signals through these waveguide structures. Signals coupled into the TE_{30} waveguide pass through a two wavelength long tapered section to allow a gradual transition between the TE_{10} and TE_{30} dimensions. Metal screws were placed into the broad

wall of the TE_{30} waveguide at the required points to act as mode traps for the TE_{10} and TE_{20} modes and to ensure the propagation of the TE_{30} mode.

The ends of the tapered sections form discontinuities in the structure. One wavelength long sections of TE_{30} waveguide were included on either side of the slot to ensure that any evanescent modes generated at the discontinuity had decayed. The TE_{10} and TE_{30} waveguide structures were constructed the same length to allow comparative measurements to be made.

The insertion loss for the TE_{30} waveguide was found to be 1dB. This was due to a small amount of signal radiation from the large slots in this structure. The insertion loss was negligible when the slots were covered with metal plates.

Tests were performed by inserting a 7cm square of attenuative card into the waveguides via the slots in their broad walls. The card was found to have 18dB insertion loss in the TE_{10} waveguide and 7dB insertion loss in the TE_{30} waveguide. The insertion loss due to the card was found to vary widely as it was moved across the slot in the TE_{30} waveguide. This was due to the lower energy density in the waveguide and the varied E field across the slot. This is shown in figure 3.1.

The use of overmoded waveguides of a higher frequency was not considered viable. A 10GHz TE_{10} waveguide would have to be ten times overmoded to produce a structure with similar physical dimensions to the 3GHz TE_{30} waveguide. The complex field variation across the slot and the low energy density in such a structure

would yield little useful information regarding sample properties.

It has been shown that the use of overmoded waveguide structures is not a practical means of sample evaluation.

3.5.3. Antennae

Horn antennae are commonly used to effect signal attenuation and phase measurements with constant geometry product streams [2,3,12]. The choice of applicator is fairly non critical where a continuous and uniform product is evaluated e.g. paper, powder stream.

When the antennae are placed close to discrete dielectric samples of varied geometry, the system performance could be adversely affected by the near field inconsistency [29] of closely spaced high gain horn antennae.

Another option exists in the form of an undersquare open waveguide antenna. These antennae can be brought closer to each other as the far field of $2D^2\backslash\lambda$ is less than that for high gain horn antennae.

Antenna impedance is given by

$$Z_A = 377*(\lambda_g/\lambda)*(b/a)$$

where λ = freespace wavelength (cm)

a = a dimension of antenna (cm)

b = b dimension of antenna (cm)

$$\lambda_g = \lambda/\sqrt{[\ 1 - (\lambda/2*a)^2\ ]} \qquad (3.1)$$

For X band with λ = 3cm, λ_g = 3.976cm, a = 2.286cm and b = 1.725cm then Z_A = 377 ohms. It can be seen that an

undersquare waveguide antenna can function as an efficient, well matched, low cost antenna which is physically small. These antennae can be connected to standard rectangular waveguide launchers as shown in figure 3.4.

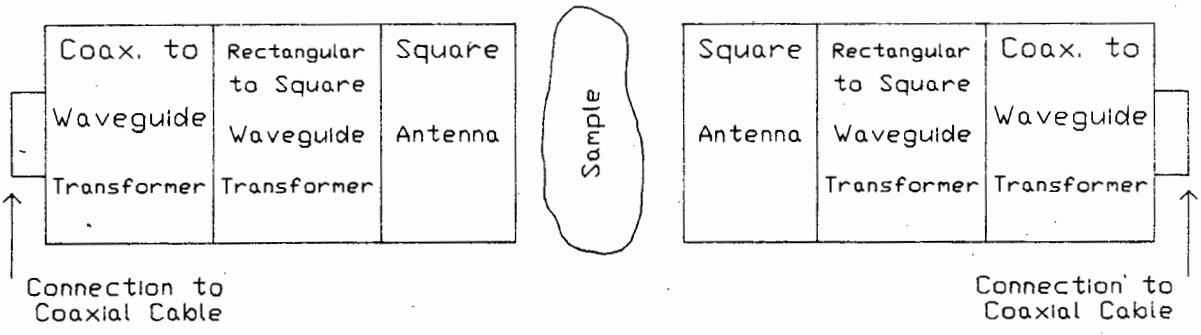

Figure 3.4. Square Waveguide Antenna Connections

Figure 3.5 depicts a quarter wavelength rectangular to square waveguide transformer. The internal dimensions of rectangular waveguide are a*b where b is the dimension of the short wall.

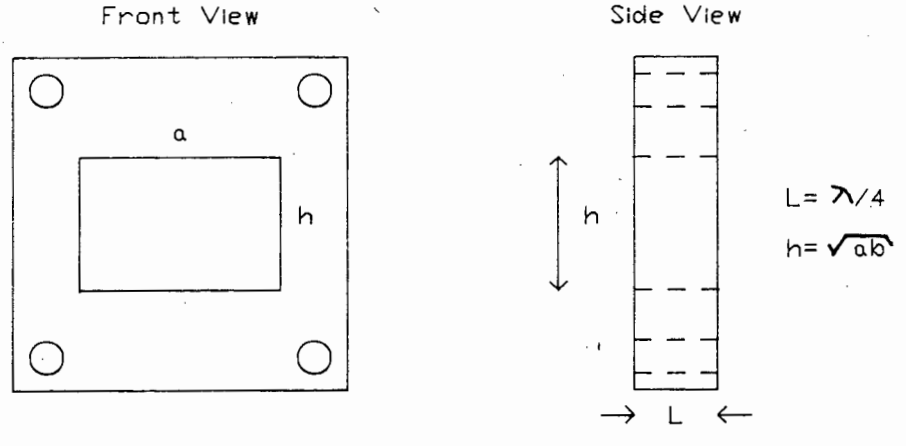

Figure 3.5. Rectangular to Square Waveguide Transformer

The height of the slot in the rectangular to square waveguide transformer is given by h= $\sqrt{a*b}$. The length of the waveguide transformer is given by L = $\lambda_g/4$. Appendix B gives the dimensions and diagrams for various transformers designed using this procedure. The design criteria for undersquare waveguide antennae are also given in Appendix B.

The antenna aperture area must be considered when discrete samples are to be processed. The sample must be of sufficient size to prevent direct signal propagation around the sample. If direct signal propagation can occur then invalid data will be obtained. The operating frequency affects the antennae dimensions. The operating frequency must be increased in order to reduce the antenna dimensions.

The use of reduced aperture antennae has been investigated as an alternative solution to the above-mentioned problem of on-line evaluation of discrete samples. Two different types of reduced aperture antennae were examined.

A resonant patch antenna is shown in Figure 3.6.

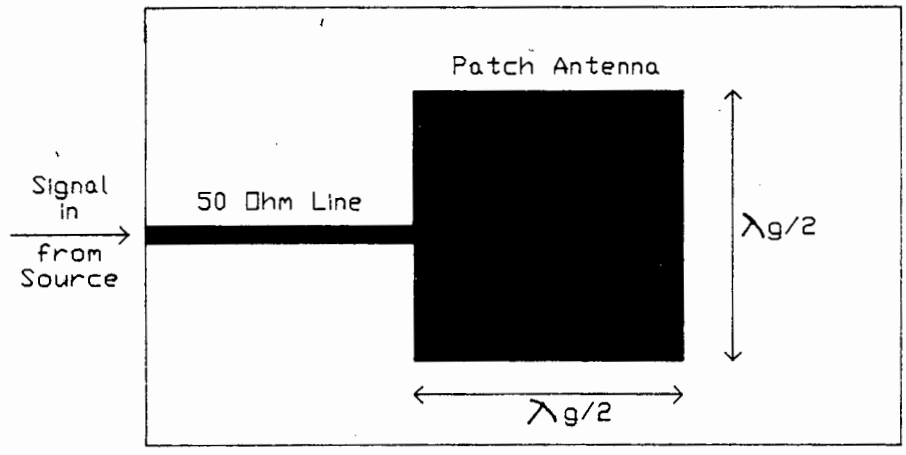

Figure 3.6. Resonant Patch Antenna

These antenna are manufactured on a dielectric substrate. Printed circuit boards with ϵ_r = 4 was used to manufacture antennae at 1GHz and RT DURIOD 5880 with ϵ_r = 2.2 was used to fabricate antennae at 3GHz and 10GHz.

Tests with these antennae proved them to be non viable. The proximity of a dielectric body such as a small water load led to a frequency pulling effect due to the resonant nature of the antenna. This meant that the antenna became matched at a different frequency, leading to invalid attenuation measurements.

Dielectrically loaded antennae were also examined. It is possible to dielectrically load an antenna to reduce its aperture area. Two possible approaches exist here. The signal can be launched directly into a dielectric waveguide or a reduced aperture antenna with a tapered dielectric transition in a closed metal waveguide can be used.

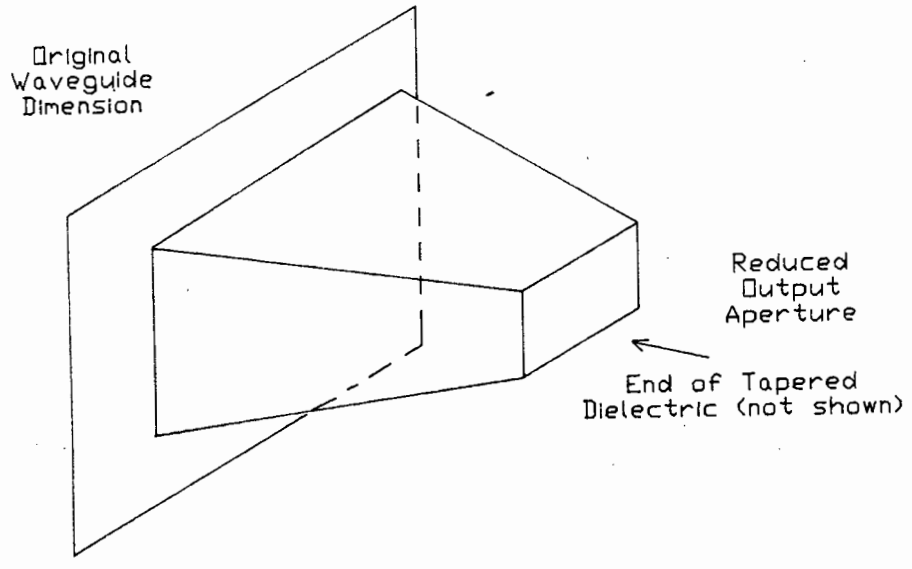

Figure 3.7. Dielectrically Loaded Antenna

It was decided to examaine the use of a dielectrically loaded waveguide antenna as shown in figure 3.7. The dielectric is tapered to provide a gradual change in impedance. This has been demonstrated to be effective by Cloete and Malherbe [30]. The dimensions of the antenna output aperture is determined by the dielectric constant of the chosen material. The antenna aperture is reduced to $1/\sqrt{\epsilon_r}$ of its original size [31].

The tapered section, shown in figure 3.8 is a half-wavelength long to prevent reflections back towards the source [32].

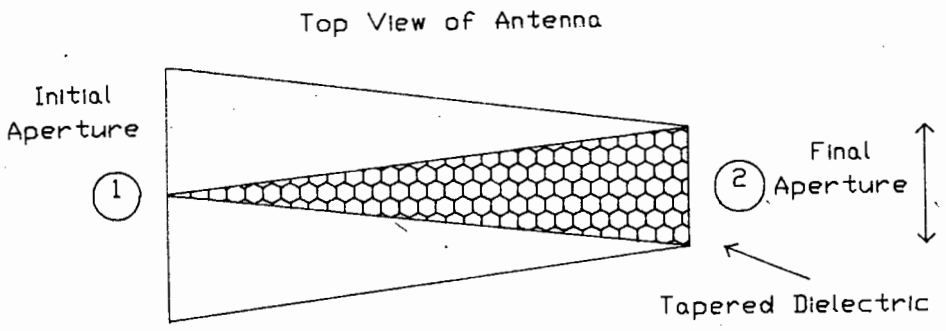

Figure 3.8. Tapered Section in Loaded Antenna

The tapered dielectric section causes two impedance discontinuities. At point (1) in figure 3.8 there is a low to high impedance discontinuity from air to the dielectric. This is similar to an open circuit termination of a line and causes a 360^{o} phase shift in any signal reflected from that discontinuity.

The discontinuity at point (2) is from high to low impedance due to the impedance change from the dielectric to air. This is similar to a short circuit termination of the line and causes a 180^{o} phase shift in any reflected signal from this discontinuity. As with a radome, this results in no nett reflected signal down the line.

The following design procedure can be used to design these dielectrically loaded antennae:

1. Choose the operating frequency and calculate the free space wavelength.
2. Use equation 3.1 to determine the waveguide wavelength.
3. Calculate the wavelength in the dielectric (λ_d).
$$\lambda_d = \lambda_g/\sqrt{\epsilon_r}$$
4. Determine the critical wavelength (λ_c) for the

dielectric.

$$\lambda_c = \lambda_d/2$$

This is the a dimension for the rectangular waveguide. Add a 20% safety factor to ensure correct operation.

5. To calculate the length, L, of the tapered dielectric

$$\lambda_{average} = (\lambda_g + \lambda_d)/2$$

Then length of taper $= \lambda_{average}/2$.

S band and X band dielectrically loaded antennae were built and tested at U.C.T. using this design procedure [33]. Unfortunately, tests indicated that the dielectrically loaded antennae did not perform as well as the normal aperture antennae at these frequencies. The use of dielectrically loaded antennae is therefore not recommended for on-line discrimination application.

3.5.4. Reflection Measurements

An object can be irradiated with a microwave signal. A certain amount of signal will be reflected from the object, dependent on the properties of that object. This reflected signal level can be monitored to deduce information regarding the objects dielectric properties.

This reflection method only allows determination of an objects permittivity and not its dielectric losses [34]. The signal reflection is largely influenced by the properties of the reflecting interface. The properties of this interface are often not representative of the properties of a bulk material. This is particularly true of inhomogenous materials. It has been shown by Chouiki [35] that it is possible

to use a open ended coaxial line for moisture measurements with powdered products.

The circuit shown in figure 3.9 was used to investigate signal reflection from various objects. This circuit employs a 10.55GHz intruder alarm oscillator and neighbouring detector diode.

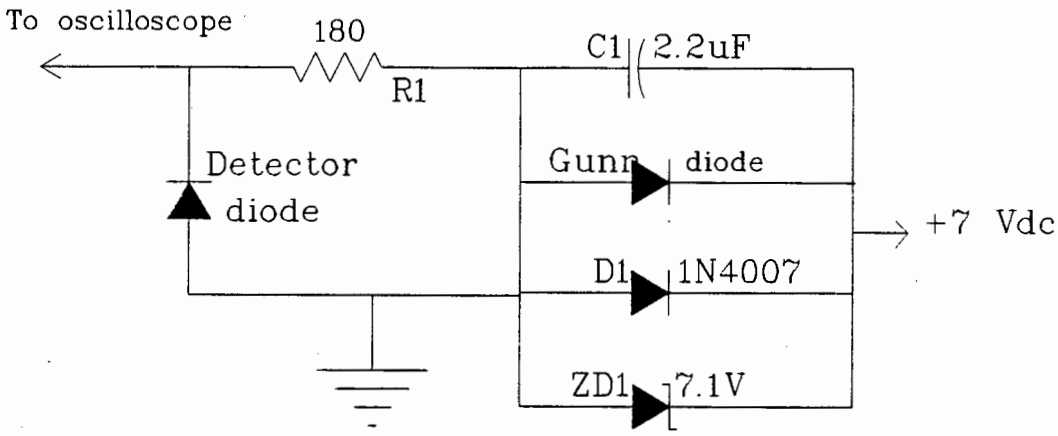

Figure 3.9. Signal Reflection Monitor

It was found, as expected, that the reflected signal level was dependent on the angle of the sample with respect to the receiver antenna. For example, widely varying reflected signal levels are observed as a flat metal plate is rotated a short distance from the antenna.

Irregular shaped objects such as a rock or coal sample were also examined. It was found that each sample exhibited widely varying results, depending on its orientation.

It is therefore clearly evident that microwave signal reflection measurements have limited application for bulk materials. An application that offers a constant geometry is required to obtain meaningful results from this technique.

3.6. LIST OF REFERENCES

[1] KRASZEWSKI, A., "Microwave Aquametry - a bibliography" J. of Microwave Power, vol. 15, pp 299-310.

[2] ZEHNDER, C.B., "Application of the Combination Microwave - Gamma ray gauge to wood chip weight and moisture measurement" Pulp and Paper magazine of Canada, 1967, vol. 10, pp T678-688.

[3] JACOBSON, R., MEYER, W., SCHRAGE, B., "Density independent moisture meter at X-band" 10th European Microwave Conference 1980, pp 216-220.

[4] MLADEK, J., "Determination of the moisture content in loose materials by microwave method", Zemedelska Tech./ Arig. Eng, 1973, vol. 19, pp 453-45.

[5] KRASZEWSKI, A., "Microwave instrumentation for moisture content measurement" J. Microwave Power, vol. 8, pp 323-325.

[6] KALINSKI, J., "Self-adjustable microwave homodyne circuit for on-line simultaneous attenuation and phase measurements" 7th European Microwave Conference 1977, pp 267-272.

[7] MEYER, W., SCHILZ, W., "A microwave method for density independent determination of the moisture content of solids" J. Phys. D: Appl.Phys, vol. 13 (1980), pp 1823-30.

[8] KENT, M., MEYER, W., "Density independent moisture metering in fish meal industry" 11th European Microwave Conference 1981, pp 448-453.

[9] KING, R.J., "On an Automatic System for Simultaneous Measurement of Amplitude and Phase of Millimeter-Wave Fields" IEEE MTT, pp 48-50, 1976.

[10] MEYER, W., SCHILZ, W., "High Frequency Dielectric Data on Selected Moist Materials" Journal of Microwave Power, 1982, vol. 17, pp 67-81.

[11] KRESS-ROGERS, E., KENT, M., "Microwave Measurement of Powder Moisture and Density" Journal of Food Engineering, 1987, vol. 6, pp 345-376.

[12] KLEIN, A., "Microwave determination of moisture compared with capacitive, infrared and conductive measurement methods. Comparison of on-line measurements at coal preparation plants" 14th European Microwave Conference 1984, pp 661-666.

[13] KLEIN, A., "Comparison of rapid moisture meters" Aufbereitungs-Technik, 1987, no. 1, pp 10-16.

[14] KLEIN, A., "Microwave moisture determination of coal - A comparison of attenuation and phase measurement" 10th European Microwave Conference 1980, pp 526-530.

[15] SUCHER, M., FOX, J., "Handbook of Microwave Measurements" vol. ii, Polytechnic Press, 1963, chapter 9.

[16] MEHDIZADEH, M., KORYU ISHI, T., WYDE, J.S., FRONCISZ, W., "Loop-gap resonator: a lumped mode microwave resonant structure" IEEE MTT31, 1983, no. 12, pp 1059-1063.

[17] OSEPCHUP, J.M., "A History of Microwave Heating Applications" IEEE MTT32, 1984, no. 9, pp 1200-1223.

[18] OHNO, J., YASHIRO, H., SHIRAKAWA, Y., TSUDA, A., WATANABE, S., HIRATA, T., HIGUCHI, M., NAGOME, M., "Microwave burden sensor for blast furnaces" IFAC Symposium, Tokyo, August 1986, pp 293-298.

[19] KAWATA, Y., KUSAKA, T., INOVE, K., HACHIYA, S., MIYAKAWA, Y., IMADA, H., "Development of Microwave Profile Meter" Transactions ISIJ, vol. 26, 1986, no. 7, pp B233-B234.

[20] CHEW, T.T., DUTRIZAC, J.E., HAQUE, K.E., WYSLOUSIL, W., KASHYAP, S., "The Relative Transparency of Minerals to Microwave Irradiation" Canadian Metallurgical Quarterly, 1984, vol. 23, no. 3, pp 349-351.

[21] FANSLOW, G.E., BLUHM, D.D., NELSON, S.O., "Dielectric Heating of Mixtures containing Coal and Pyrite" Journal of Microwave Power, 1980, vol. 15, no. 3, pp 187-191.

[22] WALKIEWICZ, J.W., KAZONICW, G., MCGILL, S.L., "Microwave heating characteristics of selected minerals and compounds" Minerals and Metallurgical Processing.February 1986, pp 39-42.

[23] BUTTS, J.R., LEWIS, J.E., STEWARD, F.R., "Microwave Heating of New Brunswick Oil Shale" Journal of Microwave Power 1983, vol. 18, no. 1, pp 37-43.

[24] WALL, E.T., "Interaction of Microwave Energy with Fuel Precursors" Journal of Microwave Power, 1983, vol. 18, no. 1, pp 31-36.

[25] BRIGGS, W.E., LEWIS, J.E., TRANQUILLA, J.M., "Dielectric Properties of New Brunswick Oil Shale"

Journal of Microwave Power, 1983, vol. 18, no. 1, pp 75-82.

[26] CHIRONIS, N.P., "Microwaves Dry Fine Coal" Coal Age, December 1986, vol. 97, pp 64-65.

[27] CHAPMAN, T.H., UK Patent GB2076 146A, filed 25 January 1980.

[28] VOSS, W.G.A., "Microwave Instruments for Material Control" Journal of Microwave Power, vol. 4, no. 3, 1969, pp 210-216.

[29] VOSS, W.A.G., "Microwave instruments for material control," Journal of Microwave Power, 4(3) pp210-216, 1969

[30] CLOETE, J.H., MALHERBE, J.A.G., "A Transition from Rectangular to Non-radiating Dielectric Waveguide" IEEE MTT33, 1985, pp 540.

[31] HARVEY, A.F., "Microwave Engineering" Academic Press Inc (London)Ltd., 1963, pg 60.

[32] HARVEY, A.F., "Microwave Engineering" Academic Press Inc.(London)Ltd., 1963, pg 45.

[33] FLEMING, E.D., "Rock differentiation at low microwave frequencies using electrically small antennas", Unpublished dissertation, University of Cape Town, 1988.

[34] KLEIN, A., "On-Line microwave meter for determining the moisture content of bulk materials on conveyor belts" IMechE Seminar on On-Line Moisture Measurement of Bulk Solids for Process Control, March, 1988, pp 37-42.

[35] CHOUIKI, S.M., "Use of R.F. Wave reflection method for moisture content determination in powdered and granulated products" IMechE Seminar on On-Line Moisture Measurement of Bulk Solids for Process Control, March 1988, pp 21-24.

CHAPTER 4

4.0 DEVELOPMENT OF MICROWAVE ORE SORTER

The third largest diamond pipe in the Southern Hemisphere is situated at Premier Mine at Cullinan, South Africa [1]. A variety of diamond bearing kimberlite rocks occur in a pipe as shown in figure 4.1.

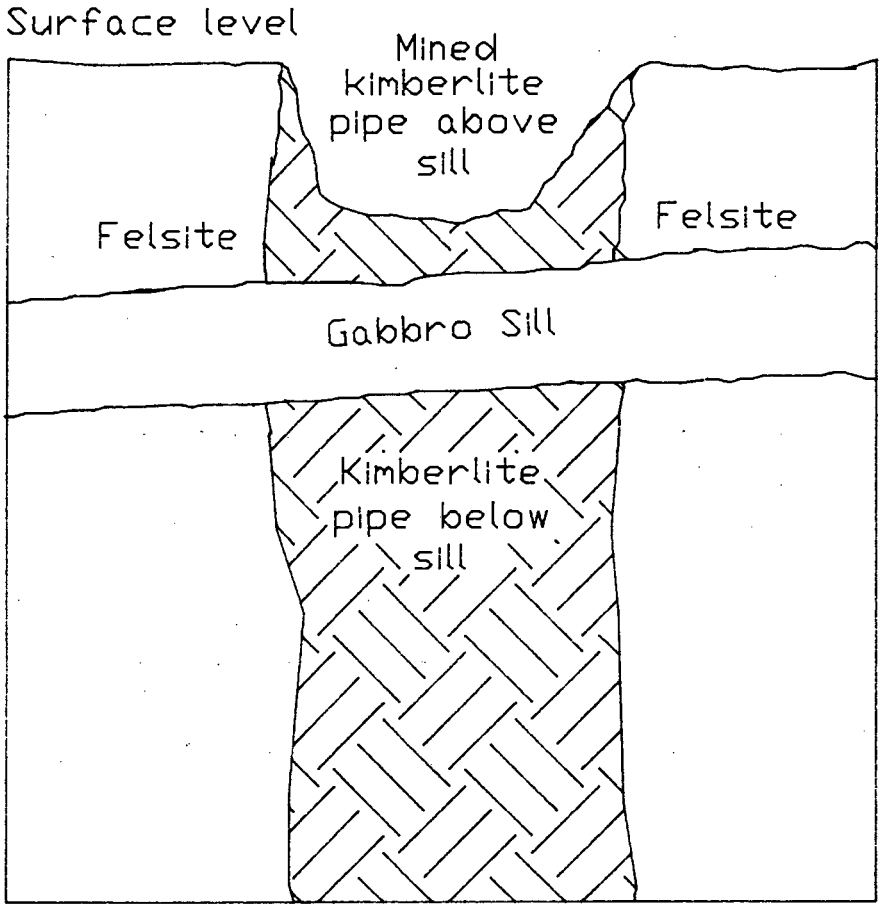

Figure 4.1. Premier kimberlite pipe

A sill of non diamond bearing gabbro has intruded into the kimberlite pipe. The sill is approximately 400m below the surface and is some 75m thick. This means that there are approximately 52 million tons of gabbro within the confines

of the pipe. The gabbro cannot be mined economically due to its volume and the high cost of removing it.

When mining began at Premier in 1902, open cast mining techniques were used. Conventional sub level or open bench mining techniques remained in use until the discovery of the gabbro sill. Mining below the sill has posed many problems to the Premier mining engineers. The most significant of these is the admixing of the barren gabbro with the kimberlite below the sill. This is due to the poor geotechnical properties of the sill. The kimberlite is diluted due to significant volumes of gabbro collapsing onto the mining areas.

The limited kimberlite reserves above the sill dictates that most of the mine's future production must come from below the sill. As the above sill kimberlite reserves diminish the gabbro problem becomes proportionally more serious.

The gabbro problem manifests itself in the following ways:

1. Gabbro replaces valuable kimberlite in the treatment plants headfeed and therefore reduces its potential revenue generating capability.

2. Gabbro is subject to the full diamond liberation and recovery process- clearly a wasteful and expensive exercise.

3. Gabbro follows the diamond route through the treatment plant. This process route is designed to concentrate diamond into a very low mass, low volume and high value stream. Serious operational difficulties occur when this process route is overloaded by large quantities of gabbro.

A means of separating the gabbro from the kimberlite was therefore required: an automatic sorting technique capable of differentiating between kimberlite and gabbro on a rock by rock basis being the ultimate goal. Further, since the rocks are of a non uniform shape and size, and for practical reasons in the treatment of large volumes of rock, a non contact discrimination technique was required. No existing commmercial technology was found to be able to differentiate between gabbro and kimberlite.

De Beers personnel discovered a difference in microwave signal attenuation between gabbro and kimberlite by heating similar sized samples in a microwave oven. The samples were irradiated for equal periods of time. It was found that the kimberlite became hotter than the gabbro, indicating that kimberlite had absorbed or attenuated the microwave signal more than the gabbro. For this reason it was decided to consider the possibility of using microwave irradiation to distinguish between samples of gabbro and kimberlite.

4.1. MICROWAVE MEASUREMENTS

The sorting of samples of gabbro and kimberlite involves the separation of irregular shaped discrete samples. Considering the information presented in section 3.5.4. reflection measurements would seem to be unsuited to this application. Tests were performed using the circuit shown in figure 3.9. It was found that samples of gabbro and kimberlite exhibited negligible differences in return signal level.

Transmission measurements were performed on different rock samples using the square horn antennae presented in section 3.5.3. A broad frequency spectrum was examined to determine if any particular frequency displayed a marked difference in signal attentuation between the two rock types. Specially

cut, parallel sided samples of gabbro and kimberlite were used in these tests in order to minimise possible errors due to scattering or reflection of the signal. Care was taken to ensure that all the samples were of sufficient size to prevent the possibility of a direct signal path around the sample.

The antennae were connected as shown in figure 3.4. A specially fabricated rigid test frame was used to mount the antennae. This test frame is illustrated in figure 4.2.

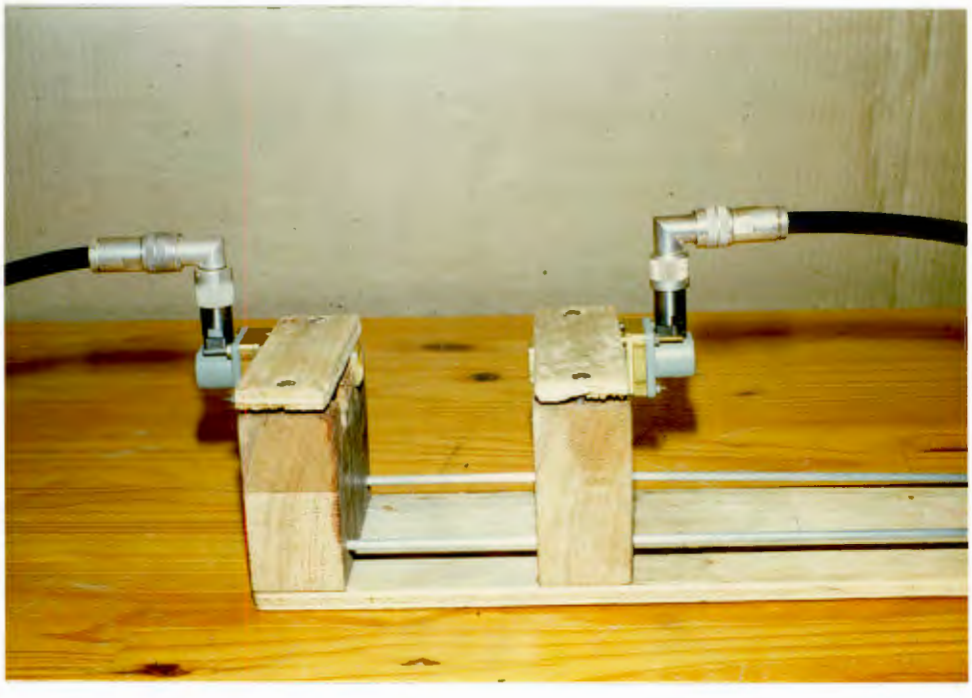

Figure 4.2. The test frame

The use of this test frame ensured accurate antennae alignment, thereby minimising the possibility of multipath reflections. Possible errors due to lateral antenna movement were prevented. The test frame had one fixed antenna and one antenna mounted on an adjustable platform. This allowed the antennae to be placed very close to the samples to reduce signal refraction around the samples.

A Hewlett Packard 8410C network analyser was used to investigate signal frequencies up to 16.4GHz. A Hewlett Packard 8746B S-parameter test set and an HP8350B sweep oscillator, capable of generating signals in the frequency range 10MHz to 26.5GHz, were coupled to the network analyser. Data capture was effected by means of an HP85 microcomputer interfaced to the network analyser via an HP59313A analogue to digital convertor. The S-parameter S_{21} was measured to determine the insertion loss due to the rock samples.

The frequency limitations of the network analyser dictated the use of a microwave power meter for signal frequencies above 16.4GHz. An HP435A power meter coupled to an HP8485A power sensor head were used for these tests. Calibration measurements were performed with no samples between the antennae. When samples were placed between the antennae, the received power level was recorded to determine the insertion loss due to the sample.

4.2. RESULTS

The S band antennae were coupled to the network analyser to perform insertion loss measurements over the frequency range from 2.6GHz to 3.9GHz. A detectable difference in signal attenuation through the two different rock types was observed - throughout the band. There was no detectable preferential attenuation at any frequency in this band. The average attenuation through these rock types, in dB/cm, at a frequency of 3GHz is shown in figure 4.3.

Rock Type	Average Attenuation in dB/cm
Kimberlite	2.01 dB\cm
Gabbro	.44 dB\cm

Figure 4.3. Average Attentuation at 3GHz.

The X band antennae were used for experimentation in the frequency range from 9GHz to 12GHz. Parallel sided 2cm thick samples of gabbro and kimberlite were used in these tests. The table displayed in figure 4.4 indicates the attenuation results at a frequency of 10GHz.

Rock Type	Average Attenuation in dB/cm
Kimberlite	2.17 dB\cm
Gabbro	.49 dB\cm

Figure 4.4. Average attenuation at 10GHz

The results shown in figure 4.4 indicate a trend of increasing attenuation with increasing frequency when compared with the results of figure 4.3. A small increase in the difference in attenuation between the different rocks is seen at the higher frequency. No single frequency in the X band range displayed a marked increase in the attentuation difference between the two rock types.

The curves presented in figure 4.5 are typical of those observed with the J band antennae over the frequency range from 12.4GHz to 16.4GHz. Two centimetre thick parallel sided rock samples were used in these tests. Repeated measurements again revealed no single frequency where a marked increase in the attenuation difference between gabbro and kimberlite could be observed.

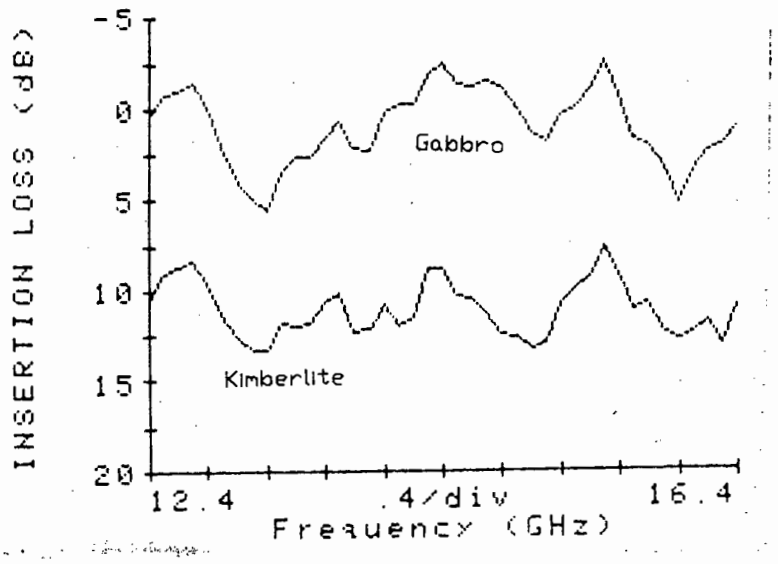

Figure 4.5. J Band insertion loss

Insertion gain can be seen for the gabbro curves in figures 4.5 and 4.6. This is observed due to the improved antenna matching promoted by the positioning of the low loss gabbro material between the closely spaced antennae.

The attenuation results for K band are presented in figure 4.6.

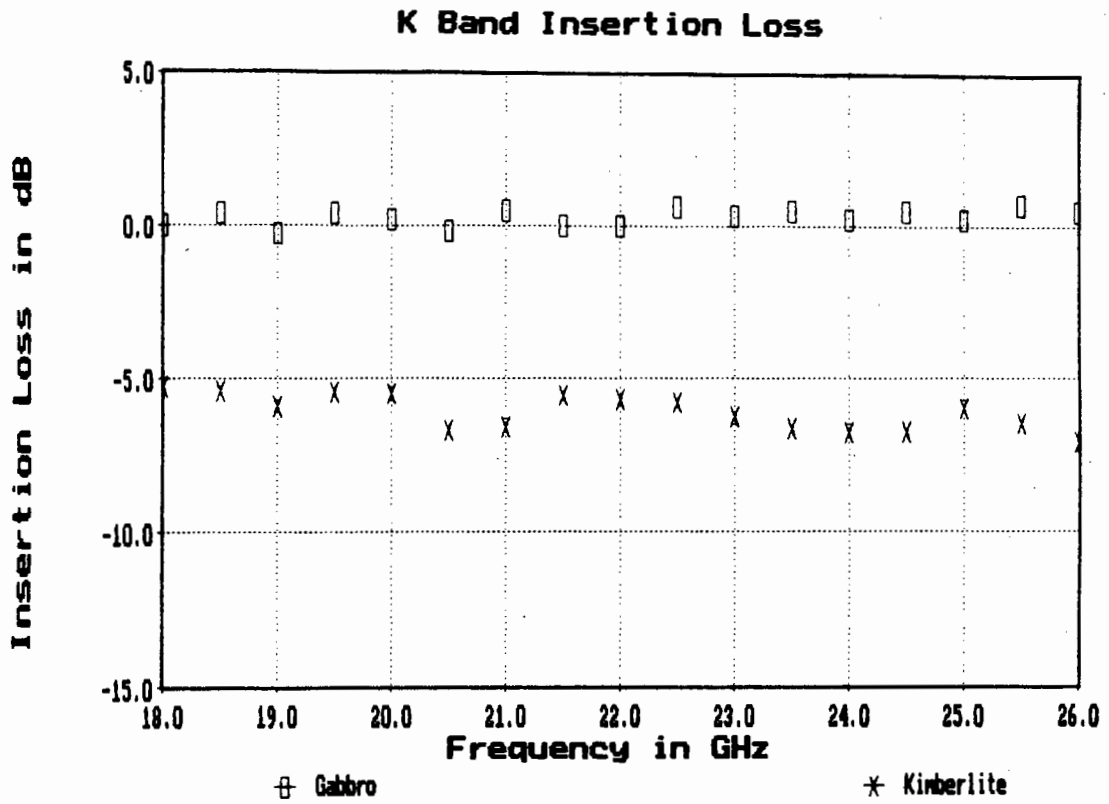

Figure 4.6. K band attenuation results

The overall attenuation through the gabbro and kimberlite samples has again increased with increasing frequency. A small increase in the attenuation difference between the rock types was observed with increasing frequency.

The effect of moisture content on insertion loss was examined in each frequency band. Samples of gabbro and kimberlite were measured when dry and after being immersed in water for 24 hours. The moisture content had negligible effect in these tests, possibly due to the small amount of water absorbed by the samples.

The effect of moisture content was most noticeable at 23GHz. At this frequency the difference in insertion loss between the rock types was altered by 1.7dB. It was therefore

concluded that the effect of moisture content was non critical provided frequencies with moisture absorption peaks (eg. 23GHz) were avoided.

4.2.1. Investigation of Kimberlite Composition

Kimberlite is composed of many different component minerals and is a generic term for a great variety of rocks. Piebald and grey kimberlite are two common kimberlite types found at Premier Mine [1]. Due to the heterogeneous composition of kimberlite, possible problems with dielectric anisotropy and anomaly were anticipated. These effects were discussed in section 2.3 and are well documented in the literature [2-10].

A study of signal attenuation using component minerals that had been separated from kimberlite was undertaken using different frequencies. The trend of increased attenuation with increasing frequency was observed. Samples were placed in a 1cm thick microwave transparent slide. Figure 4.7 shows the average attenuation through some of these component minerals at 10GHz.

Component Mineral	Average Attenuation in dB\cm
Chrome Diopside	1.55 dB\cm
Garnet	3.1 dB\cm
Ilmenite	8.47 dB\cm
tailings	5.35 dB\cm

Table 4.7. Attenuation through component minerals

It can be seen from table 4.7 that the component minerals have widely varying attenuative properties. These component minerals are present in different proportions in different samples of kimberlite. Despite it's structure, however, the various results in section 4.2. indicate that consistent attenuation values were obtained with kimberlite samples.

The observed effect of dielectric anisotropy with fifty smooth sided samples was negligible at all tested frequencies. From the above results it was concluded that, in this application where no absolute determination of a sample's dielectric constant is required, the possible effects of dielectric anisotropy and anomaly were not problematic.

4.3. DISCUSSION

The use of reflection measurements was not found to be viable for discriminating between discrete rock samples. Signal transmission between square horn antennae was

investigated over a broad frequency spectrum. A detectable difference in signal attenuation between gabbro and kimberlite was found over the investigated frequency band.

The heterogeneous composition of kimberlite was not found to be problematic in this application. No absolute measure of dielectric constant is required for rock discrimination. Due to the detectable differences in signal attenuation observed with gabbro and kimberlite it was not deemed necessary to complicate the system by incorporating signal phase measurements.

The construction of a high frequency microwave transmitter and receiver is justified in the light of the above results. The choice of operating frequency is influenced by ensuring that the antennae aperture is small enough to prevent direct signal transmission around the samples.

4.4. LIST OF REFERENCES

[1] "General information for visitors to Premier Mine", De Beers Consolidated Mines Limited, Premier Mine Division.

[2] PUGH, E.M., "Principles of Electricity and Magnetism", Addison-Wesley Publishing Co.Inc., 1970, p 147.

[3] JONES, D.S., "The Theory of Electromagnetism", Pergammon Press, 1964, pp 329.

[4] PARKHOMENKO, E.I., "Electrical Properties of Rocks", Plenum Press, New York, 1967, pp 48-51.

[5] SEN, P.N., "Dielectric anomaly in inhomogeneous materials with an application to sedimentary rocks", Appl. Phys. Lett., vol. 39, no 8, pp 667-668.

[6] SEN, P.N., CHEW, W.C., "The Frequency Dependent Dielectric and Conductivity Response of Sedimentary Rocks", Journal of Microwave Power, 1983, vol. 18, no 1, pp 95-105.

[7] WOBSCHALL, D., "A Theory of the Complex Dielectric Permittivity of Soil Containing Water; The Semidisperse Model", IEEE Transactions on Geoscience Electronics, vol. GE15, no 1, Jan 1977, pp 49-58.

[8] MENDELSON, K.S., COHEN, M.H., "The effect of grain anisotropy on the electrical properties of sedimentary rocks", Geophysics, vol. 47, no 2, Feb 1982, pp 257-263.

[9] SEN, P.N., "Relationship of certain geometrical features to the dielectric anomaly of rocks", Geophysics, vol. 46, no 12, Dec 1981, pp 1714-1720.

[10] BADZIOCH, S., CORNFORD, G.B., "Determination of moisture content of materials by electrical methods", The British Coal Utilisation Research Association, monthly bulletin, vol. 16, no 3, March 1952, pp 77-89.

CHAPTER 5

5.0 DESIGN OF MICROWAVE TRANSMITTER AND RECEIVER

The investigation of microwave signal attenuation between two antennae due to the presence of rock samples as described in section 4.2, revealed that there was a detectable difference in signal attenuation between the different rock types over a broad frequency range. It was therefore decided to construct a microwave transmitter and receiver for further laboratory testing of signal attenuation due to gabbro and kimberlite.

The transmitter and receiver had to be built in such a way that rock samples could be passed between the antennae. The transmitter and receiver were therefore housed in separate cabinets. A different version of the equipment was constructed with remote antenna housings for mounting above and below a conveyor belt.

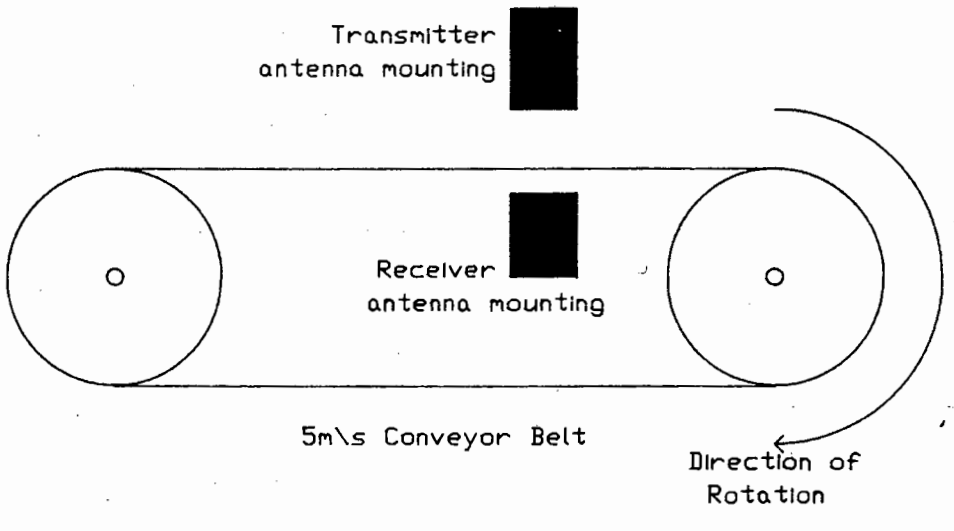

Figure 5.1 Remote Antennae Mountings

Figure 5.1 displays the mounting of the remote antenna units. This system was used to perform dynamic measurements

of signal attenuation due to rock samples. The remote antennae housings shown in figure 5.1 had to be moisture proof, dust proof and have negligible insertion loss at the chosen operating frequency. Sealed plastic containers were chosen to protect the antennae. The microwave signals passed virtually unaffected through these containers. Although the optimum container wall thickness for maximum signal transmission would be a radome of thickness $n^* \lambda/2$ where n=1,2,3 ..[1] this was not found necessary due to the low loss nature of the plastic containers.

The choice of operating frequency was influenced by a number of factors. The size of rocks to be examined relative to the antenna aperture area was an important factor to be considered. If a low operating frequency with larger antenna was chosen then the system would be limited to use with large rock samples. This is due to the fact that the smallest rock sample to be detected must completely cover the antenna aperture for the system to function correctly.

Microwave frequencies with resonant moisture absorption peaks [2] were to be avoided for the reasons mentioned in section 4.2. The attenuation difference between gabbro and kimberlite at the chosen operating frequency was also considered. It was decided to construct the transmitter and receiver so that different microwave sources and detectors could be driven from the same circuit. This allowed an examination of different operating frequencies without unnecessary circuit duplication.

A decision had to be made between continuous wave (cw) operation and pulsed mode operation. If the transmitter were used in cw mode then the receiver detector diode would function as a simple direct current (dc) rectifier. This would require dc amplification which is prone to dc offset and drift. The expected signal input at the receiver is in

the region of 10μV and 5mV and dc offsets or drift in this case could cause serious errors.

The solution to this problem is to use pulsed mode operation where pulses of microwave signal are transmitted. This is advantageous because the receiver can then be designed to avoid any dc amplification and thereby eliminate many of the possible errors involved with dc amplification. A pulsed transmitter with equal mark-space ratio was fabricated for this reason.

A decision had to be made between powering the transmitter and receiver from batteries or the mains supply. Mains operation was chosen due to the current requirements of the transmitter and to avoid the problem of battery maintenance. The pulsed operation of the transmitter may cause supply voltage spikes and variations. To prevent this from adversely affecting the operation of the receiver, separate power supplies were used for the transmitter and the receiver.

5.1 DESCRIPTION OF TRANSMITTER CIRCUITRY

A block diagram of the transmitter is shown in figure **5.2.**

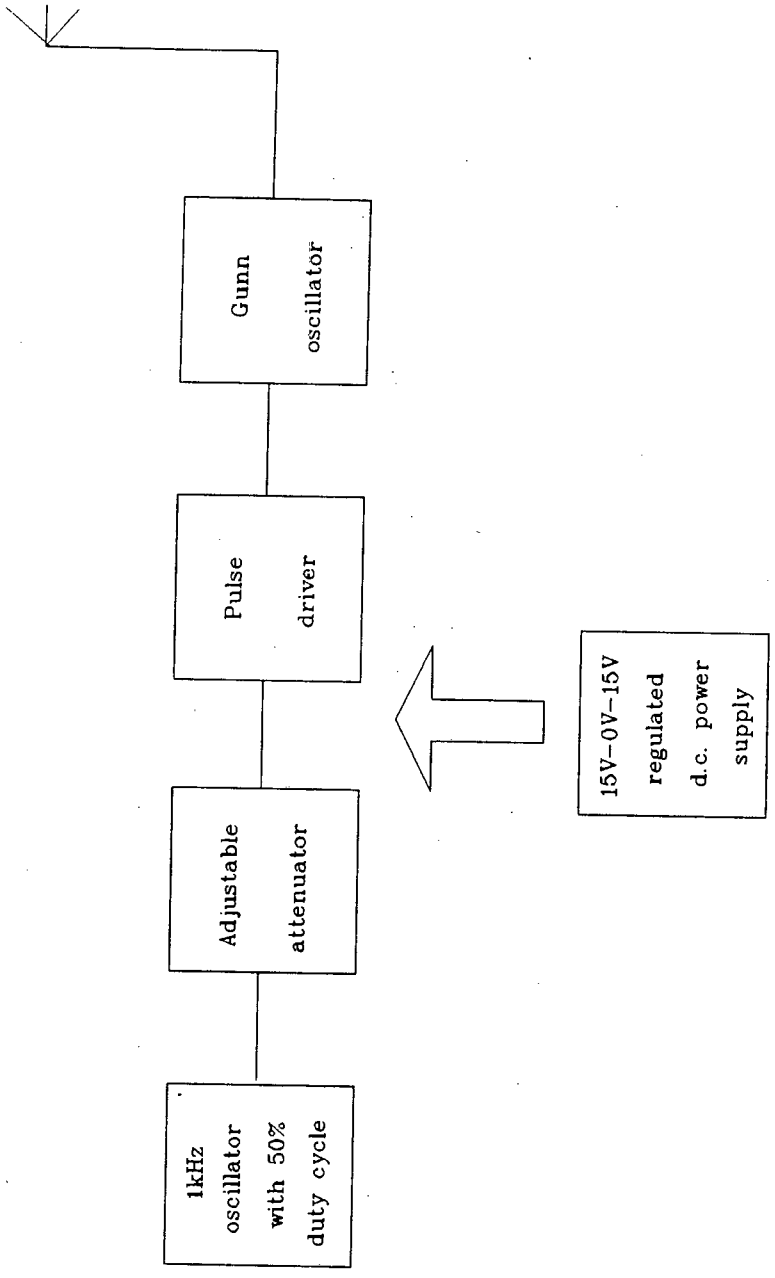

Figure 5.2 Block Diagram of Transmitter

It can be seen that the transmitter circuit consists of a 1kHz oscillator followed by an adjustable attenuator. This facilitates adjustment of the amplitude of the oscillator output voltage. The attenuator output is coupled to a current driving stage which in turn drives a Gunn oscillator. The circuit has been designed to provide a wide range of output voltages in order to be able to drive a variety of different Gunn oscillators.

A circuit diagram of the transmitter is shown in figure 5.3.

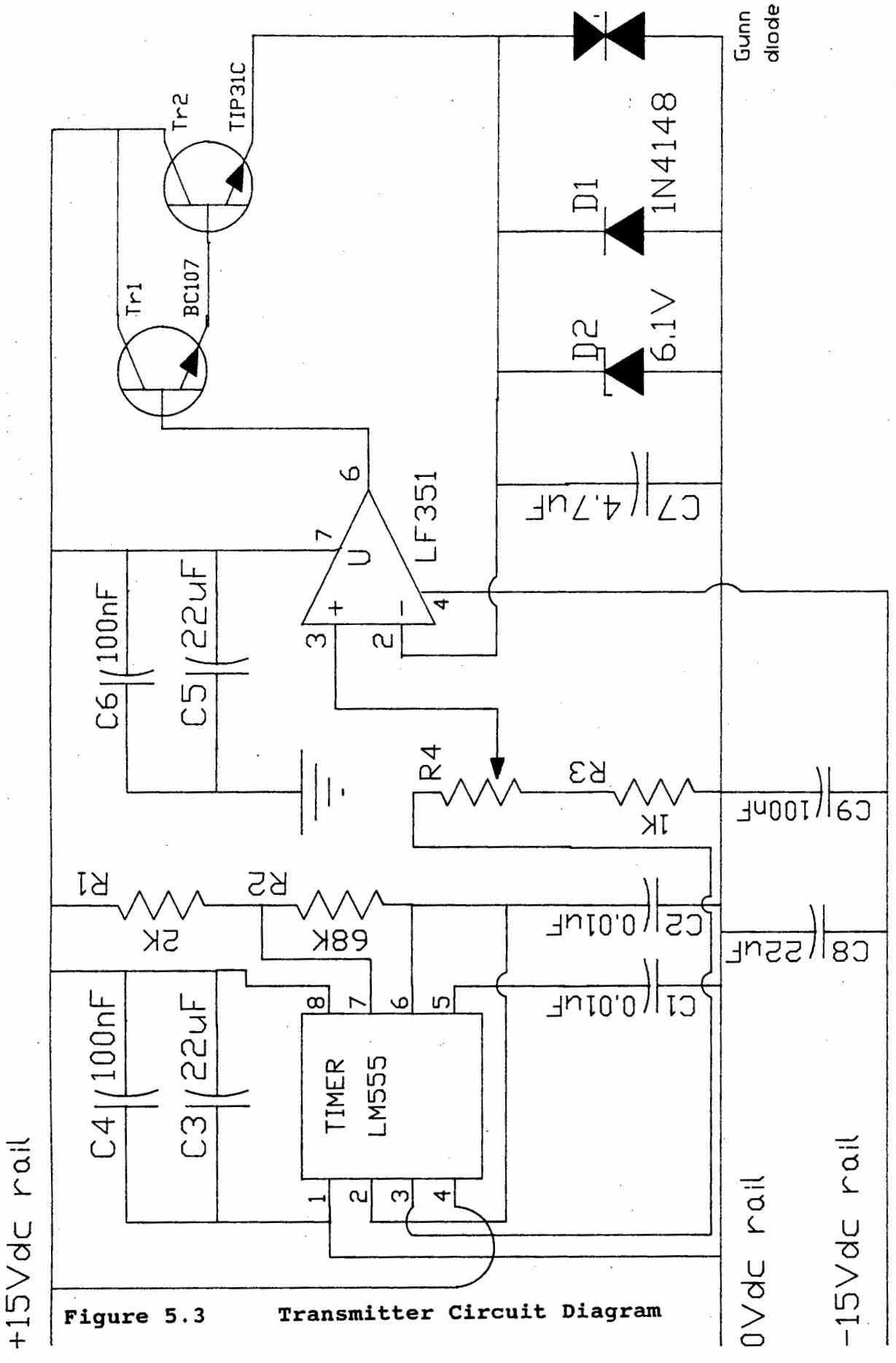

Figure 5.3 **Transmitter Circuit Diagram**

The heart of the transmitter circuit is a 1kHz square wave oscillator with a 50% duty cycle. This oscillator is realised using a LM555 timer chip. The resistors R1 and R2 and capacitors C1 and C2 were chosen to provide almost a 50% duty cycle and a 1kHz oscillation frequency as shown in figure 5.4.

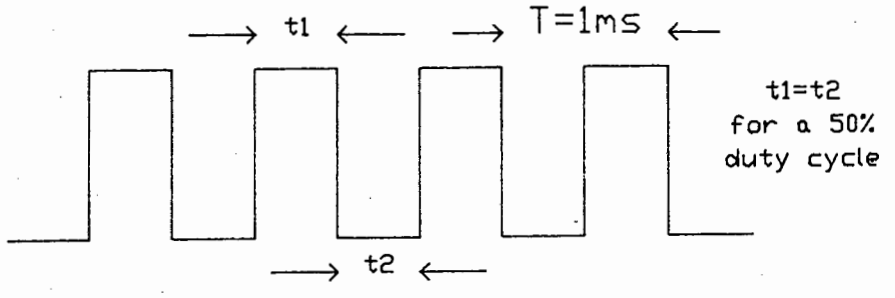

Figure 5.4 50% Duty Cycle 1kHz Square Wave

The choice of the 1kHz is non critical but should be low enough to avoid any high frequency limitations in the following stages of the circuit.

The duty cycle of 50% was deliberately chosen because this allows a smooth 1kHz sine wave (fundamental of the square wave) to be obtained in the receiver unit by means of bandpass filtering. The capacitors C3 and C4 are power supply decoupling capacitors. Capacitor C3 is included for supply smoothing while the smaller capacitance C4 will filter any sudden high frequency spikes that cannot be smoothed out by the larger and slower responding C3. Supply decoupling capacitors C5, C6, C8 and C9 were connected in pairs across the voltage supply rails as shown in figure 5.3.

The output of the LM555 oscillator is fed to an attenuator comprising of R4 and R3 to facilitate amplitude adjustment of the 1kHz square wave. Fine adjustments are made using resistor R4. The LM555 chip only has to deliver a few milliamps of current to the attenuator so that problems should not occur with the temperature stability of this component.

The square wave signal from the attenuator is fed into the non-inverting input of the LF351 operational amplifier. This op.amp is configured as a non-inverting follower whose output is used to drive the base of Tr1, a BC107 small signal transistor. The transistors Tr2, a TIP31C power transistor, and Tr1 are connected in a Darlington configuration to form a high gain output module capable of delivering an output current in excess of 1 ampere. The inverting input of the op. amp is connected to the emitter of Tr2. This negative feedback configuration improves the switching speed of the circuit.

The operational amplifier Tr1 and Tr2 form the pulse driver stage of the circuit. Output currents of up to 1 ampere may be required to drive a Gunn oscillator. The output of the operational amplifier can only supply a few milliamperes of output current. This is insufficient to drive the base of Tr2 directly hence the Darlington transistor configuration is used. The operational amplifier can easily drive Tr1 which in turn can drive Tr2.

In this way a variable voltage 1kHz oscillator is formed with the ability to deliver a high output current. The TIP31C was well heatsinked and can continuously deliver up to 3 amperes of current. Test loads drawing a current of one ampere were connected to the circuit for up to 24 hours to test it for long term output voltage stability. No output voltage droop was detectable after a 24 hour period.

The Gunn oscillator is connected between the emitter of Tr2 and the ground rail as shown in figure 5.3. Capacitor C7 is connected across the Gunn oscillator terminals to improve the stability of the circuit. The zener diode D2 is connected across the Gunn oscillator terminals to protect it from the possibility of becoming reverse biased when the voltage supply is switched off.

The rise time of the pulses applied to the Gunn oscillator is an important factor related to the frequency stability of the oscillator. The pulse rise time should be as short as possible to reduce the frequency drift of the oscillator. In this application, however, absolute frequency stability is not required. The amplitude of the received signal will be more important than its frequency.

The transmitter circuit in figure 5.3, with the exception of the Gunn oscillator, was mounted on a printed circuit board designed to accommodate it. A copy of the printed circuit board foil pattern is given in Appendix C.

5.1.1. The Gunn Oscillator

The Gunn oscillators used in this transmitter are commercially manufactured varactor tunable units. The X band Gunn oscillator required a 10Vdc supply and the 35GHz unit required a 6Vdc supply. The attenuator shown in figure 5.3 was adjusted to suit the oscillator used. The Gunn sources were connected to square waveguide antennae as shown in figure 5.5.

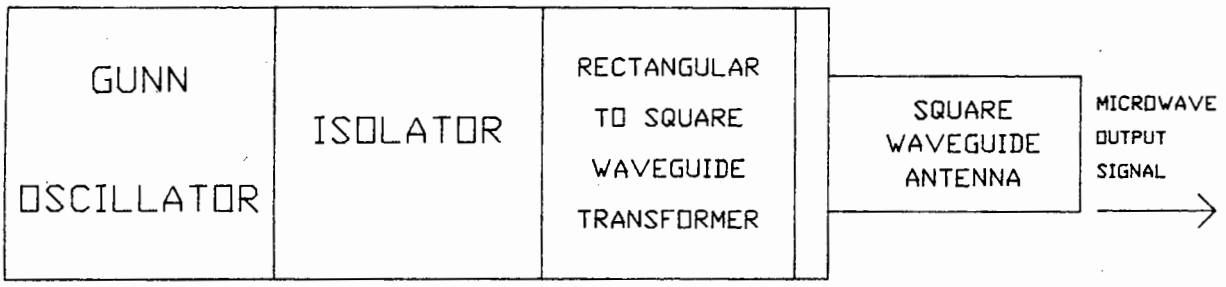

Figure 5.5 Connection of Gunn oscillator to Antennae

An isolator was connected to the source to prevent any possible impedance mismatch due to the presence of a rock sample from reducing the output power or even causing the Gunn oscillator to switch off and stop oscillating. The design details for the square antennae and the rectangular to square waveguide transformers are given in Appendix B.

5.2. DESCRIPTION OF RECEIVER CIRCUITRY

A block diagram of the receiver circuit is given in figure 5.6.

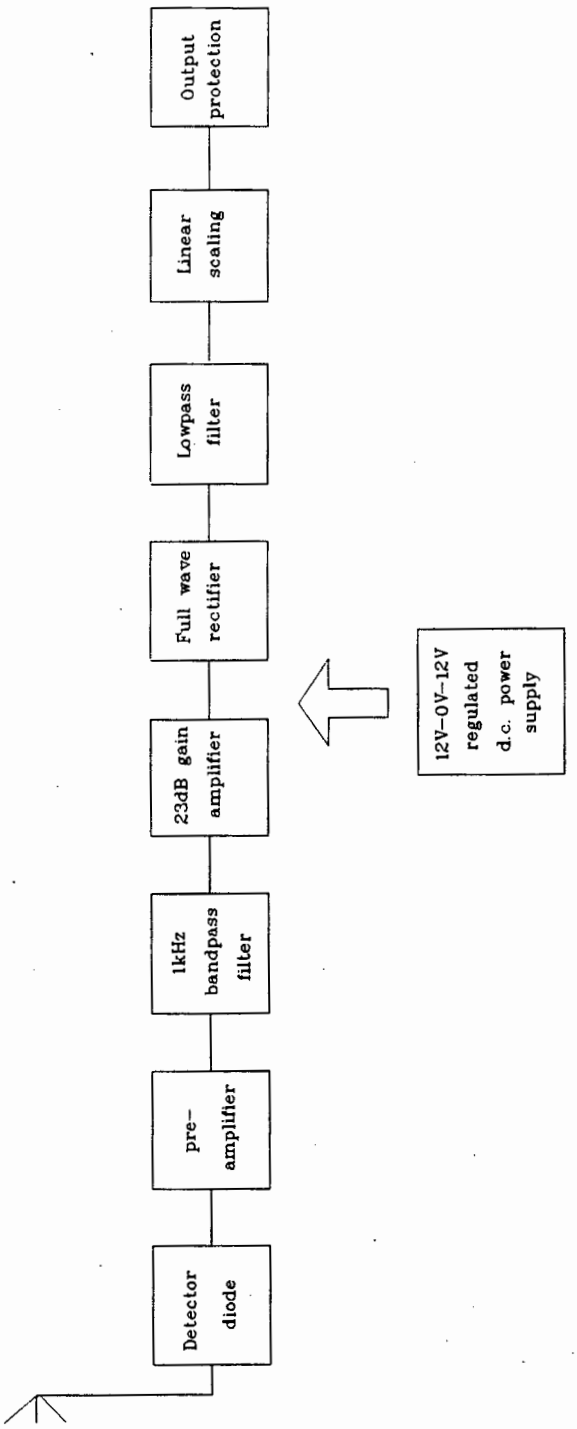

Figure 5.6 Receiver Block Diagram

The microwave detector diode was mounted as shown in figure 5.7. The microwave input signal is received via the square waveguide antennae. The antennae is connected to a rectangular to square waveguide antenna. This in turn is coupled to the detector diode in its rectangular waveguide mounting. The construction of the antennae and rectangular to square waveguide antennae was discussed in Chapter 3.

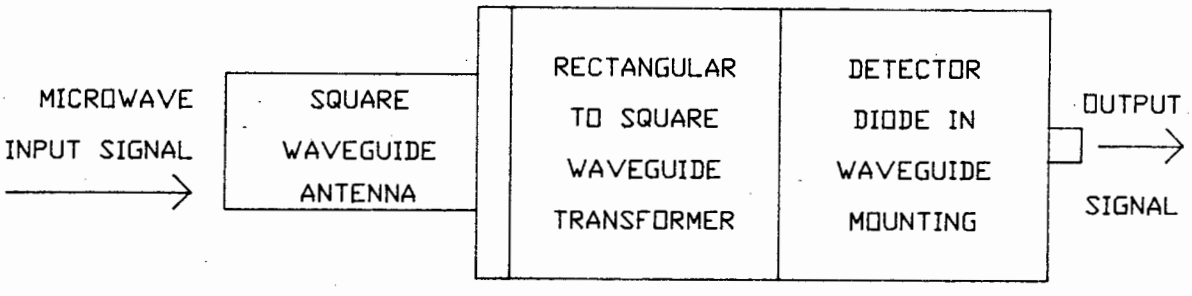

Figure 5.7 Detector Diode Mounting

The receiver was designed so that detector diodes of different frequencies, with their respective antennae, can be used interchangeably in the circuit. It can be seen from the block diagram of figure 5.6 that the output from the detector diode is first amplified before being bandpass filtered. The detector diode output is a square wave when the transmitter of section 5.1 is used. The square wave's amplitude is less than 10mV and undergoes 40dB of amplification by means of the preamplifier.

The bandpass filter centred at 1kHz extracts the 1kHz sinewave fundamental from the squarewave. The sinewave is then further amplified and rectified using a full wave rectifier. A low pass filter is used to produce a dc level from the rectifier output. This dc signal is then scaled to vary within the range 0-5Vdc. This output can be connected to a personal computer via an analogue to digital convertor

card to effect data capture. The unit is equipped with output protection to prevent any possible damage to the A/D convertor in the event of equipment failure.

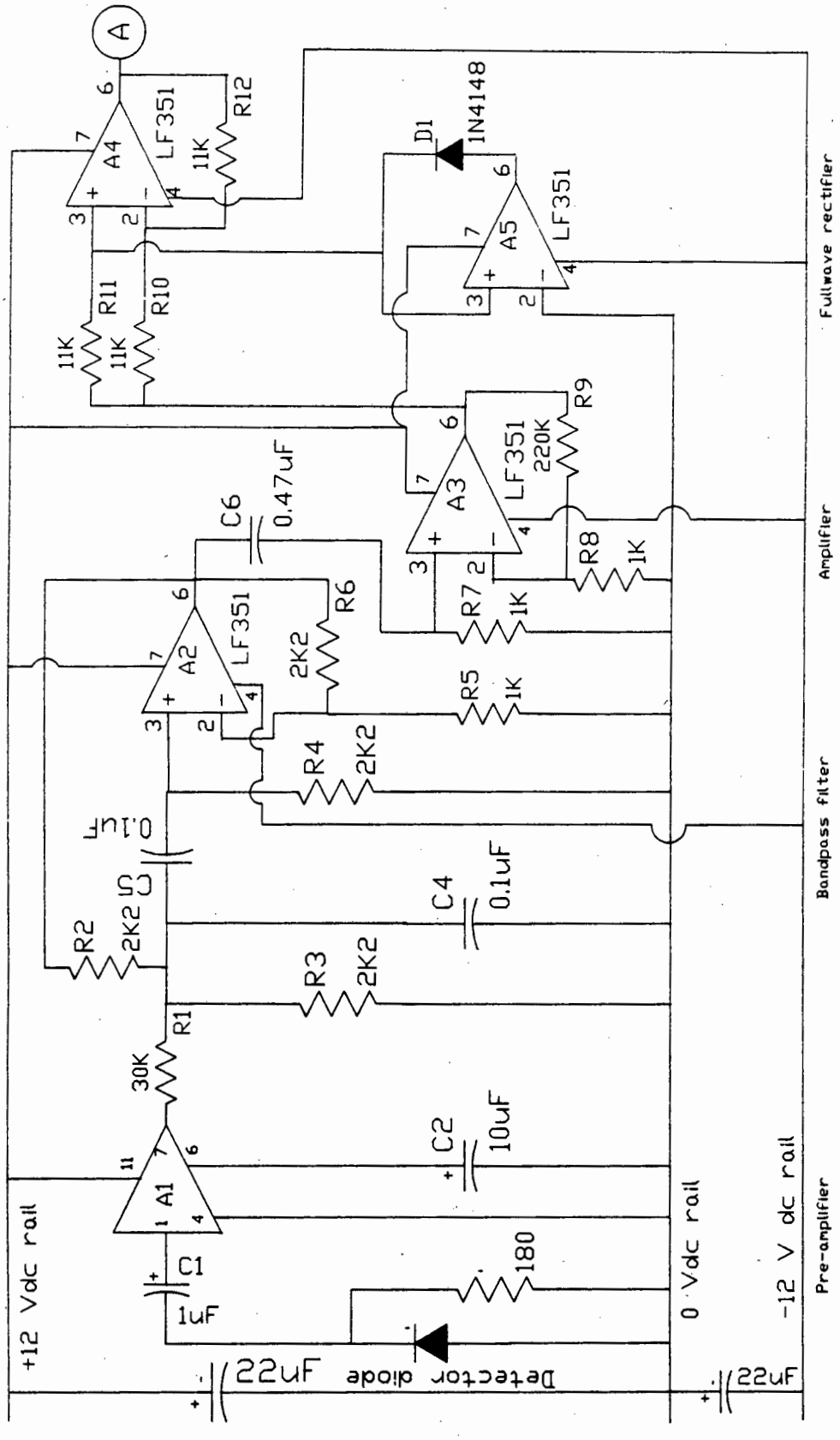

Figure 5.8 Receiver Circuit (a)

The receiver circuit diagram up to the full wave rectifier is shown in figure 5.8. The remainder of the circuit is shown in figure 5.9. From figure 5.8 it can be seen that the detector diode is ac coupled to amplifier A1 via capacitor C1. Amplifier A1 is a LM382 low noise preamplifier configured to provide a fixed voltage gain of 40dB. The connection of capacitor C2 between pin 6 and ground presets this voltage gain. A high quality tantalum capacitor was used here to try to improve the long term gain stability.

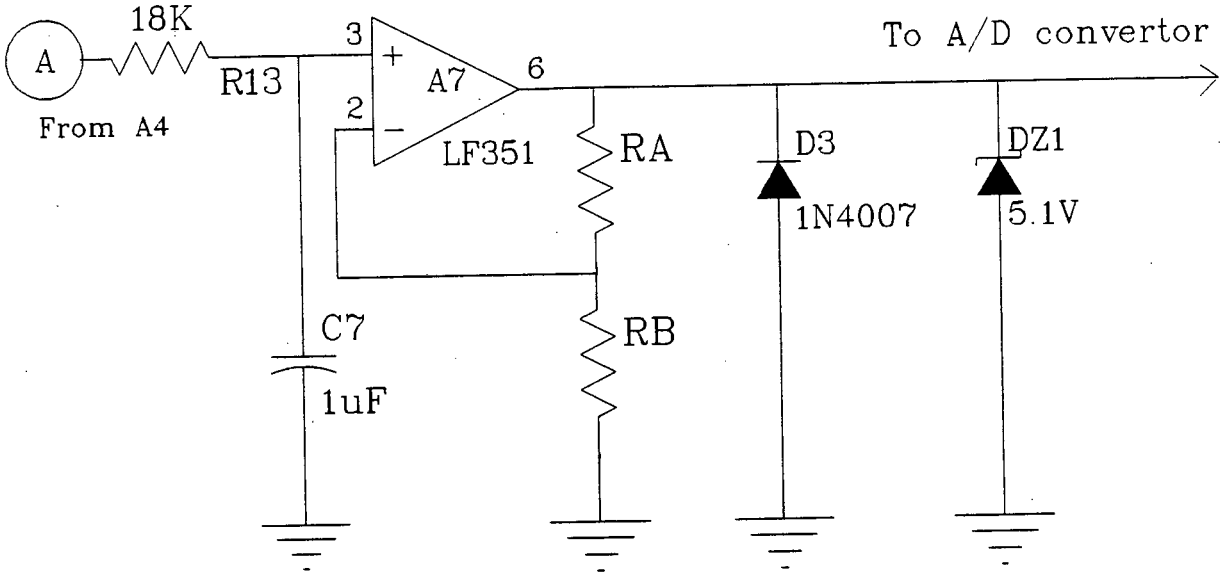

Figure 5.9 Receiver Circuit (b)

The LM382 chip was chosen for its good noise performance. A single supply rail is used for this chip so its output has a large dc offset (approximately 6Vdc) to ensure that there is sufficient signal voltage swing. This dc offset is removed by the next stage in the circuit, the bandpass filter.

The components R1, R2, R3, R4, R6, C4, C5 and A2 form the bandpass filter. This unit gain filter was designed to have a centre frequency of 1kHz and a bandwidth of 200Hz. The design procedure is given below.

$Q_p = f_o/B = 5.1$ and $w_p = 2\pi f_o = 6408.8$ radians/second
where $f_o = 1kHz$
so $w_p/Q_p = 1256.6$

The required transfer function is therefore

$$T(s) = 1256.6s \; / \; [s^2 + 1256.6s + 4.1 \times 10^7]$$

Now let C4 = C5 = 1F and
let R1 = R2 = R4 = $\sqrt{2}/w_p = 2.21 \times 10^{-4}$ Ω
R6/R5 = $3 - \sqrt{2}/w_p = 2.723$

These values are then scaled in amplitude by a factor of 10^7 to give:
C4 = C5 = 0.1μF and
R1 = R2 = R4 = 2210Ω
Let R5 = 1kΩ then R6 = 2723Ω
The gain factor K = $w_p(2\sqrt{2}-1/Q_p) = 16870.2$
but K must be = $w_p/Q_p = 1256.6$
so the attenuator comprised of R1 and R3 is used to arrange this R3/R1 = 0.0745.
so R1 = 29664Ω
and R5 = 2388Ω

The closest manufactured values were used in the circuit shown in figure 5.8. This design process is well covered by Daryanani [3].

The bandpass filter was tested separately and the measured parameters are given in figure 5.10.

Filter Parameters	Frequency in Hz
Centre Frequency	962 Hz
Half Power Frequency (1)	847 Hz
Half Power Frequency (2)	1111 Hz

Figure 5.10 Measured Filter Parameters

The difference between the measured and theoretical values is due to the use of closest value components. Capacitor C6 is used to ac couple the bandpass filter to the next stage of amplification.

Amplifier A3 is configured as a non inverting amplifier. Resistor R7 provides a dc bias path for this ac coupled stage. The resistor ratio R8 + R9/R8 determines the gain of this stage. The circuit is shown with a gain of 46dB.

An active clamp is used to switch an "optional inverter" op amp configuration to achieve full wave rectification. Precision 2% tolerance resistors were used in this stage to ensure accurate signal rectification. Diode D1 and op. amp. A5 form the active clamp which switches the polarity of A4. This active rectifier circuit should not introduce any errors due to diode voltage drops. The simple low pass filter formed by R13 and C7 is used to filter the full wave rectified signal. The time constant of this circuit is 0.018 seconds.

The linear scaling circuit centres around op.amp. A7. The variable resistors RA and RB were adjusted to limit the signal output level to the range 0-5Vdc. The output of A7 was then connected to an A/D convertor to provide data to a personal computer. Overvoltage protection is provided by zener diode DZ1 which clamps the output level to prevent possible damage to the data capture unit. Diode D3 was used to prevent the possibility of a negative output voltage. A copy of the receiver printed circuit board foil layout is included in Appendix C.

5.3. DESCRIPTION OF POWER SUPPLIES

The transmitter power supply circuit is shown in figure 5.11. The receiver power supply circuit is given in figure 5.12.

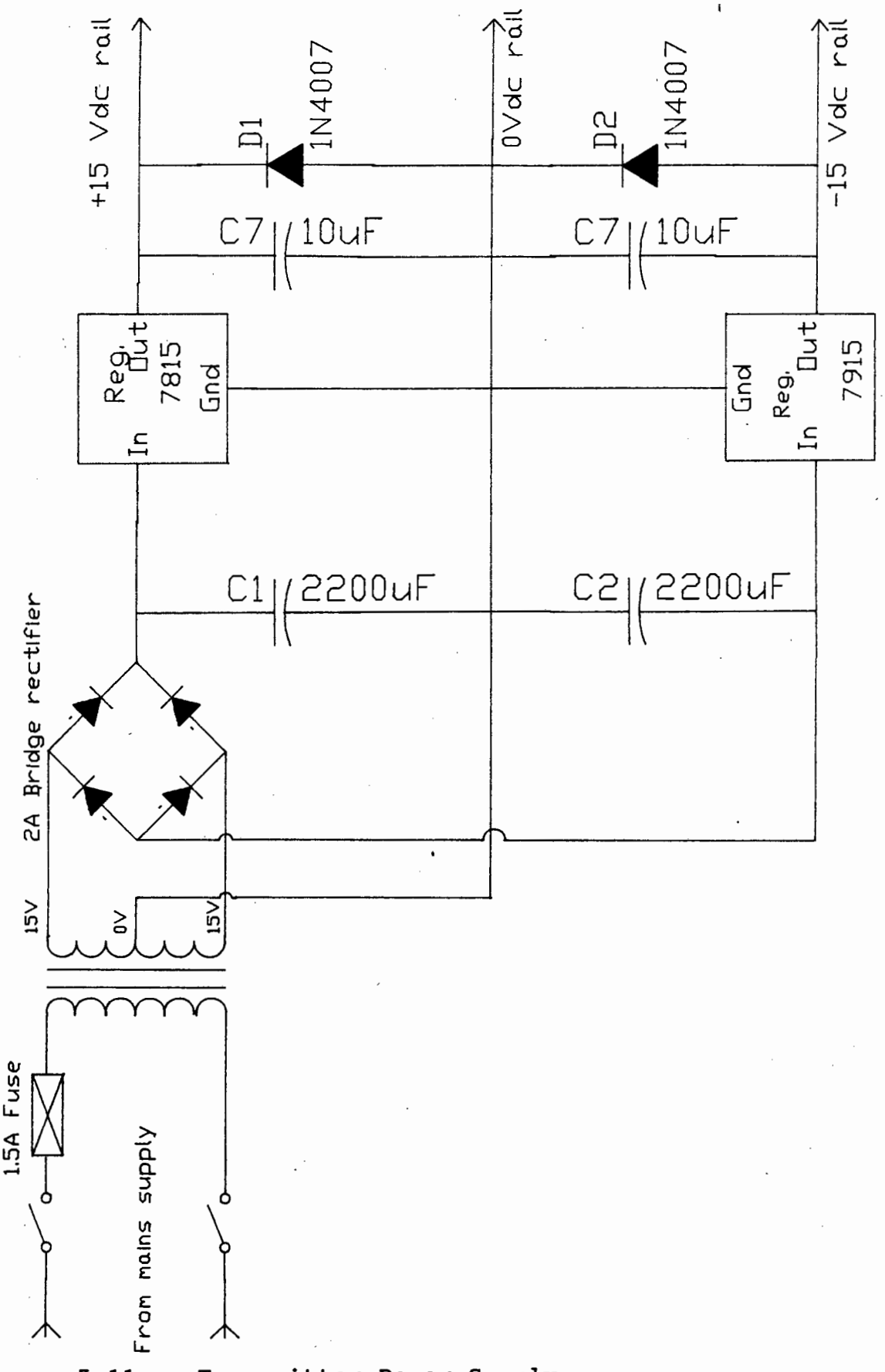

Figure 5.11 Transmitter Power Supply

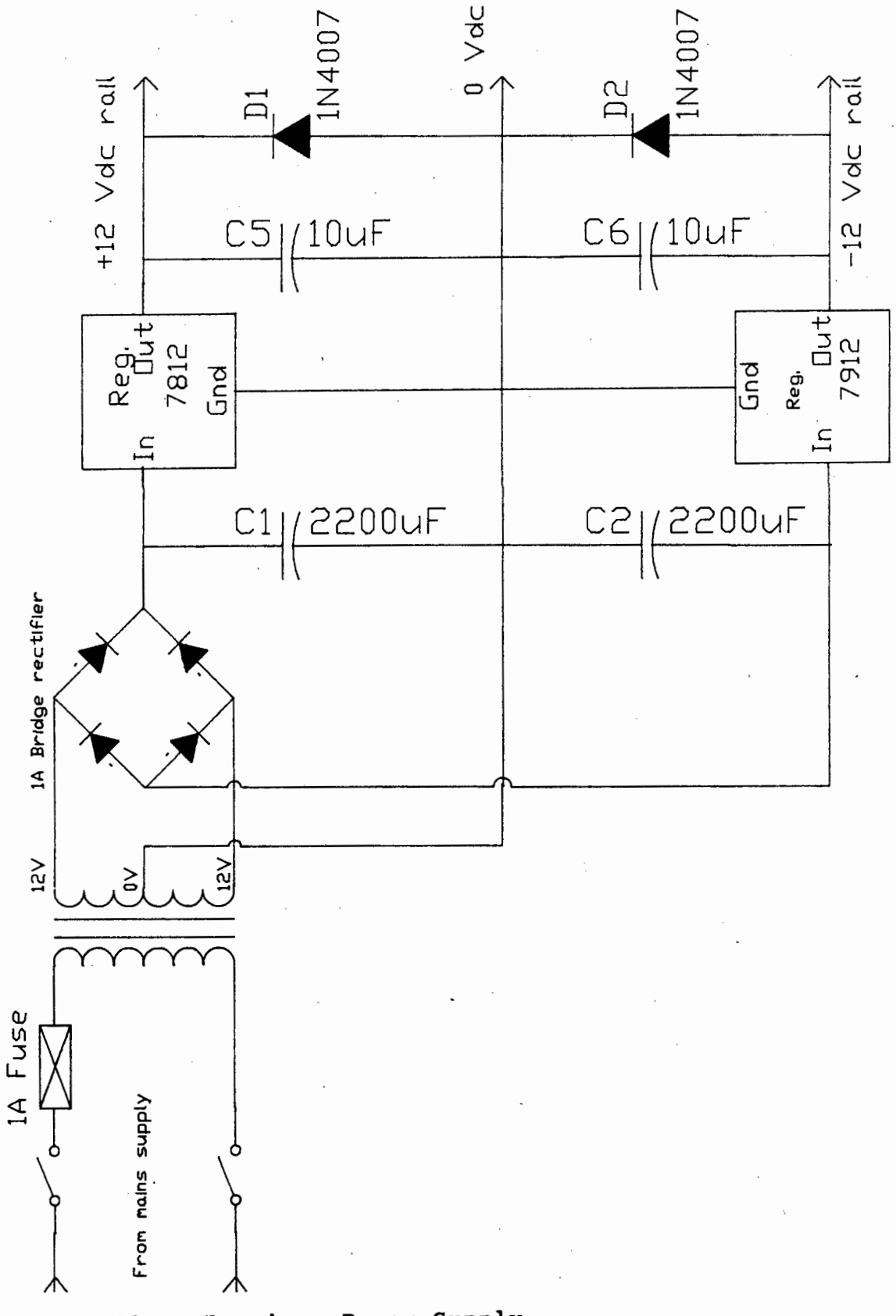

Figure 5.12 Receiver Power Supply

In each case a mains switch is used to switch the mains supply live and neutral wires which are connected across the primary windings of the mains stepdown transformers. The transformers primary windings are protected against current overload by means of a series connected 1A fuse.

The centre taps on the primary windings are grounded. The transformer in figure 5.11 has an 15V, 0V, 15V secondary winding rated at 1.5 amperes. The transformer in the receiver power supply has a 12V, 0V, 12V secondary winding rated at 1.5A. In each case the transformer's outputs are connected to a bridge rectifier with conservatively rated current handling capabilities.

The positive and negative outputs of the bridge rectifiers are connected to 2200μF smoothing capacitors rated at 40V each.

The capacitively smoothed rectifier outputs are then fed into voltage regulators. A 7815 positive voltage regulator and a 7915 negative voltage regulator are used in the transmitter power supply. The receiver power supply employs a 7812 positive voltage regulator and a 7912 negative voltage regulator. These voltage regulators can provide output currents of up to 1.5A each and are adequately heatsinked to improve thermal dissipation.

The diodes connected between ground and the output of each voltage regulator provide output short circuit protection for the power supplies. The components for these power supplies, with the exception of the transformer, fuse and switch, are all mounted on a specially designed printed circuit board. A copy of the printed circuit board foil pattern is given in Appendix C.

5.4. LIST OF REFERENCES

[1] HARVEY, A.F., "Microwave Engineering", Academic Press Inc.(London)Ltd, 1963, p 670.

[2] HARVEY, A.F., "Microwave Engineering", Academic Press Inc.(London)Ltd, 1963, p 1075.

[3] DARYANANI, Gobind., "Principles of Active Networks Synthesis and Design", John Wiley and Sons, New York, 1976, p 287.

CHAPTER 6

6.0 TEST RESULTS

The microwave transmitter and receiver described in Chapter 5 were fabricated, and extensive tests were performed with these production prototypes.

6.1. STATIC TESTS

Microwave components for operation at 10GHz and 35GHz were used with the circuitry described in Chapter 5. Static signal attenuation due to rock samples was measured directly in decibels (dB) by means of Rotary Vane Attenuators. These were connected as shown in figure 6.1.

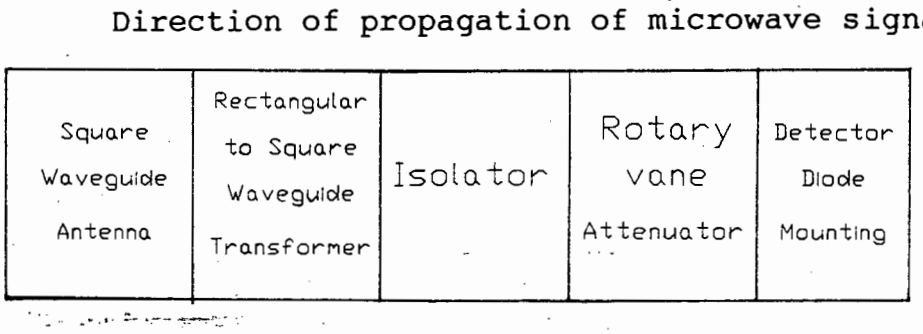

Figure 6.1. Use of Rotary Vane Attenuator

The isolator shown in figure 6.1 was used to eliminate the effect of possible detector impedance mismatching. The attenuator was set to 0dB insertion loss and the detector diode output was observed on an oscilloscope. A rock sample was then placed between the transmitting and receiving antennae. The new detector diode output level was observed using the oscilloscope and the rock sample was subsequently removed. The rotary vane attenuator was used to reduce the signal level to that noted when the rock sample was in place between the antennae. The attenuation due to the rock sample was then read off of the attenuator directly in dB.

The test results obtained at 10GHz were virtually identical to those shown in figure 4.4. It was therefore concluded that the 10GHz equipment was functioning correctly. The 35GHz units performed well, as shown in figure 6.2. These units, with their reduced antenna aperture area, are useful for differentiating between small rocks.

Rock Type	Average Attenuation in dB\cm
Kimberlite	9.33 dB\cm
Gabbro	2.38 dB\cm

Figure 6.2. 35GHz Attenuation Results

It was shown in equation 2.19 that the attenuation constant for a medium is dependent on the dielectric properties and the conductivity of that medium - two different dielectric media such as gabbro and kimberlite would be expected to demonstrate different amounts of signal attenuation at a particular frequency.

It can be seen from figure 6.2 that there is a detectable difference in signal attenuation between gabbro and kimberlite at 35GHz. A small laboratory system was constructed for dynamic testing using an operating frequency of 35GHz.

A 60GHz Gunn oscillator was made available for experimentation. The use of such a high frequency system has the advantage of very small antenna aperture, allowing the detection of very small rock samples. Signal attenuation, however, increases with increasing frequency as

shown by equation 2.19. The overall signal attentuation at 60GHz was found to be too high to effect reliable rock differentiation with the samples used for the 35GHz tests. The 60GHz operating frequency would only be useful for work with very small rock samples.

6.1.1. Signal Differentiation and Multiple Reflections

Some irregularities were observed with microwave signal attenuation through samples of gabbro. Flat, parallel sided samples of gabbro, placed perpendicularly between the antennae exhibited low signal attenuation. The attenuation due to the gabbro appeared to vary as the orientation of the sample was changed. It was found that the signal attenuation due to randomly shaped gabbro samples was also orientation dependent. This meant that if the sample of gabbro had a particular orientation between the antennae then it appeared to exhibit high signal attenuation and could be incorrectly detected as the highly attenuative kimberlite.

A number of possible mechanisms were explored to determine the cause of the observed phenomenon. Signal reflection from the rock surface was shown to be similar for gabbro and kimberlite in section. Neither rock type exhibited any large differences in reflected signal level with varying sample orientation. It was therefore concluded that excessive signal reflection from the rock surface was not causing the observed phenomenon.

Signal diffraction through samples of gabbro was considered as a possible cause for the apparent position dependent attenuation through gabbro. The

occurrence of microwave signal diffraction through samples was demonstrated as shown in figure 6.3.

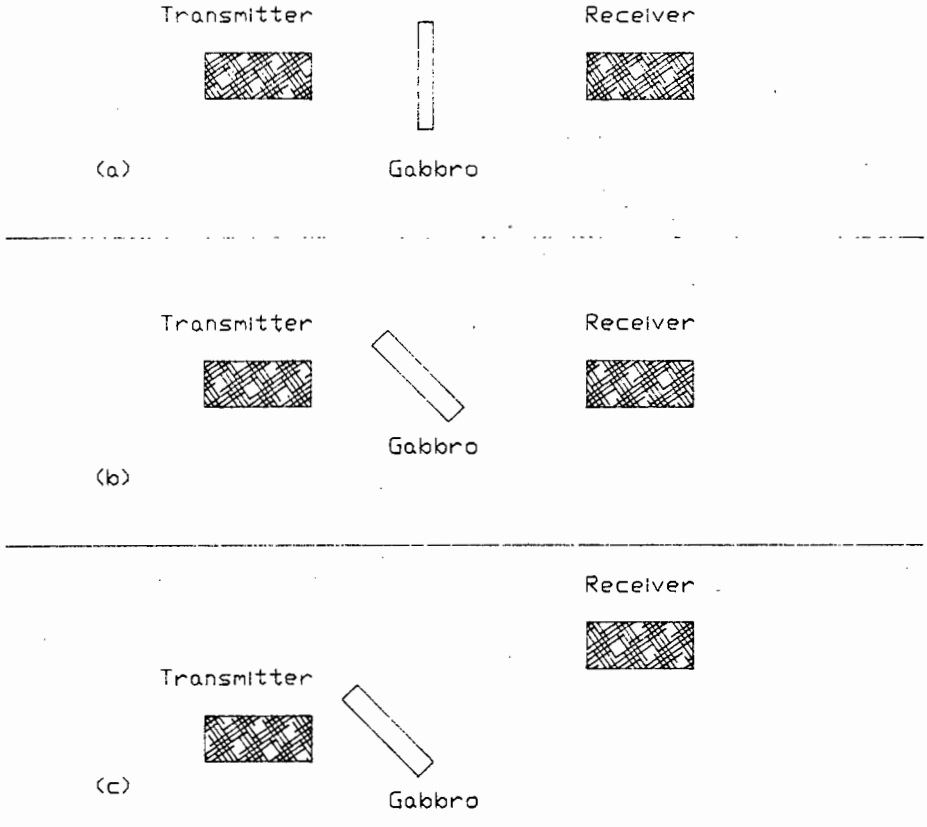

Figure 6.3. Signal Diffraction through Gabbro

Low signal attenuation was recorded when a flat sided gabbro sample was placed perpendicular to the antennae as shown in figure 6.3a. The signal attenuation appeared to have increased when the sample was re-orientated as shown in figure 6.3b. When the receiver antenna was repositioned as shown in figure 6.3c the original received signal level was again observed. The rock was large enough to prevent any direct signal transmission between the antennae. This experiment indicated that signal diffraction had occurred through the gabbro sample.

Randomly shaped gabbro samples were examined with the antennae aligned as shown in figure 6.3c. The results of this experimentation varied widely. Rocks that had faces close to flat improved the received signal level. Some samples, however, demonstrated up to 26dB variation in received signal level due to orientation dependent signal scattering.

The received signal level was reduced by some samples, regardless of their orientation. These were the most irregular shaped samples of gabbro. This indicated that the microwave signal had been scattered by these rocks. The samples were chemically analysed to ensure that they had the same composition as other gabbro samples. With the correct antenna alignment shown in figure 6.3a it was found that the level of signal attenuation was highest for rocks whose shapes were the most irregular.

Multiple signal reflections between the samples of gabbro and the antennae, resulting in standing waves, were also observed. Impedance discontinuities due to poorly matched detectors or antennae can give rise to standing waves. This resulted in a signal level which varied cyclicly with antenna spacing. The effect of a poorly matched detector (VSWR about 4 to 1)can be eliminated by means of an isolator as shown in figure 6.4. The isolator acts as a well matched load. A standing wave exists between the isolator and the detector due to the impedance discontinuity between them. The isolator prevents reflected signals from point B in figure 6.4 from reaching point A by absorbing the reflected signal.

The use of isolator at the transmitter and receiver eliminates the effect of standing waves between the antennae thus the cyclic signal amplified with antennae

was removed. The impedance mismatch at the antenna/air interface could still establish a standing wave between the antennae but careful antenna design eliminated this effect.

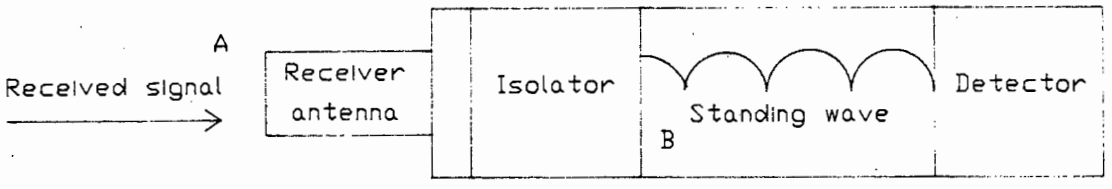

Figure 6.4. Effect of an Isolator

The microwave antennae were initially housed in metal containers. The possible problem of signal reflections from the metal sidewalls was removed by fixing microwave absorbent foam to the appropriate surfaces.

When a low loss dielectric material such as gabbro was placed between closely spaced antennae then standing waves were established between the transmit antennae and the material sample. This is shown in figure 6.5.

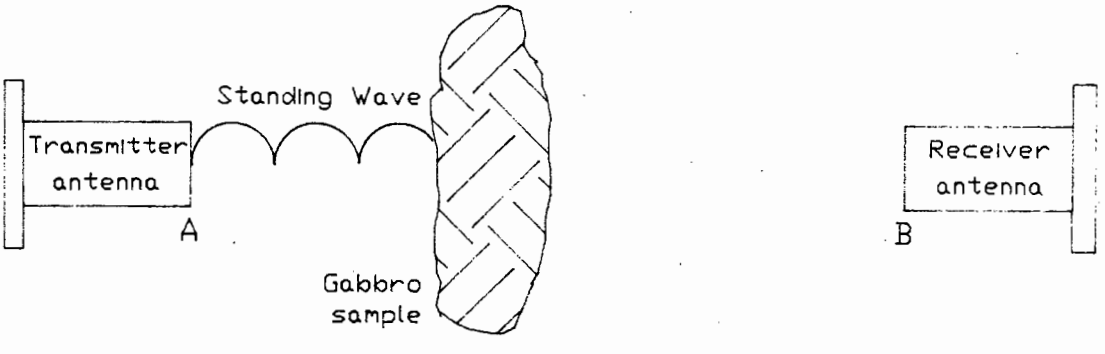

Figure 6.5. Standing Waves due to Sample

These standing waves were observed as periodic variations in the received signal amplitude as the position of the gabbro sample was varied from point A to point B between the antennae. The standing waves occurred as a result of addition or cancellation of reflected signals from the different surfaces of the rock. The abovementioned problems were discovered by experimentation with static samples. The importance of these effects could only be gauged by means of dynamic experimentation.

6.1.2. Attenuation due to Conveyor Belt Samples

Conveyor belt samples were tested for use with the system shown in figure 5.1. Eighty-one different belt types were examined. These were manufactured from various rubber and plastic compounds and had widely varying dielectric properties.

The conveyor belt should exhibit the lowest possible attenuation to prevent it from adversely affecting the system performance. Some conveyor belts are steel reinforced and could not be used as the microwave signal could not pass through the conductive steel layer. The conveyor belt thickness was also considered. The ideal belt thickness is a radome thickness of $n*\lambda/2$ where n is an integer [1]. This would allow maximum signal transmission through the belt. Conveyor belt thicknesses of $(2n+1)/4$ should be avoided as these allow minimum signal transmission through the belt.

The attenuation through the conveyor belt samples varied widely from 0.22dB to 15dB at 35GHz. A conveyor belt with approximately 2dB insertion loss was chosen for use with the laboratory system. Although the

conveyor belt loss is constant and was calibrated out of the system it could adversely effect the system dynamic range if the insertion loss were too high.

6.2. DYNAMIC RESULTS

An experimental laboratory scale conveyor belt system was provided by De Beers Diamond Research Laboratories. This conveyor belt was capable of transporting rocks at a speed of 5 m/s, this is the belt velocity commonly used in high throughput automatic sorting machines. The antenna configuration of figure 5.1 was used for the laboratory machine. The low loss conveyor belt was channelised to ensure that the rock samples passed directly between the antennae as shown in figure 6.6.

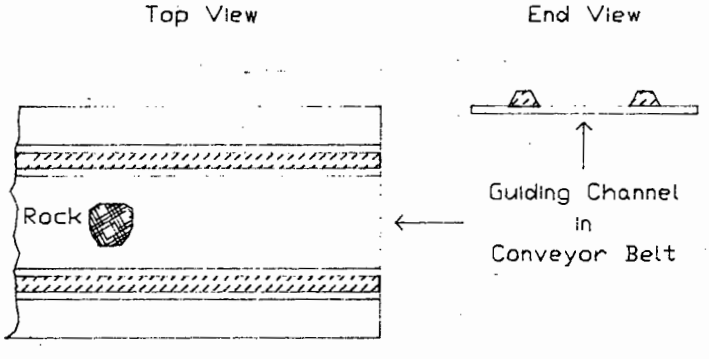

Figure 6.6. Channelised Conveyor Belt

The pre-production model microwave receiver was linked to a personal computer via an A/D convertor with a 0-5Vdc input. Using this equipment, the received signal level was recorded as the rocks were passed between the antennae. Repeated attenuation measurements were performed with many different samples of gabbro and kimberlite. This work was performed in conjunction with De Beers personnel at De Beers Diamond Research Laboratories.

The data displayed in figure 6.7 indicates the frequency distribution of received signal level through samples of gabbro and kimberlite. The percentage of each rock type producing a particular receiver voltage is shown. This data was obtained from 5640 tests on the rock samples.

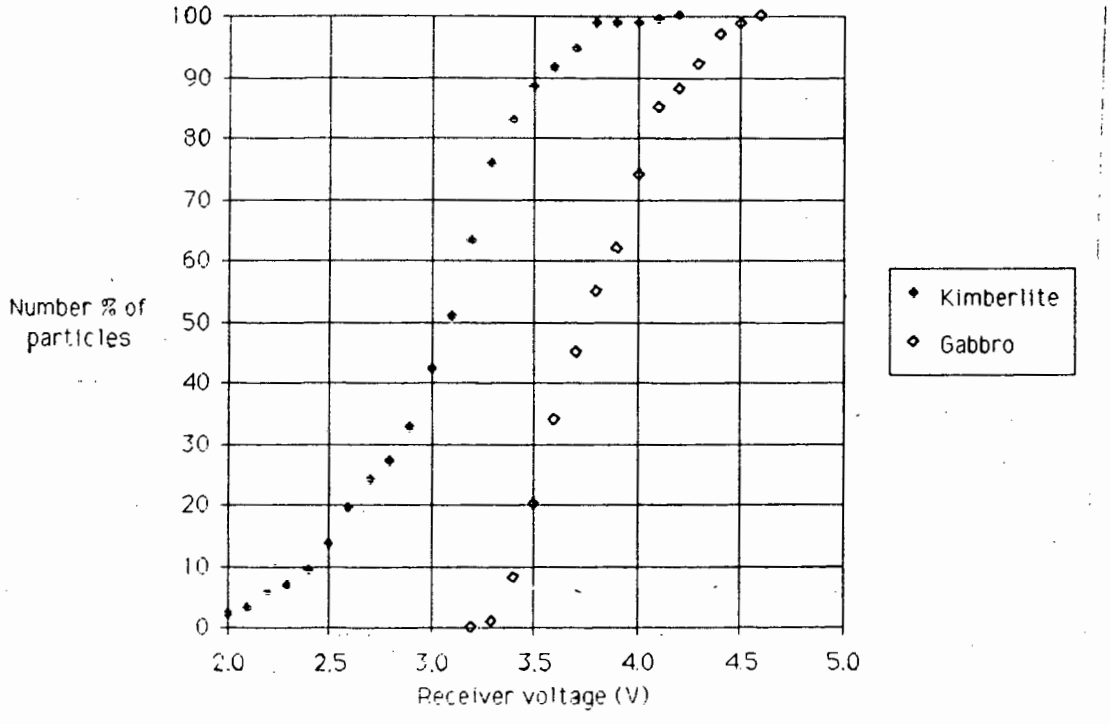

Figure 6.7. Cumulative Transmitted Power Number Frequency Distribution

The coefficients of variation for gabbro and kimberlite samples were calculated. Forty replications on 146 different rock samples were performed to obtain the data shown in figure 6.8. These data indicate the distribution of the coefficients of variation for each set of 40 replicates.

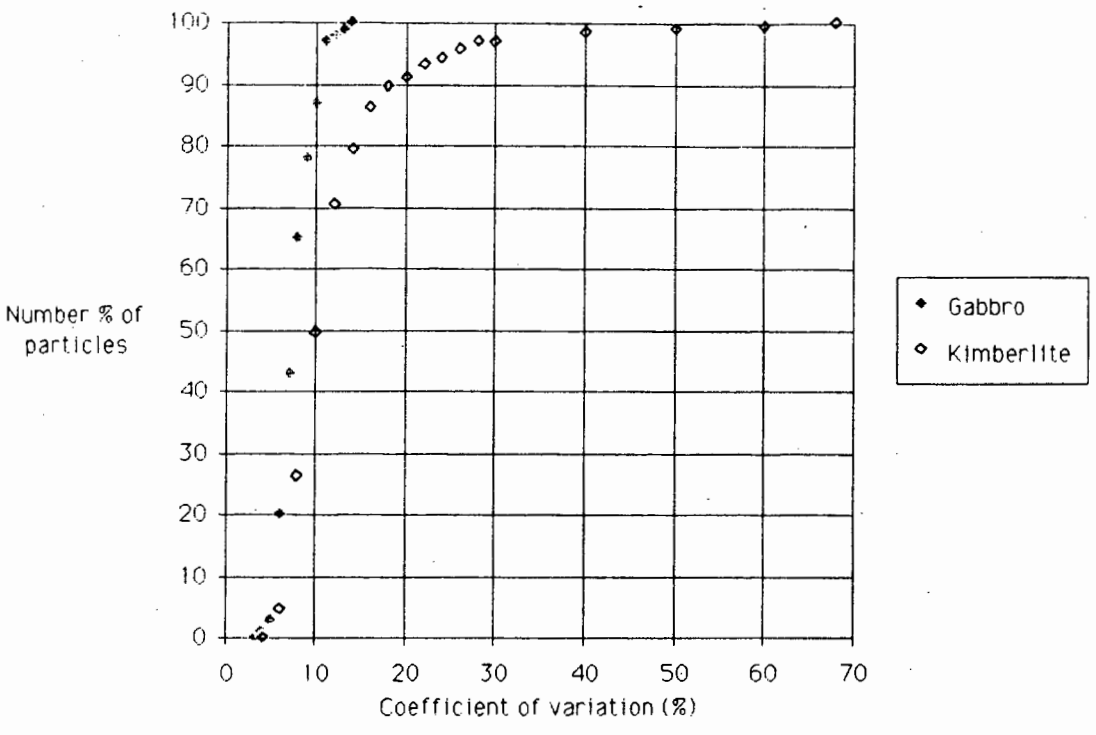

Figure 6.8. Distribution of Coefficients of Variation

It is clear from figure 6.8 that the gabbro samples displayed a 10% variation in signal level whilst the coefficient of variation for kimberlite was much greater. This was probably due to the inhomogenous composition of kimberlite which results in anisotropy of dielectric constant through this rock type. The size and shape of the samples were also influential factors.

The gabbro rejection curve is shown in figure 6.9. The percentage of correctly identified kimberlite versus the percentage of correctly identified gabbro is plotted. These data were obtained from 5640 tests on rock samples. It can be seen from figure 6.9 that a trade off is possible between the percentage of retained kimberlite and the percentage of

rejected gabbro. The highest percentage of kimberlite is retained when the lowest percentage of gabbro is rejected. When 93% of the kimberlite is retained it is possible to reject 67% of the waste gabbro.

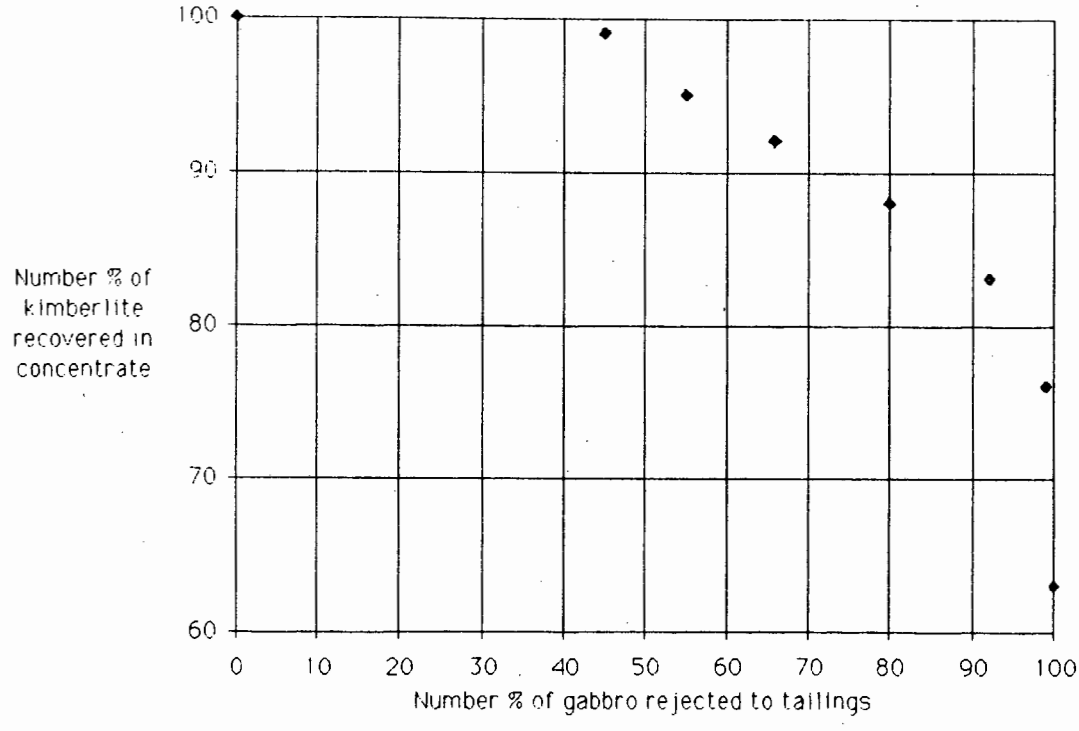

Figure 6.9. Gabbro Rejection Curve

It was found that the rejection of gabbro was dependent on the shape of the sample. The scattering of microwave signal by some gabbro samples led to their misidentification as kimberlite. The size variation of rocks was also found to be a critical factor in the identification of rock samples. A thin sample of kimberlite was occasionally misidentified as gabbro due to the low signal attenuation through the thin slice.

Experimentation with a height measuring device to measure the height of the rock samples as they pass the antennae has proved to be successful. The signal attenuation through a sample will be affected by the sample thickness. The thicker the sample ,the greater the the attenuation through the sample. The height measurement was used in conjunction with the attenuation measurements to provide a correction factor for the attenuation measurements. This signficantly reduces the abovementioned error of kimberlite misidentification and greatly improves the overall system performance. This system is being developed for industrial use. This work gave rise to both publications [2,3] and a patent [4].

It is considered that a substantial source of error and resulting anomalous high attenuation readings from some Gabbro samples are caused by signal scattering and diffraction, described in section 6.1.1. This apppears to be worse at higher frequencies and a system designed to eliminate this effect is described in Chapter 7.

However, the system described in this chapter, in conjunction with height measurement proved to be a viable on line system for waste rock sorting of gabbro from kimberlite.

6.3. LIST OF REFERENCES

[1] HARVEY, A.F., "Microwave Engineering", Academic Press Inc.(London)Ltd, 1963, p 670.

[2] MERCER, S.R., DOWNING, B.J., SALTER, J.D., NORDIN, L., "Microwave Discrimination Techniques for Rock Sorting", SAIEE 2nd Joint Symposium on Antennas and Propagation and Microwave Theory and Techniques, August 1988.

[3] MERCER, S.R., DOWNING, B.J., SALTER, J.D., NORDIN, L., "Microwave Discrimination Techniques for Rock Sorting", Elektron, Nov/Dec 1988, pp 19-20.

[4] NORDIN, L., SALTER, J.D., DOWNING, B.J., "Sorting Method and Apparatus", SA. Patent 87/8309, Filed 28 November 1986.

CHAPTER 7

7.0 INVESTIGATION OF DIFFERENT MICROWAVE MEASUREMENT STRUCTURES

A system for sorting regularly shaped dielectric samples was discussed in Chapter 6. Problems were experienced with irregularly shaped samples. An investigation of different microwave structures was undertaken to identify a structure that could be used to eliminate sample orientation dependence. Particular attention was given to on-line applications.

Many different types of microwave structures exist. The family of stripline structures, loop gap resonators and various resonant cavities can be considered for sample discrimination purposes.

Resonant cavities have been the most widely examined of these structures for the purpose of investigating sample dielectric constant. Most applications have not been on-line but rather for precision laboratory measurements [1]. The use of cylindrical cavities was investigated by Horner et al. [2]. Sproull and Linder [3] described a measurement technique using an oscilloscope. The cavity axial length was often varied as part of the measurement technique [2,3]. This type of system required specially prepared disk shaped samples.

The preparation of needle shaped samples was required for use with an accurate laboratory measurement system by Higgs [5]. Other researchers [6] have also developed precise methods for measuring changes in resonant frequency. Numerous systems have been developed in recent years [7-14]. The use of cylindrical cavity resonators is common [8, 12-16]. One system that operates at X band [14] will only cater for small samples.

The use of different types of microwave resonant structures is examined in this chapter. The properties of stripline structures, coaxial structures and rectangular waveguide structures are studied and compared.

7.1. STRIPLINE STRUCTURES

A stripline structure consists of a strip conductor and a ground plane. The conductor and the ground plane are separated by a dielectric material. An air dielectric is required if dielectric samples are to be passed between the conductor and the ground plane. The E field and H field are not entirely contained within the dielectric substrate (air) between the conductor and the ground plane. This means that wave propagation is not a pure transverse electromagnetic mode (TEM) but a quasi-TEM mode [17].

The family of stripline structures have different dimensions and positions of the strip conductor with respect to the ground plane. Microstrip, parallel stripline, coplanar stripline and shielded stripline are all members of the stripline family of structures. The shielded stripline structure is the most viable of these structures for on-line usage. The E field is more confined than with the other structures. The E field distributions of these different structures are shown in figure 7.1.

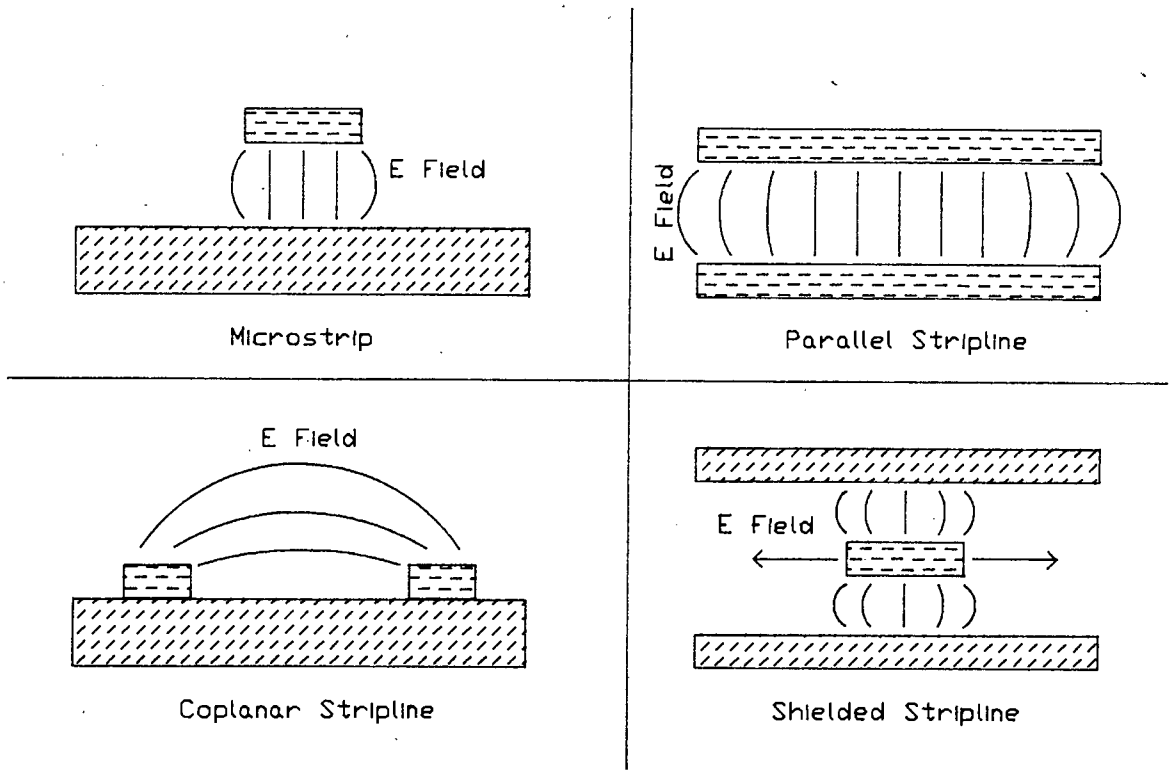

Figure 7.1. Field Distributions for Stripline Structures

A resonant structure using shielded stripline has been documented in the literature [18] for the grading of apples.

7.2. LOOP GAP RESONATORS

The loop gap resonator is a recently developed microwave structure that has a field distribution between lumped and distributed [19]. A loop gap resonator and it's E field distribution is shown in figure 7.2.

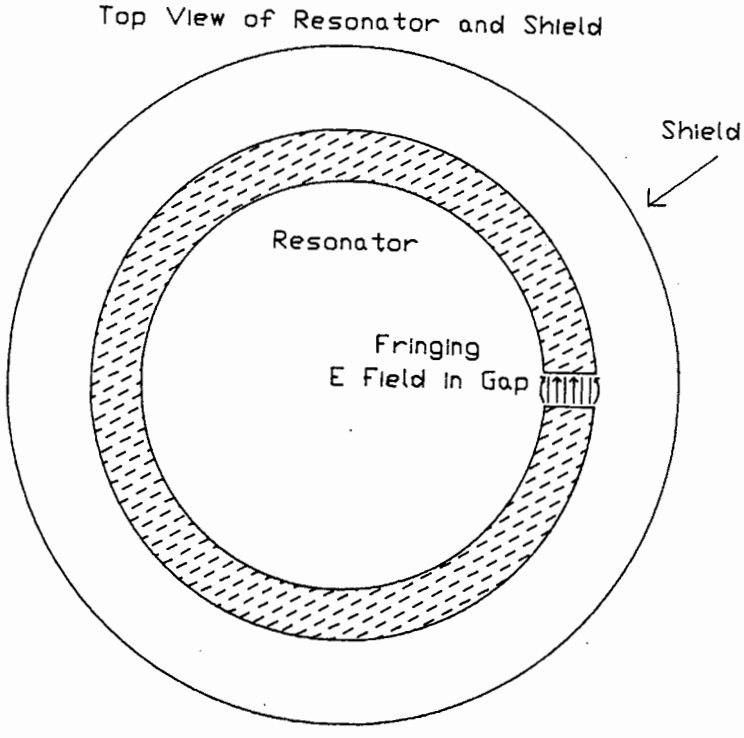

Figure 7.2. Loop Gap Resonator

The gap is kept small and coupling is made to the fringing field. A conveyor belt can be passed through the centre hole. This structure was extensively investigated by Celliers [20] for use in a moisture metering application. The use of this structure was not found to be successful due to the poor coupling to the weak fringing field. It was also found that the Q-factor dropped too low as the physical size of the structure was increased.

7.3. COMPARISON OF WAVEGUIDE, COAXIAL AND STRIPLINE STRUCTURES

The properties of fundamental mode rectangular waveguide, coaxial line and stripline were examined to evaluate the

suitability of these structures for dielectric sample evaluation.

A non radiating slot can be cut in the centre of the broad wall of a fundamental mode rectangular waveguide as shown in figure 7.3.

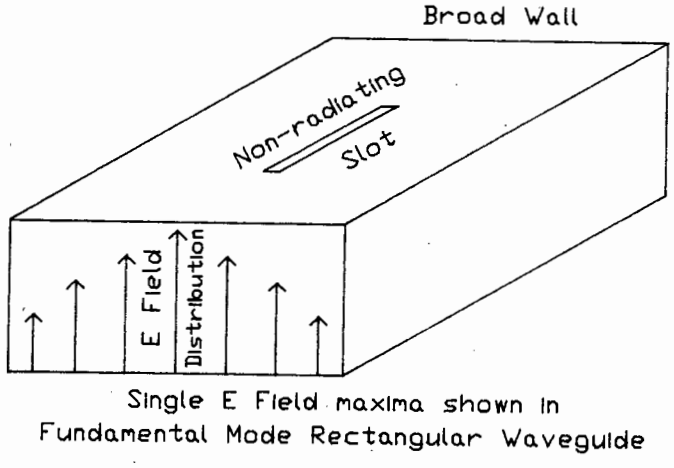

Figure 7.3. TE_{10} Rectangular Waveguide with Non Radiating Slot

A dielectric sample inserted into this non radiating slot is positioned in the E field maxima. No other mode can be established in the waveguide when a dielectric slab is placed into it. The electric field must reduce to zero at the surface of the sample as shown in figure 7.4.

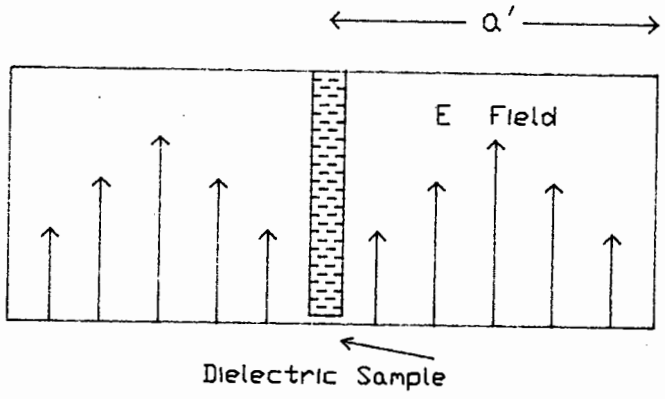

Figure 7.4. Bisected Waveguide

The field distribution shown in figure 7.4 however, is not possible as the waveguide dimensions a' are below cut off. Hence the effect of a dielectric inserted into the electric field maxima is to attenuate the field. The electric field is constrained to pass through the lossy material. This principal has been used in the Rotary Vane Attenuator.

When a conductor is placed into the waveguide as shown in figure 7.5 the effect is to reduce the b dimension to b'.

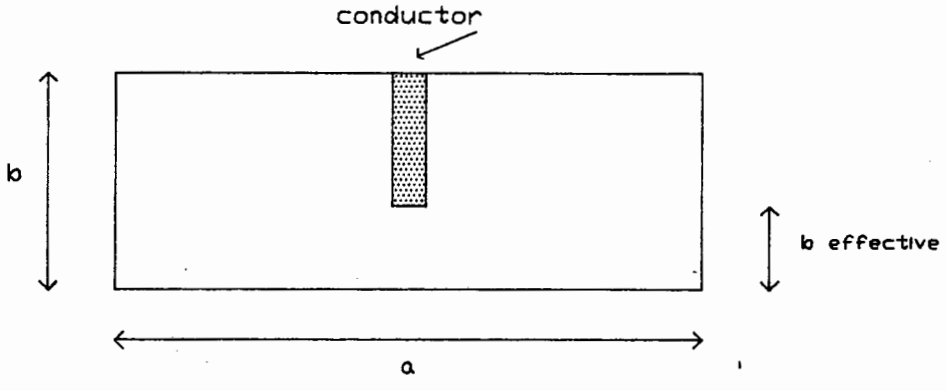

Figure 7.5. Waveguide with Conducting Slab

This alters the characteristic impedance Z_o of the waveguide in accordance with the formula $Z_o = Z_w \lambda_g * b / \lambda_o a$

where Z_w = Wave impedance

λ_g = waveguide wavelength

λ_o = free space wavelength

a,b = waveguide dimensions

Structures such as coaxial lines and stripline structures which support TEM modes can exhibit an electric field distortion. The E field is not constrained to pass through the dielectric material but may distort around the sample. This effect is demonstrated in section 7.3.2.

Propagation of TEM modes is not possible in a single conductor structure such as rectangular waveguide [21]. Suppose a TEM wave, which has no axial electric or magnetic field component, to exist in any shaped hollow guide. Then the lines of magnetic field must lie entirely in the transverse plane. Also, in non-magnetic materials, del.H=0. This constrains the lines of magnetic field to be in closed loops. Therefore if a TEM wave exists in the waveguide then the lines of magnetic field will be closed loops in the plane perpendicular to the axis.

According to Maxwell's first equation, the magnetomotive force around each of these current loops must be equal to the axial current through the loop. For a hollow guide with no inner conductor, this axial current must be a displacement current. An axial electric field is required to allow the existence of an axial displacement current and there is no axial electric field in a TEM wave. Hence a TEM wave cannot exist in a single conductor waveguide.

It therefore follows that the electric field is constrained to pass through any dielectric material positioned in the

electric field maxima in a fundamental mode waveguide cavity.

A rectangular waveguide structure, a coaxial structure and a stripline structure were fabricated to allow comparative measurements to be made.

7.3.1. Construction of Test Structures

The rectangular waveguide structure was fabricated from a length of X band rectangular waveguide with flanges on each end to facilitate coupling to waveguide launchers. A one wavelength long non-radiating slot was cut in the centre of the broad wall as shown in figure 7.3. There was a one wavelength long length of transmission line on either side of the slot to allow any evanescent modes to decay before reaching the launchers. A rotating vane was used to insert the dielectric material into the waveguide.

A picture of this rectangular waveguide structure is shown in figure 7.6.

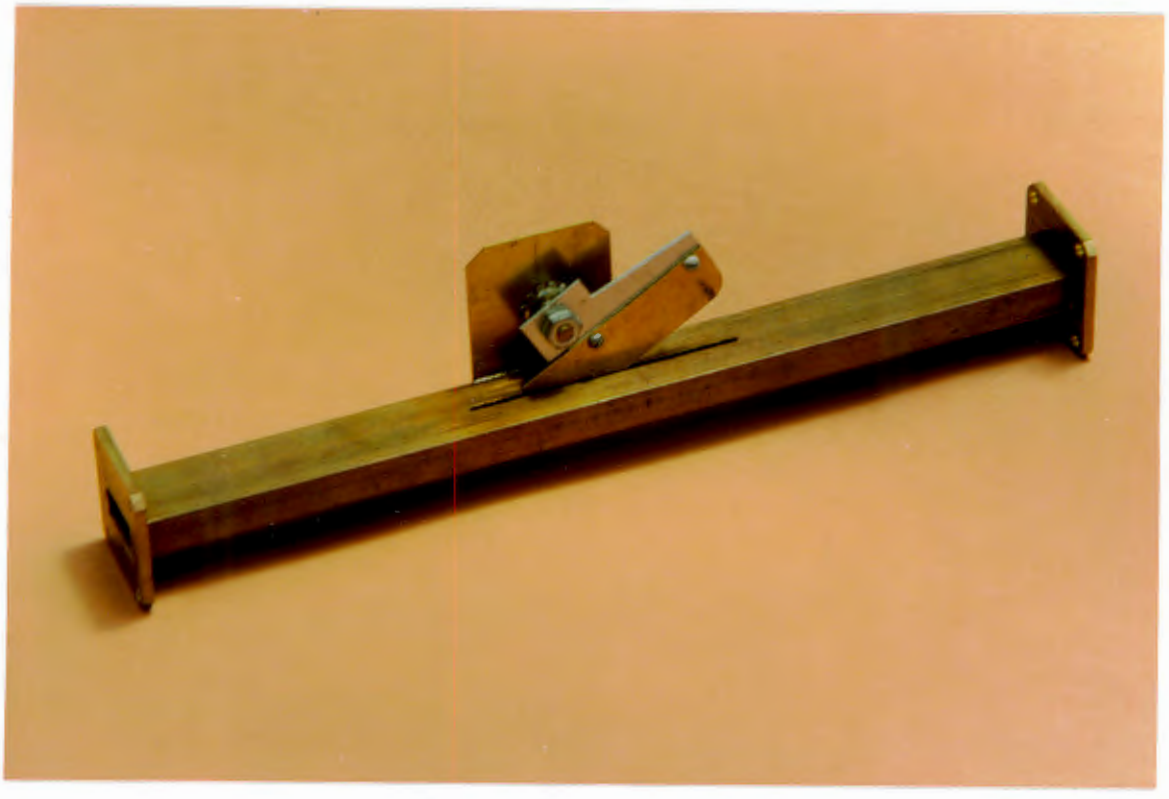

Figure 7.6. Rectangular Waveguide Test Structure

The characteristic impedance of a coaxial line is given by $Z_o = 138*\sqrt{\mu_r/k_r}*\log_{10}(R0/R1)$ where R0 and R1 are the inner and outer radii shown in figure 7.7.

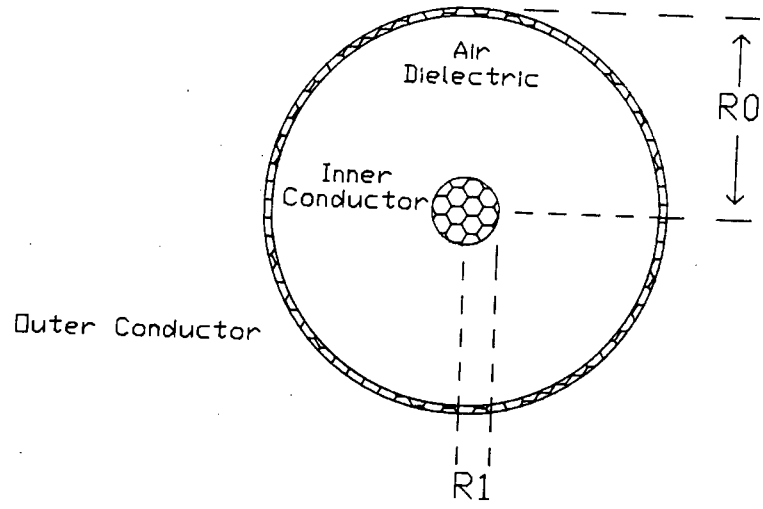

Figure 7.7. Coaxial Line dimensions

If an air dielectric is used as shown above then μ_r = k_r = 1. Choosing Z_o = 50Ω the ratio R0/R1 = 2.3. For ease of construction at X band, R0 was matched to a standard N type connector so R0 = 8.2mm. Consequently R1 = 3.6mm.

The total length of this structure was three wavelengths (9cm). This allowed a one wavelength sample to be centred in the structure with one wavelength of transmission line on either side to allow for the decay of any evanescent modes arising from impedance discontinuities.

The coaxial test structure is shown in figure 7.8.

Figure 7.8. Coaxial Test Structure

The N type connectors could be removed for sample insertion and positioning. Samples were placed perpendicularly between the inner and outer conductors as shown in figure 7.9. The sample will have maximum interaction with the E field in this position.

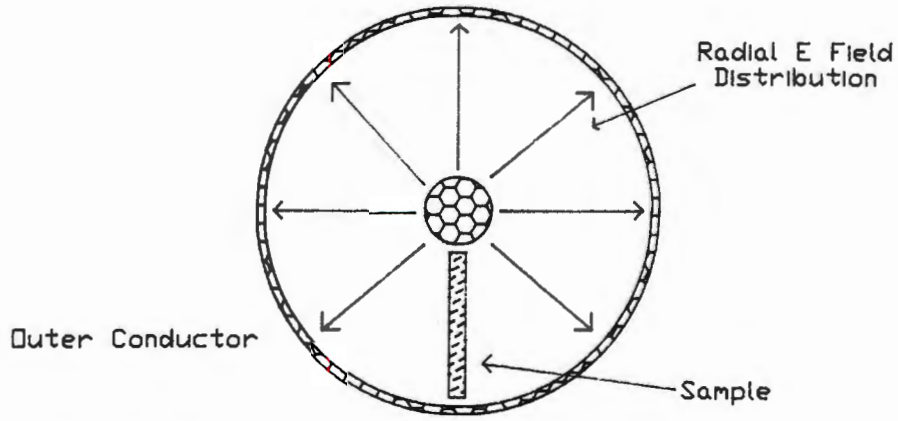

Figure 7.9. Sample position in Coaxial Structure

The samples were correctly positioned by mounting them in specially prepared expanded polystyrene foam sections. Expanded polystyrene was found to be virtually transparent to the X band signal.

A diagram of the X band stripline structure is shown in figure 7.10. An aluminium ground plane was chosen for convenience. A 50Ω line with an air dielectric was required to facilitate comparative measurements with the waveguide and coaxial units.

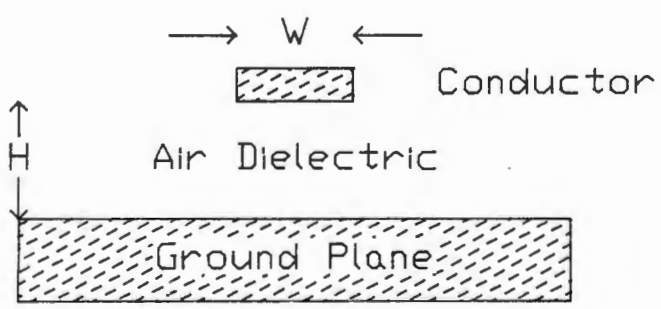

Figure 7.10. Diagram of Stripline

For an air dielectric $\epsilon_r = 1$
At 10GHz, $\lambda = c/f = 3cm$
Using Wheeler's curves [22], $\lambda_o/\lambda_g = 1$
therefore $\lambda_o = \lambda_g$
With $\epsilon_r = 1$, W/H = 5
Choosing H = 1.2mm we get W = 6mm

The airgap H had to be chosen large enough so that a sample could be placed perpendicularly in the gap as shown in figure 7.11.

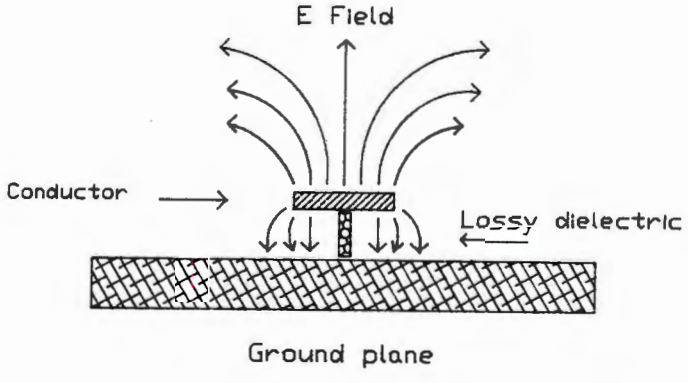

Figure 7.11. Sample Position in Stripline Structure

Samples were correctly positioned using a slotted strip of expanded polystyrene. The structure was fabricated slightly more than three wavelengths long to ensure that any spurious evanescent modes due to impedance discontinuities could decay without adversely affecting the measurements.

Standard SMA launchers were fixed to the ground plane. The 50Ω line was tapered at either end to allow a gradual impedance change from the launchers to the 6mm wide strip. A picture of this stripline structure is shown in figure 7.12.

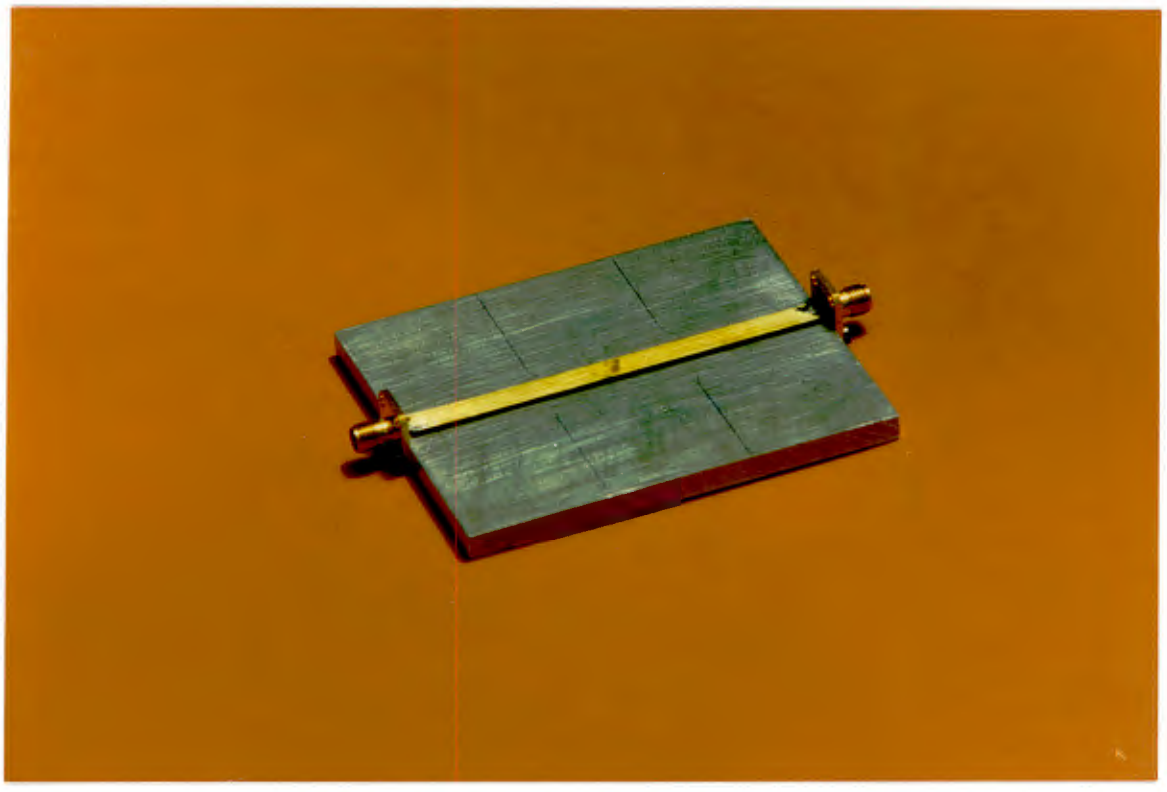

Figure 7.12. The Stripline Test Structure

7.3.2. Test Results

A one wavelength long section of microwave attenuative card was inserted into each structure using the method described in section 7.3.1. The results obtained are quantified in figure 7.13.

Microwave Structure	Waveguide	Coaxial Line	Stripline
Insertion Loss	14dB	2.9dB	0.33dB

Figure 7.13. Effect of Lossy Material in Each

These results demonstrate that the sample has the most interaction with the microwave signal in the waveguide structure. The experiment was repeated with metal conductors. A strip of metal bisecting the waveguide had virtually the same effect as covering the rectangular aperture with a metal plate.

This was not the case with the other structures. An annular metal disk blocking the coaxial structure severely attenuated the signal as expected. A metal conductor positioned as shown in figure 7.9, however, had almost the same effect as the lossy material mentioned in figure 7.13.

A metal strip positioned in the stripline structure had virtually the same effect as the section of lossy card. These results demonstrate that field distortion occurs in both stripline and coaxial structures. Fundamental mode rectangular waveguide structures were shown to have a far greater interaction with an inserted dielectric sample than the coaxial and stripline units.

7.4. CONSTRUCTION OF RECTANGULAR WAVEGUIDE CAVITY SYSTEM

A 500MHz TE_{01} mode rectangular waveguide cavity was designed. The design procedure is discussed in depth by Montgomery [23]. A diagram of the 500MHz cavity, with dimensions, is shown in figure 7.14.

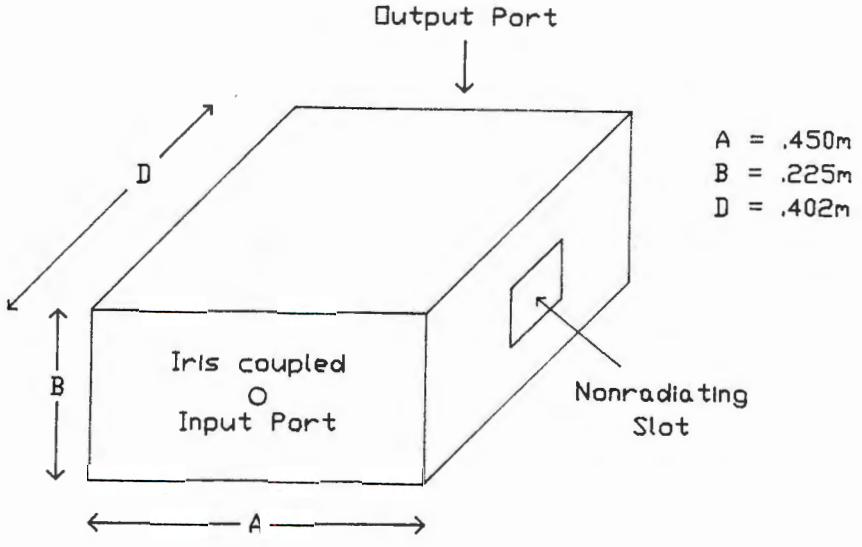

Figure 7.14. Rectangular Resonant Cavity

The RF signal was iris coupled into the cavity as indicated in figure 7.14. Non-radiating slots are also shown in the above diagram. This allowed samples to be passed through the cavity. A perspex tube, transparent to the 500MHz signal, was fixed into cavity to guide the samples through the cavity.

Different samples were dropped through the cavity as shown in figure 7.15. This method facilitated sample speeds of up to 5m/s.

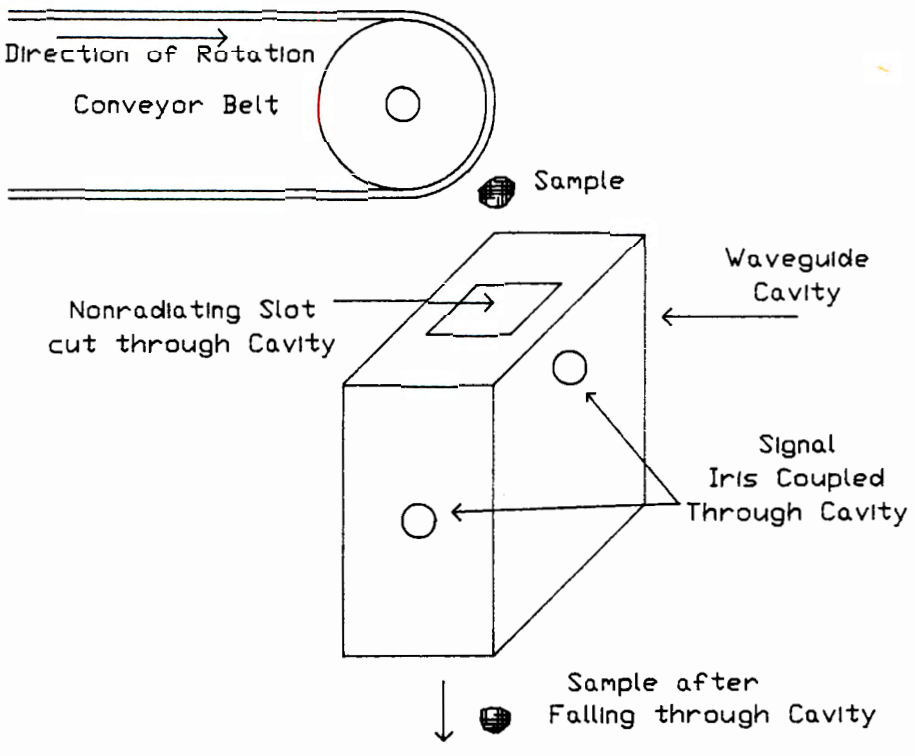

Figure 7.15. Samples Dropped through Cavity

7.4.1. System Design

The 500MHz waveguide cavity was connected to the system shown in figure 7.16.

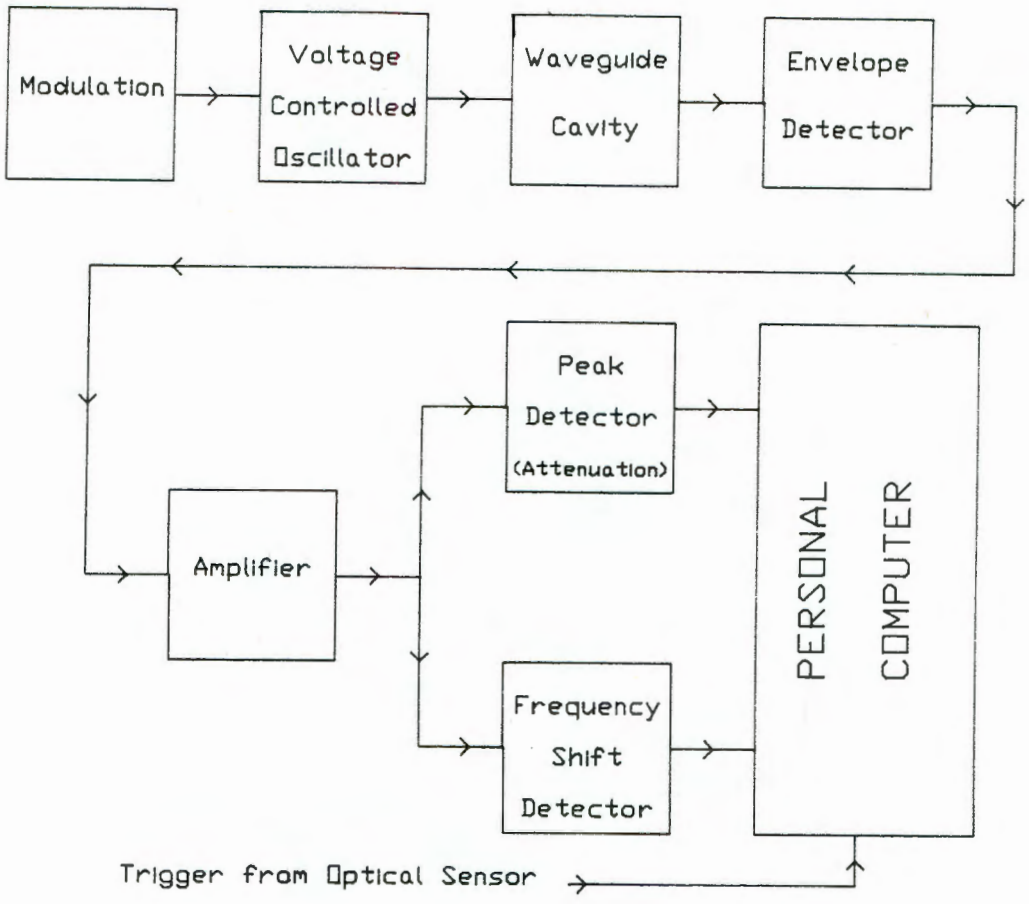

Figure 7.16. Block Diagram of Transmitter, Cavity and Display

The transmitter consisted of a 500MHz varactor tuned transistor oscillator with an output power of 30mW. The varactor was linearly modulated using a 10kHz triangular voltage waveform. Some signal waveforms observed at various points in the system are shown in figure 7.17.

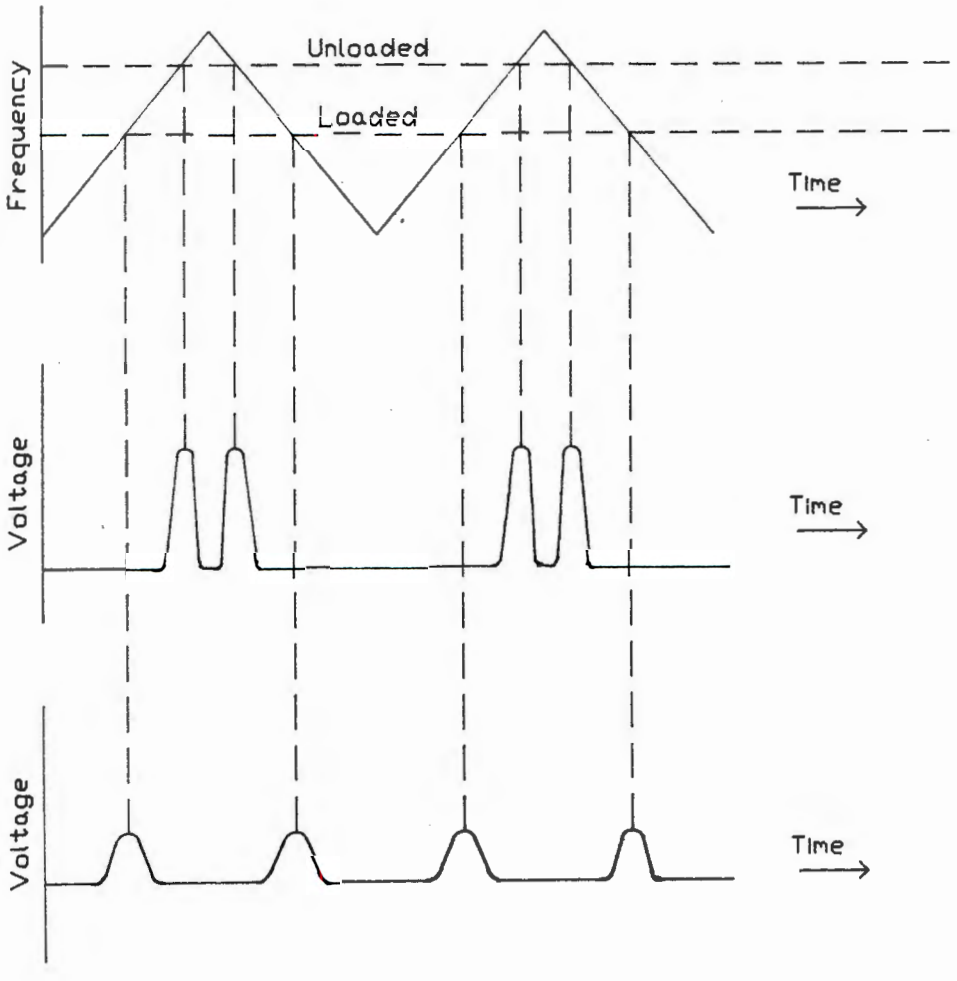

Figure 7.17. System Signal Waveforms

The transmitter frequency is varied linearly by means of the varactor. The curve labelled unloaded output represents the output of the waveguide cavity as the transmitter sweeps through it's resonant frequency and back again. If a dielectric sample is introduced into the cavity then it's resonant frequency will drop. The waveform "loaded output" represents the cavity output in this state.

The pulses in this second waveform have moved apart and have reduced in amplitude. An active peak detector was used to obtain a measure of the signal attenuation due to a sample. Interpeak timing logic circuitry was used to measure the time between pulses. This information is then related to the resonant frequency shift of the cavity. A personal computer was used to effect data capture. Each measurement was triggered by a sample interrupting a light beam across the entrance to the cavity. The circuitry used in this system was reported in detail by De Waal [24].

7.4.2. Results Using 500MHz Waveguide Cavity

Samples were dropped through the cavity at a rate of 5m/s using the configuration shown in figure 7.15. The transmitter sweep frequency was sufficiently high enough to ensure that measurement accuracy was not limited by the sample velocity. One thousand eight hundred samples were recorded as each dielectric body passed through the cavity at 5m/s.

This system was successfully applied to the weighing of regular shaped samples of fruit [25]. Apples and oranges consist of more than 80% moisture (ϵ_r=80). The determination of the volume of water results in an accurate measure of the weight of the fruit. As the fruit passed through the cavity the variations in resonant frequency and signal attenuation were recorded as described above. The resonant frequency shift is greatest when the fruit is positioned at the E field maxima in the centre of the cavity.

Accuracies of greater than 5% were recorded for apples and oranges. The most repeatable results were obtained with the oranges which have the most regular shape. The

main source of error when measuring apples was the orientation dependent resonant frequency shift due to the less symmetrical shape of this fruit. The problem here is the variation in coupling between the irregular shaped sample and the E-field in the linearly polarised waveguide cavity where the E-field is limited to a single plane of polarisation.

The use of this resonant cavity system for rock sorting was studied by De Waal [24]. The system was found to be 100% successful for separating regular shaped samples of gabbro and kimberlite. The kimberlite, with a consistently higher dielectric constant than gabbro, displays a greater frequency shift than the gabbro rocks. This system has led to the filing of numerous patents [26-32].

Problems were, however, experienced with irregular shaped samples. The amount of resonant frequency shift was shown to be orientation dependent for irregular shaped rocks. This problem of orientation dependence is fully examined in section 7.5.

7.5. ORIENTATION DEPENDENCE IN LINEARLY POLARISED WAVEGUIDE CAVITY

A fundamental mode waveguide is shown in figure 2.18. A dielectric sample is positioned in figure 2.18a such that it will experience a maximum coupling with the electric field. The sample position indicated in figure 2.18b will have minimum coupling with the electric field.

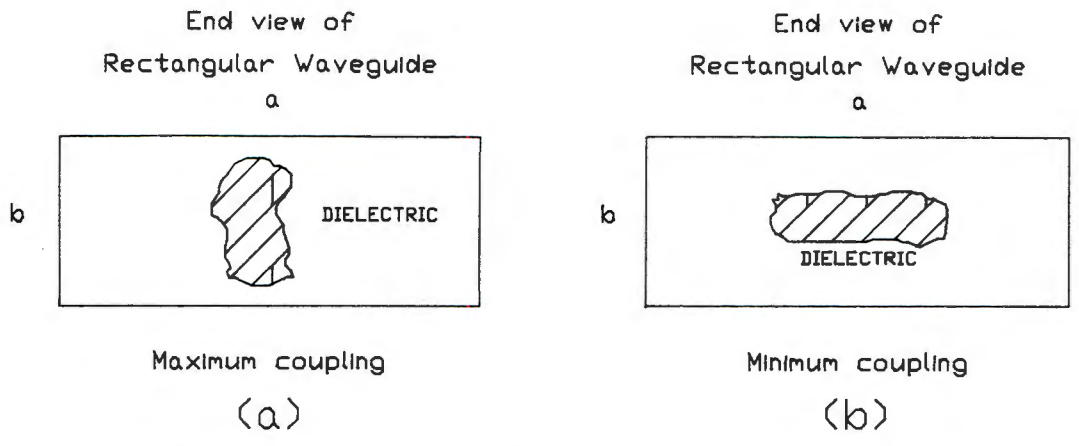

Figure 7.18. Coupling to E-Field in TE_{01} Waveguide

The 500MHz waveguide cavity shown in figure 7.14 was tested with a 31.8ml cylindrical shaped water load. Three different orientations of this cylindrical load in the centre of the cavity are presented. This data was obtained using a HP4195A network analyser.

The resonant peak for the unloaded cavity is shown in figure 7.19.

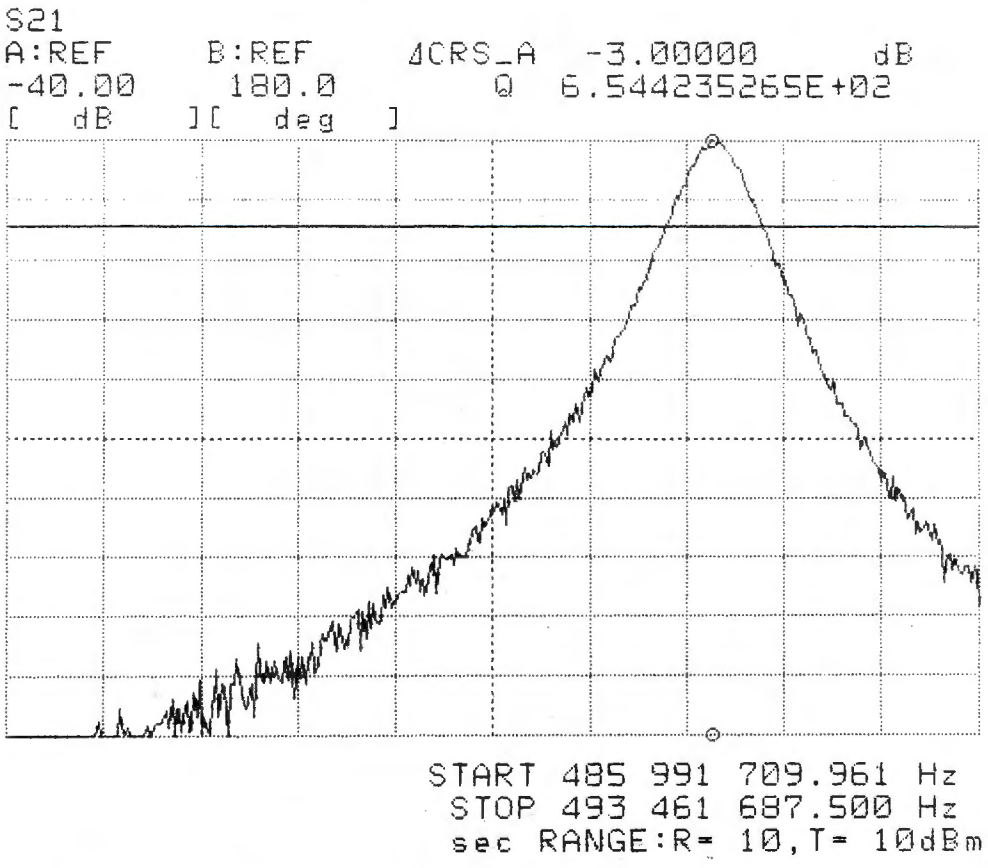

Figure 7.19. Unloaded Cavity Response

A vertical orientation of the cylindrical water load is shown in figure 7.20.

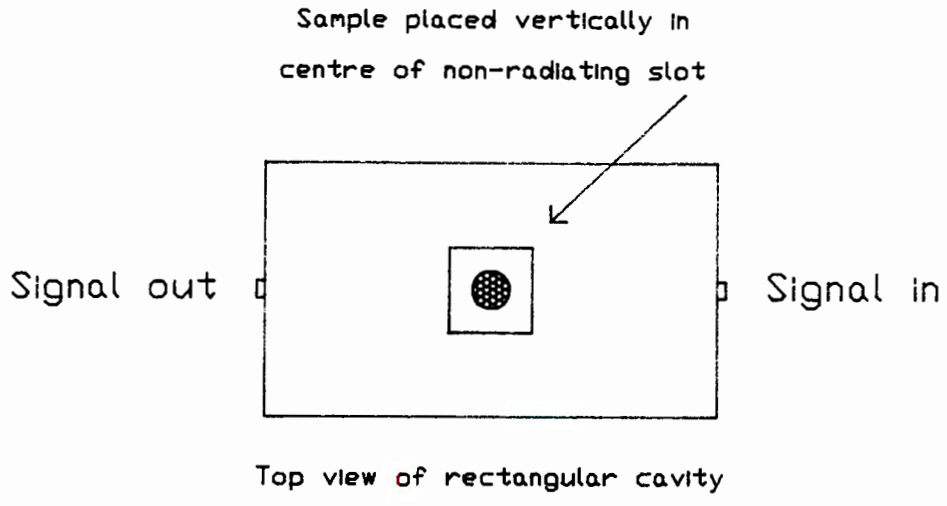

Figure 7.20. Vertical Sample Orientation

The cavity response with this sample orientation is shown in figure 7.21. The unloaded cavity response is also shown for reference.

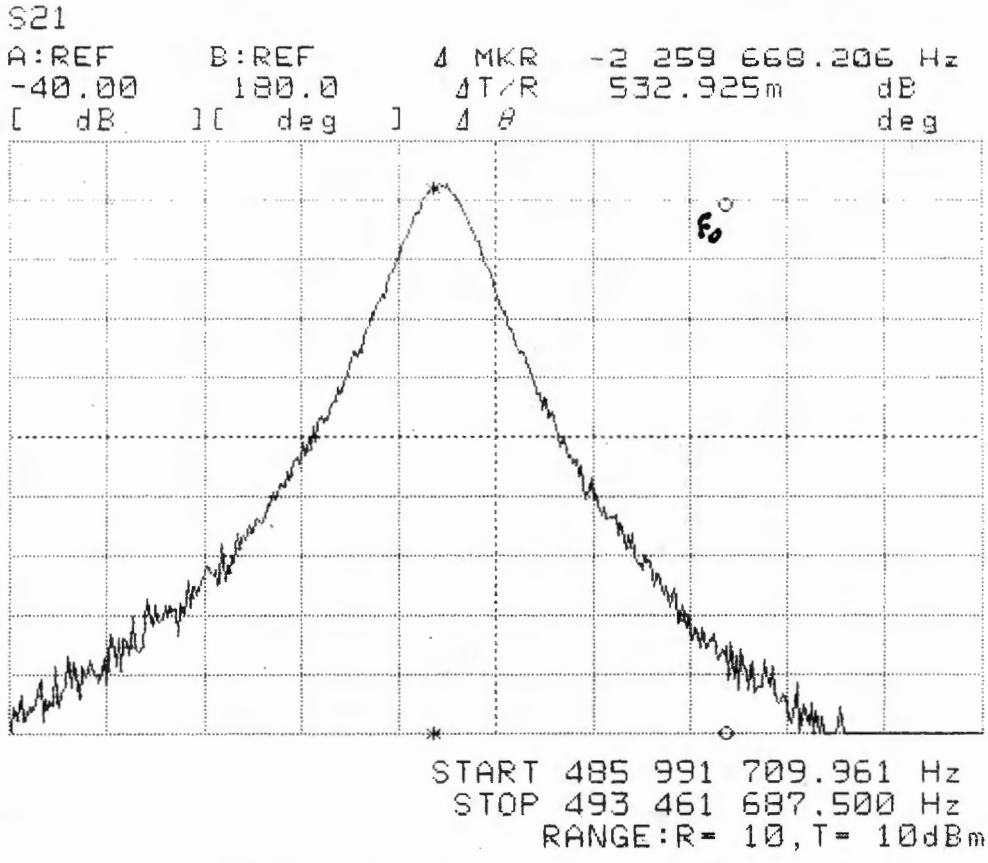

Figure 7.21. Cavity Response with Vertical Sample

The cylindrical load was then positioned horizontally in the centre of the cavity as shown in figure 7.22.

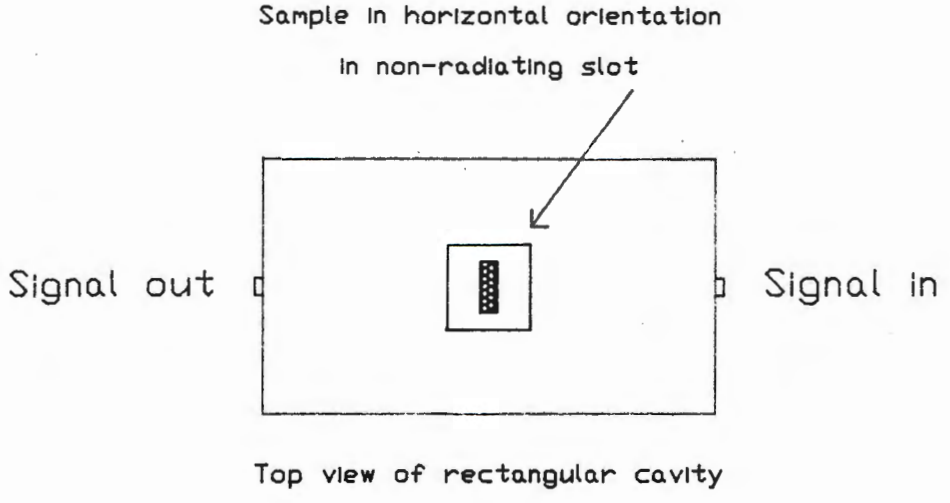

Figure 7.22. Horizontal Sample Orientation

The cavity response relative to the unloaded cavity with this horizontal sample orientation is given in figure 7.23.

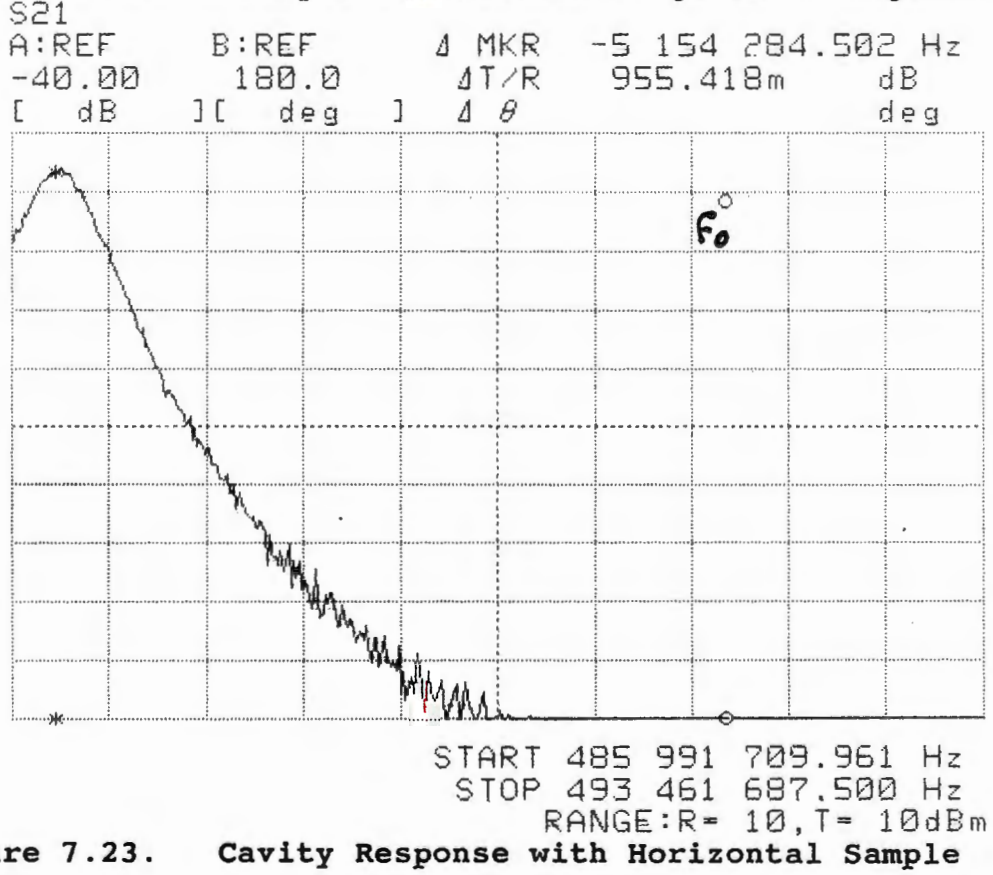

Figure 7.23. Cavity Response with Horizontal Sample

A different horizontal position of the sample illustrated in figure 7.24, was then adopted.

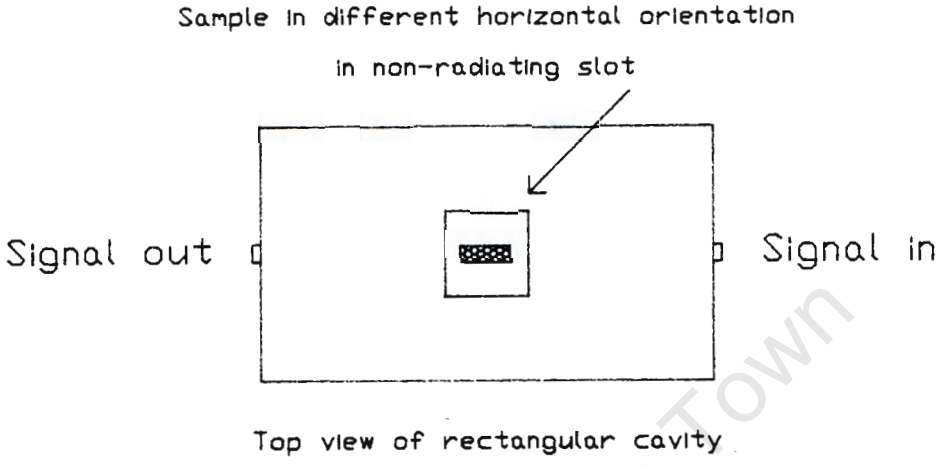

Figure 7.24. Different Horizontal Orientation

The cavity response with the sample configuration of figure 7.24 is shown below in figure 7.25. The unloaded cavity response is also shown for reference.

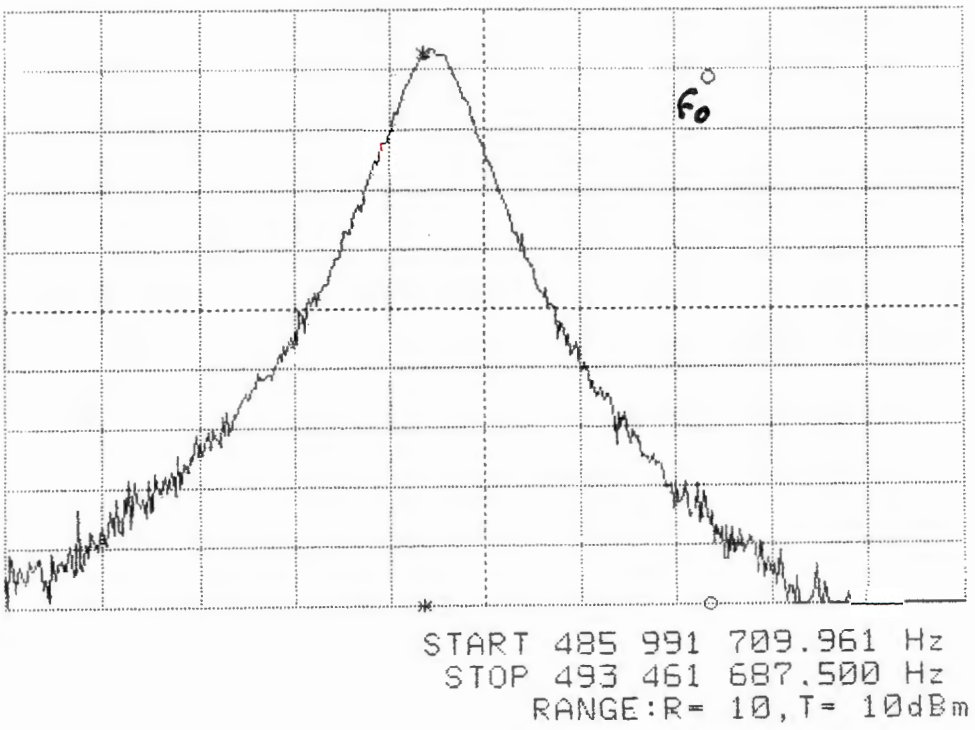

Figure 7.25. Cavity Response for Second Horizontal Orientation.

A study of figures 7.21, 7.23 and 7.25 reveals that all three sample orientations result in different cavity responses. The curves of figure 7.21 and 7.25 are very similar and represent a much smaller change in resonant frequency than the plot illustrated in figure 7.23. This is due to the fact that the sample orientation of figure 7.22 is that which intersects the maximum amount of E-field.

These results clearly demonstrate the problem of sample orientation dependence with irregular shaped samples. Although a successful system was developed for work with regular shaped samples using a resonance approach, a solution capable of processing irregular shaped samples (eg.minerals and fruit) was desired.

7.6. LIST OF REFERENCES

[1] RZEKECKA, M.A., HAMID, M.A.K., "Automatic Digital Method for Measuring the Permittivity of Thin Dielectric Films", IEEE MTT-20, No 1, Jan. 1972, pp 30-37.

[2] HORNER, F., TAYLOR, T.A., DUNSMUIR, R., LAMB, J., JACKSON, W., "Resonance methods of dielectric measurement at centimetre wavelengths", Proc. Inst. Elec. Eng.(London), vol. 93, pt III, pp 53-68, 1946.

[3] SPROULL, R.L., LINDER, E.G., "Resonant Cavity Measurements", Proc. I.R.E., May 1946, pp 305-312.

[4] SAITO, S., KUROKAWA, K., "A Precision Resonance Method for Measuring Dielectric Properties of Low-Loss Solid Materials in the Microwave Region", Proc. I.R.E., Jan 1956, pp 35-42.

[5] HIGGS, A.W., "A System for measuring complex permittivity at microwave frequencies", J.Phys. E:Sci. Instrum., vol 19, 1986, pp 1019-1025.

[6] LAND, D.V., "Improved method for resonant-frequency perturbation measurements", Electronics Letters, vol 23, no 21, 1987, pp 1166-1167.

[7] NEY, M., GARDIOL, F.E., "Automatic Monitor for Microwave Resonators", IEEE vol. IM-26, no 1, March 1977, pp 10-12.

[8] AGDUR, B., ENANDER, B., "Resonances of a Microwave Cavity Partially Filled with a Plasma", J. App. Phys., vol 33, no 2, Feb. 1962, pp 575-581.

[9] HUME, A.L., AUCHTERLONIE, L.J., "Assessment of moisture content of fibres and fabrics by measurement of extinction cross-section in an open resonator", Electronics Letters, 18th Aug. 1988, vol. 24, no 17, pp 1097-1098.

[10] BOSISIO, R.G., "A Digital Non-Contact Microwave Instrument for Egg Size and Shape Index Measurements", IEEE vol. IECI-20, no 3, Aug. 1973, pp 174-177.

[11] LAKSHMINARAYANA, M.R., PARTAIN, L.D., ALLAN COOK, W., "Simple Microwave Technique for Independent Measurement of Sample Size and Dielectric Constant with Results for a Gunn Oscillator System", IEEE vol. MTT-27, no 7, July 1979, pp 661-665.

[12] AKYEL, C., BOSISIO, R.G., APRIL, G., "An Active Frequency Technique for Precise Measurements on Dynamic Microwave Cavity Perturbations", IEEE vol. IM-27, no 4, Dec. 1978, pp 364-368.

[13] LI, S., AKYEL, C., BOSISIO, R.G., "Precise Calculations and Measurements on the Complex Dielectric Constant of Lossy Materials Using TM_{010} Cavity Perturbation Techniques", IEEE vol. MTT-29, no 10, Oct. 1981, pp 1041-1047.

[14] MARTINELLI, M., ROLLA, P.A., TOMBARI, E., "A Method for Dielectric Loss Measurements by a Microwave Cavity in Fixed Resonance Condition", IEEE vol. MTT-33, no 9, Sept. 1985, pp 779-783.

[15] MARTIN, E., HERNANDEX, M.C., SANCHEZ, M.C., ZAMARRO, J.M., MARGINEDA, J., "Automatic measurement of Q factor and resonant frequency of microwave resonators", J. Phys. E: Sci. Instrum., vol. 14, 1981, pp 961-962.

[16] HAMID, M.A.K., RZEPECKA, M.A., "Microwave resonators for fruit and vegetable grading", Journal of Microwave Power, vol. 11, no 2, 1976, p 195.

[17] LIAO, S.Y., "Microwave circuit analysis and amplifier design", Prentice-Hall, New Jersey, 1987, p 197.

[18] KASHYAP, S.C., VACHON, F., "A Microwave Method for Grading Agricultural Products", Journal of Microwave Power, vol. 14, no 1, 1979, pp 35-39.

[19] MEHDIZADEH, M., KORYUISNII, T., HYDE, J.S., FRONCISZ, W., "Loop-gap Resonator: A Lumped Mode Microwave Resonant Structure", IEEE vol. MTT 31, no 12, Dec. 1983, pp 1059-1063.

[20] CELLIERS, S.,"Online Moisture Measurement of Rocks using Microwave Techniques." MSc Thesis, University of Cape Town, 1989.

[21] JORDAN, E.C., BALMAIN, K.G., 'Electromagnetic Waves and Radiating Systems", Prentice-Hall, Inc., 1968, p270.

[22] WHEELER, H.A.,"Transmission-line properties of parallel strips separated by a dielectric sheet.", IEEE Trans. MTT13 no.3, March 1965, pp172-185.

[23] MONTGOMERY C.G.,"Techniques of Microwave Measurements", MIT Radiation Laboratory Series, vol.11 p 294.

[24] DE WAAL, A., "Kimberlite / Gabbro Rock Discrimination using a 500MHz Resonant Waveguide Cavity.", Undergraduate Thesis, Department of Electrical Engineering, University of Cape Town, 1987.

[25] DE WAAL, A., MERCER, S., DOWNING, B.J., "On Line fruit weighing using a 500MHz waveguide cavity", Electronics Letters, 18th Feb. 1988, vol. 24, no 4, pp 212-213.

[26] DOWNING, B.J., MERCER, S.R., SALTER, J.D., NORDIN, L., "Sorting Particulate Material on the Basis of Size or Composition", S.A. Patent 88/7740, filed 17 October 1988.

[27] DOWNING, B.J., MERCER, S.R., SALTER, J.D., NORDIN, L., "Sorting Particulate Material on the Basis of Size or Composition", Australian patent AU 2404088.

[28] DOWNING, B.J., MERCER, S.R., SALTER, J.D., NORDIN, L., "Sorting Particulate Material on the Basis of Size or Composition", Brazilian patent BR 18805383.

[29] DOWNING, B.J., MERCER, S.R., SALTER, J.D., NORDIN, L., "Sorting Particulate Material on the Basis of Size or Composition", Canadian patent Ca 5804281.

[30] DOWNING, B.J., MERCER, S.R., SALTER, J.D., NORDIN, L., "Sorting Particulate Material on the Basis of Size or Composition", South West African patent SW 88/0106.

[31] DOWNING, B.J., MERCER, S.R., SALTER, J.D., NORDIN, L., "Sorting Particulate Material on the basis of Size or Composition", United Kingdom patent U.K. 88244447.

[32] DOWNING, B.J., MERCER, S.R., SALTER, J.D. NORDIN, L., "Sorting Particulate Material on the Basis of Size or Composition", USA patent U.S. 07259843.

CHAPTER 8

8.0 A RESONANT STRUCTURE FOR ORIENTATION INDEPENDENT RESULTS

Use of fundamental mode rectangular waveguide cavities for on line determination of complex dielectric constants were shown in section 7.5 to have problems with the orientation of irregular shaped samples. This was due to the orientation dependent coupling of the irregular shaped sample to the linearly polarised E-field. It was decided to investigate the use of other cavity geometries and structures to reduce or eliminate the effect of sample orientation in the cavity.

The analysis of field patterns in loaded cavities and dielectrically loaded waveguides is complex and is only possible for relatively simple geometries [1-10]. The use of tubular waveguides [11] and cyclindrical cavities, particularly TM_{011} and TE_{111} cavities, has been well documented in the literature [12-18]. Most of these cavities have been used to examine axial dielectric rods or disks. This type of structure is therefore seldom applied to on-line usage. The sample insertion hole has been shown to affect the field structure within the cavity and correction factors have been derived for very accurate laboratory type measurements [19,20].

Consideration is given to structures with two independent planes of polarisation and to those with three independent planes of polarisation, with a view to on-line usage.

8.1. STRUCTURES WITH TWO INDEPENDENT PLANES OF POLARISATION

8.1.1. Investigation of TE_{111} Cylindrical Cavity System

A TE_{111} cylindrical cavity has been used for the study of axial dielectric rods [12]. The cavity was used in a linearly polarised sense.

It was decided to develop two different TE_{111} cavity systems in parallel. One system investigates two independent planes of polarisation and the other system uses circular polarisation. A system using two independent planes of polarisation is shown in figure 8.1.

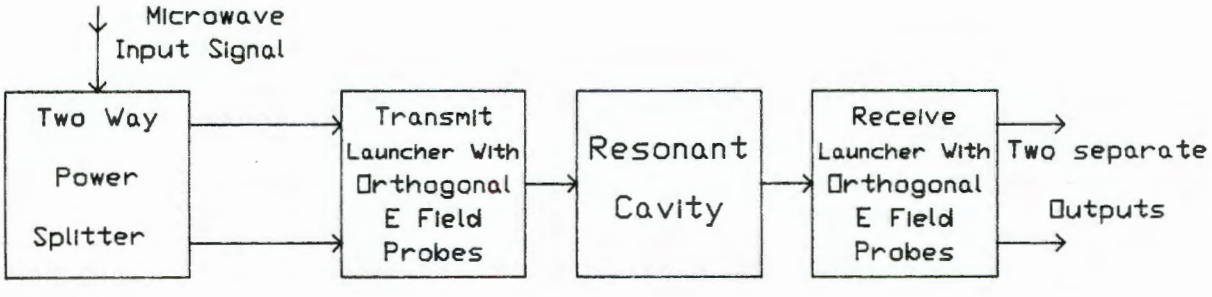

Figure 8.1. Linearly Polarised System

A two way power splitter with zero degrees phase delay between the outputs was used to provide two in phase signals to the orthogonally placed E field probes. The signals were coupled into the cylindrical cavity via circular iris holes. The received signals were observed using the E field probes on the receiving launcher.

A circularly polarised cavity system is shown in figure 8.2.

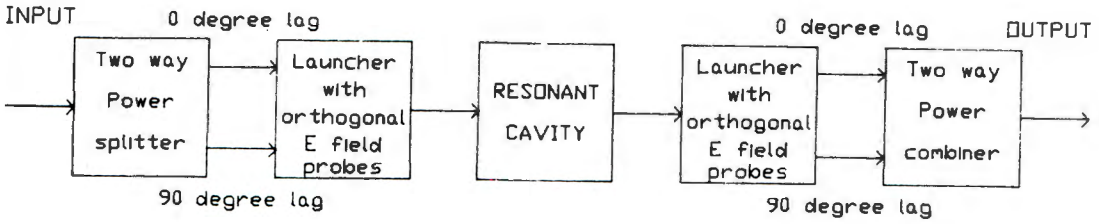

Figure 8.2. Circular Polarised System

The microwave input signal was fed into a two way quadrature power splitter. The outputs from this power splitter were coupled through equal length cables to the orthogonally placed E field probes in the cylindrical waveguide launcher. This would result in a rotating E field propagating through the cavity as shown in figure 8.3. The orthogonal placement of the E field probes is also visible in this diagram.

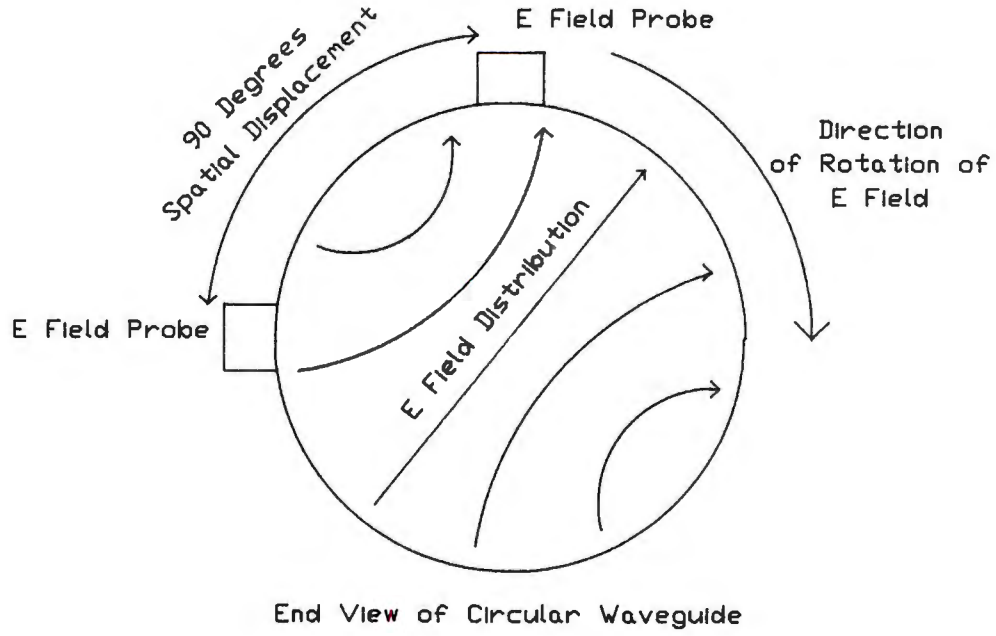

Figure 8.3. Rotating E field

The circularly polarised field in the cavity would result in an average resonant frequency change and an average Q factor change related to the cross sectional area of the sample and not the linear dimension in the direction of the E field. This would result in sample orientation independence in two planes.

The signals are coupled into the resonant cavity through a circular iris. The circular iris is a symmetrical structure and will not affect the polarisation and coupling of the signal passing through it. The signal output from the cavity in figure 8.2 is processed via a reciprocal system. The construction of the system components shown in figure 8.2 is detailed in the following sections.

8.1.1.1. Construction of TE_{111} Cavity and launchers

For the TE_{111} mode to be the dominant mode the cavity diameter D shown in figure 8.1 must be less than or equal to the axial length L. The cavity is designed using the formula [21]:

$$\lambda = 2/\sqrt{\left[(2X_m/\pi D)^2 + (n/L)^2 \right]} \qquad (8.1)$$

where X_m is a Bessel function [21].

It was chosen to fix D = 0.4L. This is substituted into equation 8.1 to reduce the number of variables. The above procedure was used to produce a 2.4GHz TE_{111} cavity with dimensions D = 0.093m and L = 0.101m.

Circular iris coupling holes in the cavity end plates were used to couple the microwave signal

into the cavity. The cavity and the sample insertion hole are illustrated in figure 8.4.

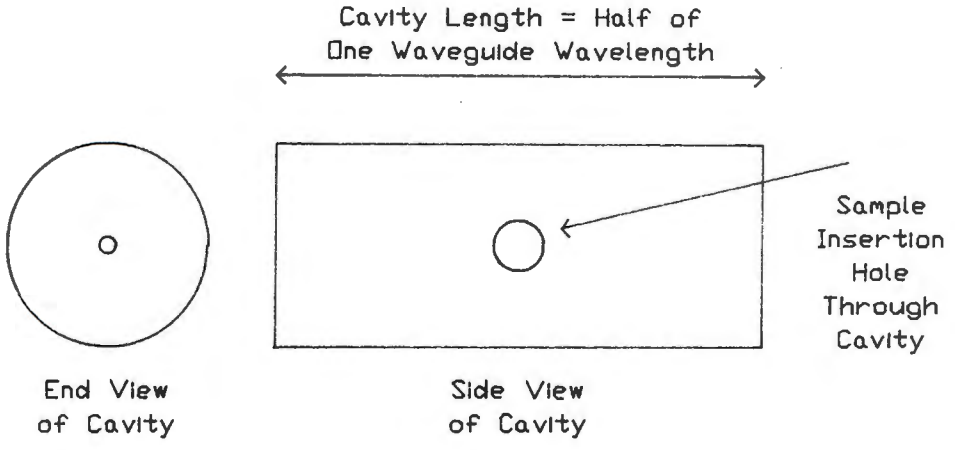

Figure 8.4. TE_{111} Cylindrical cavity

The cylindrical waveguide launchers were also fabricated from the tubing with internal diameter D = 0.093m. The launchers were flange mounted onto the cavity. The launcher sections were constructed at least four wavelengths long to ensure that the correct field distributions were established before being coupled into the cavity.

A problem was encountered with the matching and positioning of the E field probes as no reference launcher or standard 50Ω termination was available for testing these probes. To overcome this problem a tapered load consisting of lossy card was placed into the waveguide to provide a well matched load. This functioned well as a matched load.

The probes were then optimally positioned and trimmed to obtain a better than 10dB return loss (S_{11}) from 2.2GHz to 2.5GHz.

8.1.1.2. Construction of two way Power Splitters

Different types of quadrature power splitter were examined [22-24] and a Wilkinson in-phase power splitter [25] with unequal length cables was chosen for ease of fabrication. This was fabricated using RT Duroid 5880 microstrip board.

A two way Wilkinson divider/combiner (a reciprocal device) is shown in figure 8.5.

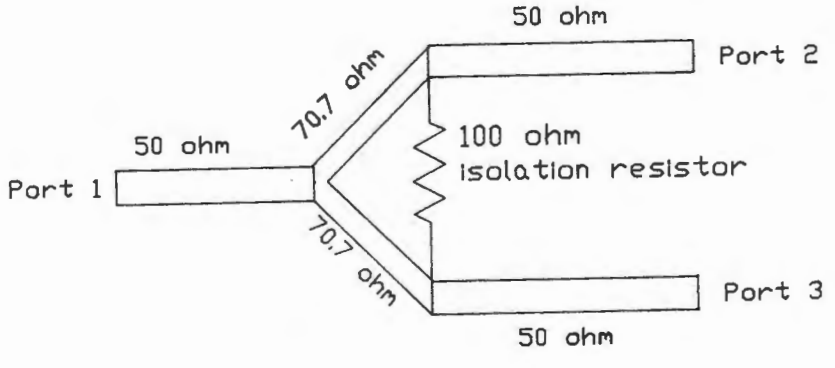

Figure 8.5. 2 Way Wilkinson power divider/combiner

The line thicknesses and lengths for the 50Ω and 70.7Ω lines were determined using the software package LINECALC. The response of a 2GHz two way power splitter is shown in figure 8.6.

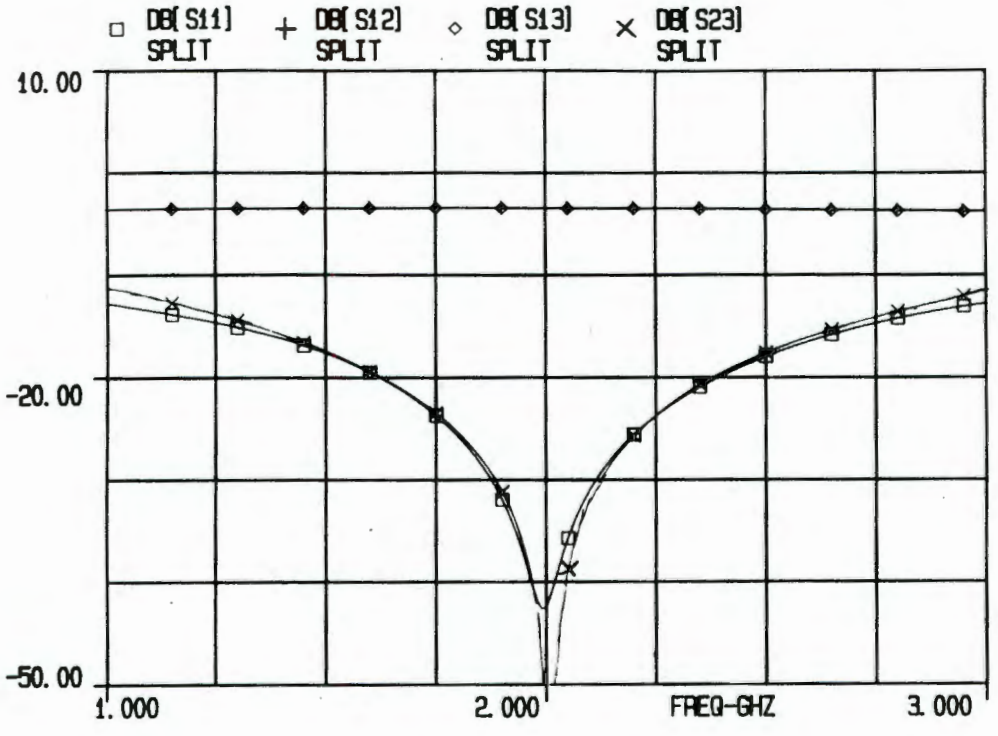

Figure 8.6. Response of Wilkinson Power Splitter

This plot was produced by entering a nodal model of the device into the software package TOUCHSTONE. This nodal model is shown in Appendix D. This device was designed to operate at 2GHz but will still function satisfactorily at 2.4GHz. A 90^{o} electrical length of line at 2.4GHz was added to one leg to produce the required phase difference between the two output ports. This is shown in figure 8.7.

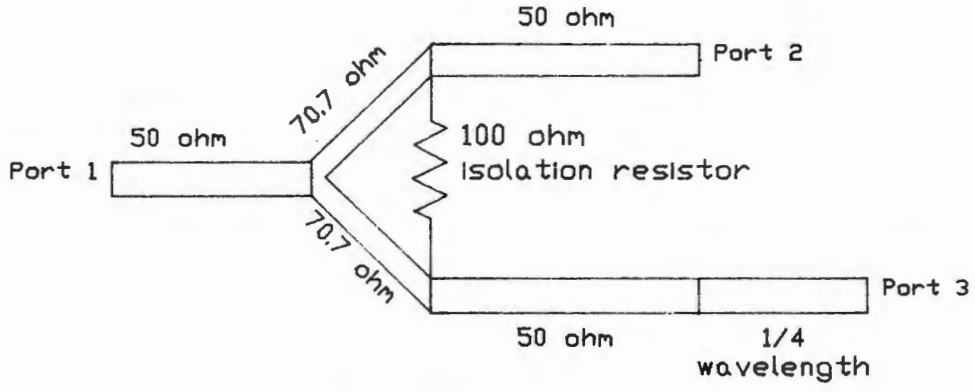

Figure 8.7. Wilkinson coupler with 90° phase lag.

The foil pattern for these couplers is given in Appendix D. The phase difference between the two outputs was measured to be 90° at 2.4GHz. A HP8410C network analyser was used for this investigation. The insertion loss for the device was measured to be 0.2dB.

8.1.1.3. Results

A study of the linearly polarised TE_{111} cavity revealed problems with signal polarisation twisting (repolarisation). The cavity shown in figure 8.8. has the sample insertion hole in line with the E field probes in the launchers.

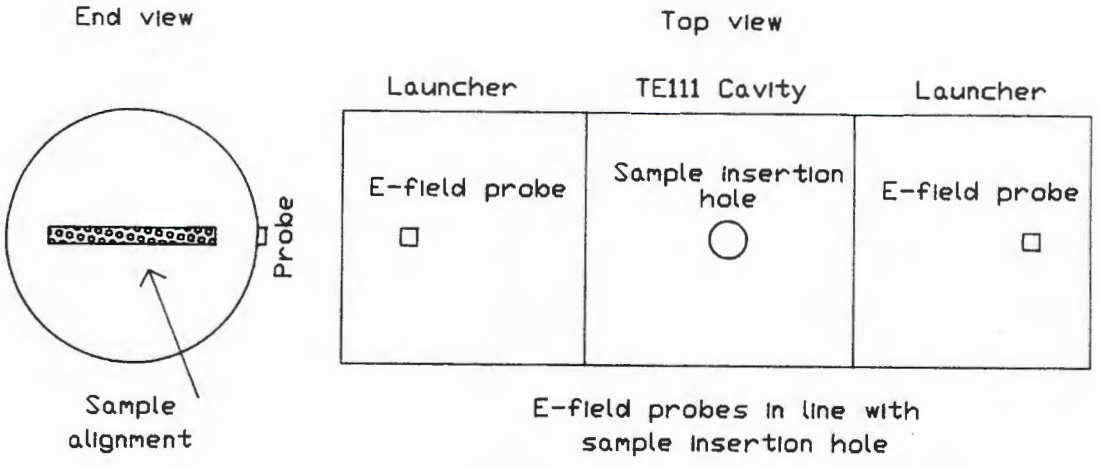

Figure 8.8. Alignment of E field probes and sample hole

A cylindrical sample (a water load or moist chalk) was placed into the cavity as indicated in figure 8.8. The system appeared to function correctly with this geometry ie. the sample was inserted and a resonant frequency change and a Q factor change were noted.

The system was then reconnected as shown in figure 8.9.

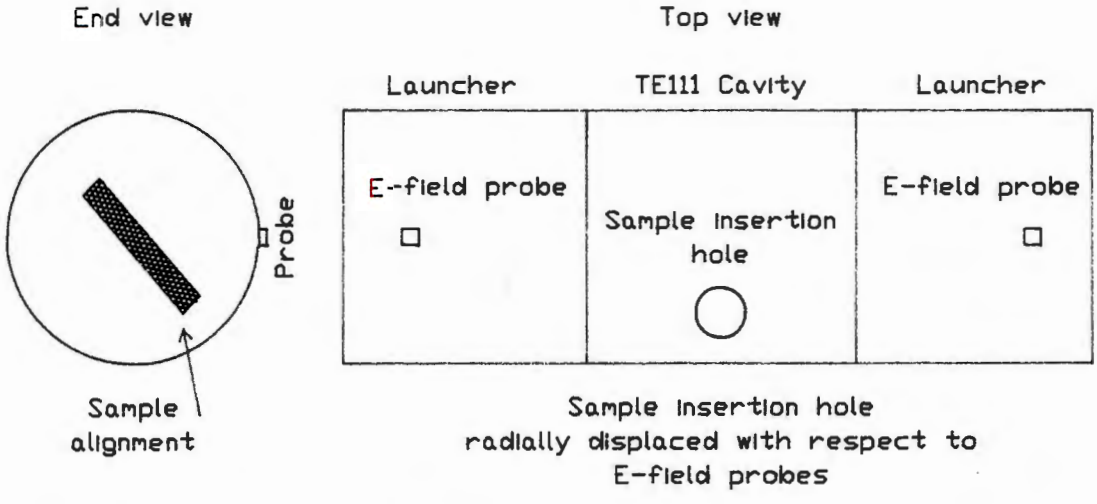

Figure 8.9. Cavity with misaligned sample hole and E field probes

The sample insertion hole was displaced from the E field probes by 45^{o}. The E field probes were aligned with each other. When a cylindrical sample was inserted as shown in figure 8.9. then no output signal was visible. The receiving launcher was then rotated until it's E field probe was in line with the sample. At this point the resonant peak was visible again. Thus energy is transferred from the original plane of polarisation and this energy will not be detected by the receiver probes. This test was repeated with different displacements of the sample hole and similar, repeatable results were obtained.

The above results clearly demonstrate that polarisation twisting can occur in TE_{111} cavities. This did not occur in the rectangular waveguide cavity described in chapter seven as the b dimension was chosen so that it was below the cut off frequency. This type of cavity is therefore

not suited to on-line processing of irregular shaped samples.

The circular polarised system was unsuccessful due to practical problems of maintaining polarisation over the swept frequency range caused largely by poorly matched launchers. Isolators, linearly polarised devices, can be used to improve the impedance match in a linearly polarised system but not for circularly polarised systems. Matching sections could not be fabricated from microwave attenuative material as, due to it's high dielectric properties, it could not be machined accurately enough to preserve the orthogonal phase relationship of the launched signals.

8.1.2. Investigation of TM_{011} Cylindrical Cavity

The lowest frequency of operation for a cavity is referred to as it's dominant mode. Referring to figure 8.10, for the TM_{011} mode to be dominant, the cavity diameter D must be greater than or equal to it's axial length L. The design procedure for this type of cavity is given by Montgomery [21].

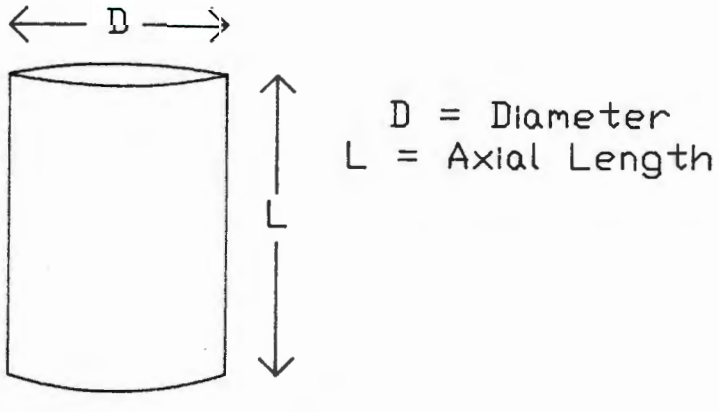

Figure 8.10 Cylindrical cavity

The field distribution for a TM_{011} cavity is shown in figure 8.11. The H-field consists of closed annular loops and the E-field is radially symmetric. The E-field maxima is in the centre of the cavity and decays to zero at the cavity walls in order to satisfy Maxwell's equations.

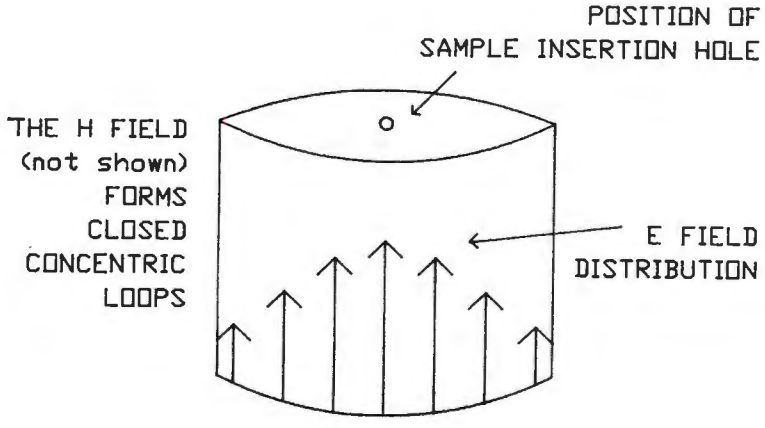

Figure 8.11. TM_{011} cavity field distribution

A 1GHz TM_{011} cavity, excited by H field loops was available for investigation. A non-radiating hole was cut into the centre of the cavity as shown above. This hole is non-radiating because, due to the field distribution in the cavity, the flow of surface currents in the walls is not interrupted by the hole.

The radially symmetric E-field distribution offers some degree of orientation independence. A 30ml cylindrical shaped water load was inserted into the cavity in a horizontal plane as shown in figure 8.12.

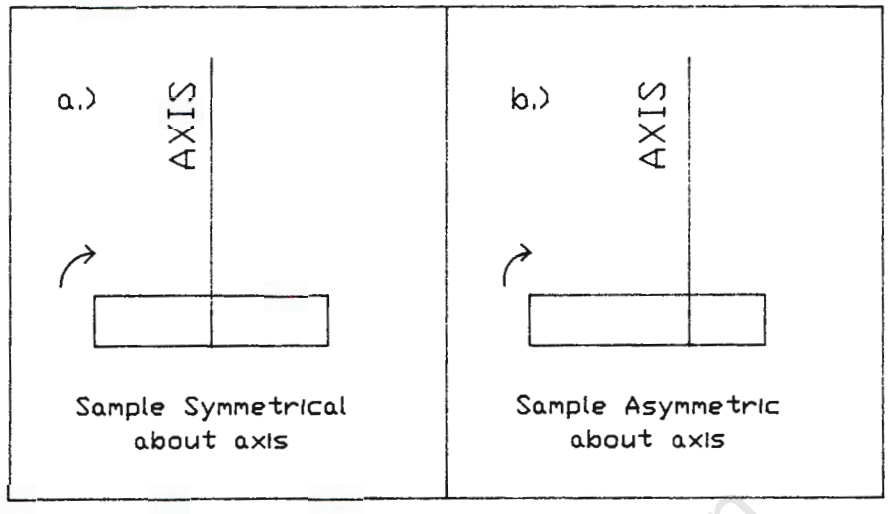

Figure 8.12. Cylindrical load in TM_{011} cavity

The cylindrical load was swung about an axis as shown in a) and b) above. In both instances, there was no change in resonant frequency or Q factor as the sample was rotated about the axis.

The vertical orientation of the sample is shown in figure 8.13.

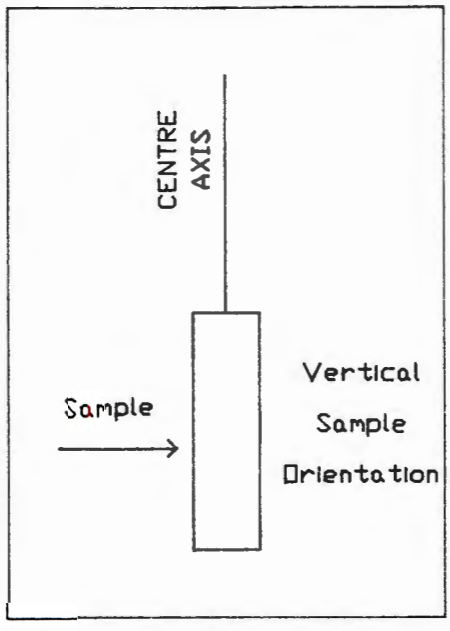

Figure 8.13. Vertical sample orientation

The vertical sample orientation gave very different results to those orientations shown in figure 8.12. A much greater frequency shift was observed due to the greater coupling to the E field in the vertical orientation.

The above results indicate that sample orientation independence was achieved in two planes due to the inherent E field structure of this cavity. No fundamental problems such as signal repolarisation were observed with this cavity. It would therefore appear that the TM_{011} cavity geometry is better suited to on-line product evaluation than the TE_{111} cavity.

A system that evaluates an irregular shaped object in two planes is advantageous compared to the simple linearly polarised system presented in chapter seven.

The optimum performance, however, would be obtained if the sample could be simultaneously monitored in three independent planes.

8.2. STRUCTURES WITH THREE INDEPENDENT PLANES OF POLARISATION

8.2.1. Spherical Resonant Structures

The possible use of a spherical resonant structure for on-line processing of irregularly shaped samples was considered [26]. It has been shown by Currie [27] that "The perfect geometry of a spherical resonator allows its modes to possess a high degree of degeneracy". This means that many independent field configurations have the same natural frequency of operation.

This problem, together with the problem of polarisation twisting demonstrated for a cylindrical structure (polarisation twisting would also exist in a spherical geometry) led to the conclusion that spherical cavities would not be suitable structures in this application.

8.2.2. Resonant Cube

A resonant cube was examined in an attempt to eliminate orientation dependence of irregular shaped samples. This structure was linearly polarised but was simultaneously excited in three orthogonal planes.

A diagram of this cubical cavity is given in figure 8.14. The microwave signal was coupled into the faces labelled 1, 2 and 3. The signals were coupled out of opposite faces. The samples are passed through the structure from point A to point B.

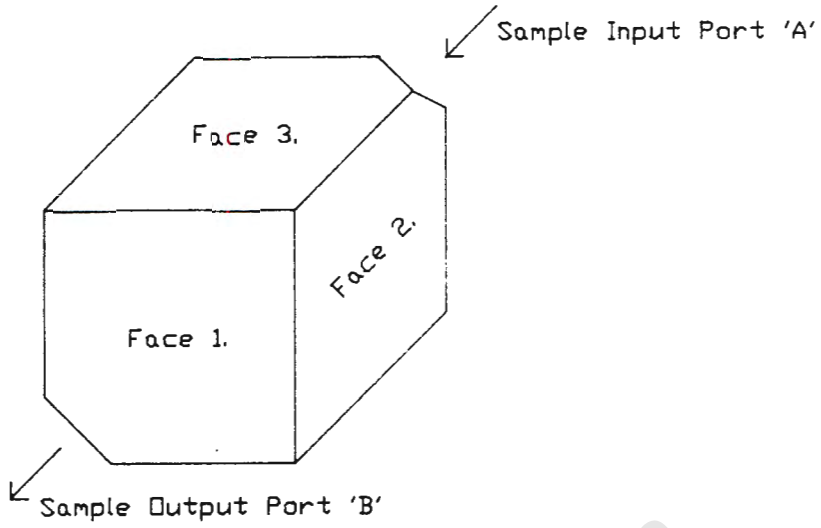

Figure 8.14. Resonant cube

With this structure it is possible to create three different directions of E-field polarisation and therefore three different directions of propagation. This is shown in figure 8.15.

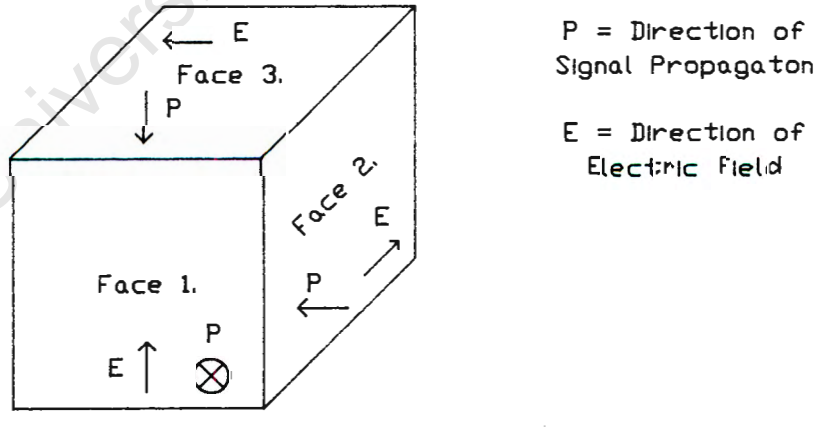

Figure 8.15. E-fields in resonant cube

At face 1 the E-field is vertical and the direction of signal propagation is away (into the page). At face 2 the direction of the E-field is away (into the page) and the direction of signal propagation is from right to left across the page. The direction of signal propagation at face 3 is vertical (from top to bottom of page) with the E-field direction from right to left across the page. It was hoped to eliminate the effect of sample orientation by performing measurements in these three mutually perpendicular planes.

The resonant cube could be connected as shown in figure 8.16.

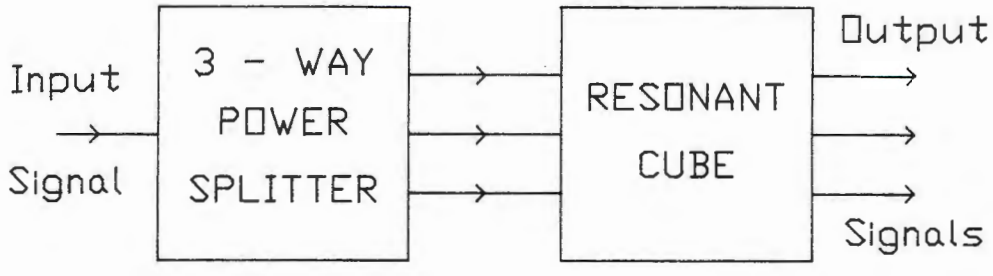

Figure 8.16. Connection of resonant cube

The input signal is fed to each face by means of a three way in phase power splitter. This is convenient for use with a network analyser. The three output signals from the cube can be processed as required. Alternatively, each face of the cube can be individually excited with separate oscillators.

A resonant cube was constructed at a frequency of 3GHz to facilitate laboratory testing. The availability of various microwave components, such as a reference

waveguide launcher, was an influential factor in the choice of operating frequency.

8.2.2.1. Construction of cavity and launchers

The microwave signals were iris coupled into the resonant cube. The signals were launched from coaxial cable to rectangular waveguide via coaxial to waveguide transformers. These were fixed onto each face of the cavity. A commercially manufactured 3GHz coaxial cable to rectangular waveguide transformer was available as a reference unit.

Figure 8.17 shows the theoretical location of the E-field probe in a waveguide launcher. This is often varied in practise in order to optimise the operating bandwidth of the unit. The properties of the E-field probe such as length, thickness and dielectric coating are also influential when determining the probe position.

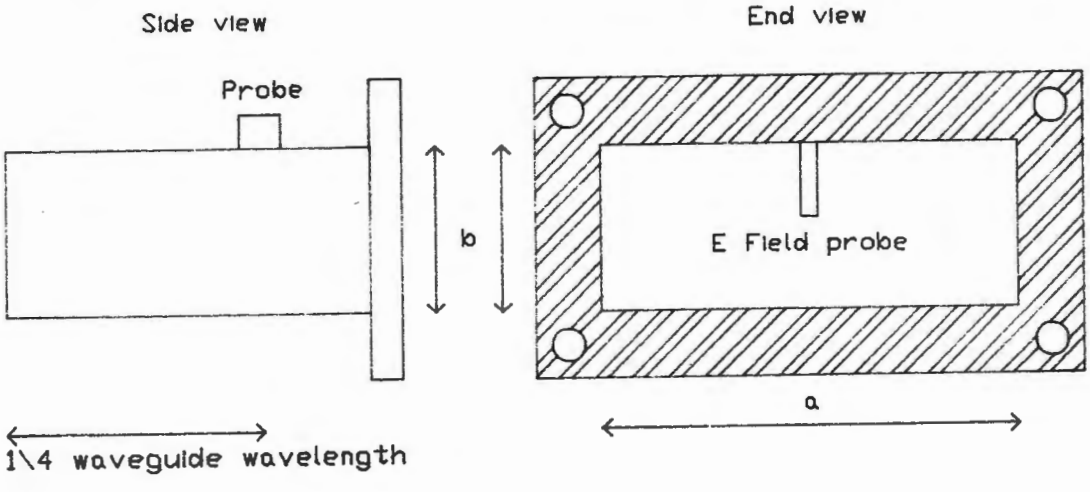

Figure 8.17. Coaxial cable to rectangular waveguide transformer

The coaxial cable to rectangular waveguide transformers were fabricated from brass. The E-field probes were matched using the commercial unit as a reference. The performance of these units was adequate with a return loss of better than 10dB from 2.5GHz to 3.1GHz.

The cavity was initially constructed as a cube with all three faces the same size. The sides of the cavity were $\lambda_g/2$ long as shown in figure 8.18. This was equal to the a dimension of the launcher rectangular waveguide.

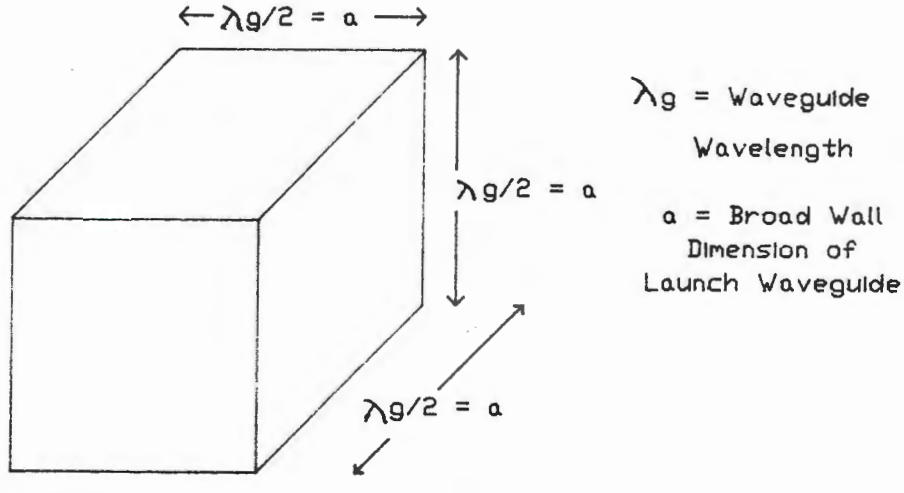

Figure 8.18. Cube dimension

In this case a = 72mm. From figure 8.18, $\lambda_g/2$ = a therefore the waveguide wavelength can be calculated. This information can be substituted into equation 3.1 to determine the freespace wavelength. Using this approach, the resonant frequency of each plane was found to be 2.946GHz. The dimensional tolerances of the cube led to a

difference of 13MHz between the lowest and highest frequency resonant peaks. The signals were iris coupled into the copper cavity through the centre of each face.

8.2.2.2. Construction of Power Splitter

The three way power splitter illustrated in figure 8.9 was implemented by fabricating a four way power splitter and terminating the fourth port in a matched 50ohm load. The four way splitter comprised of three two way Wilkinson power splitters configured as shown in figure 8.19.

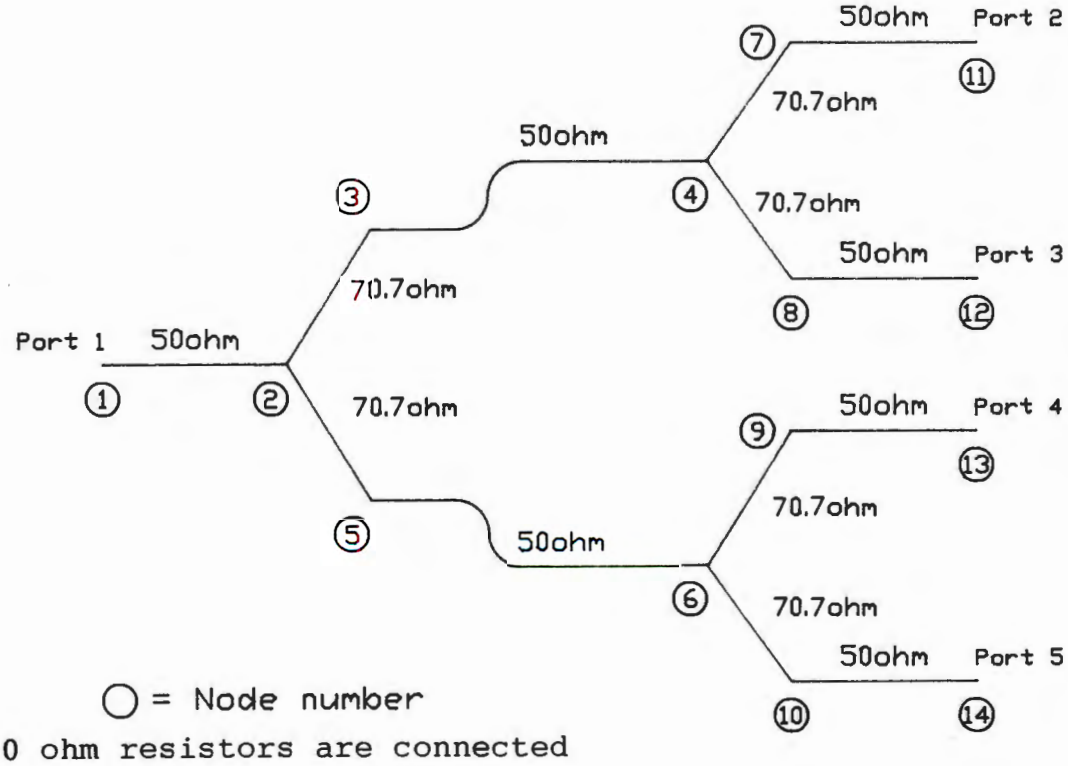

○ = Node number

100 ohm resistors are connected between nodes 3&5, 7&8, 9&10

Figure 8.19. Nodal model of four way power splitter

The software package LINECALC was used to determine the various line lengths and widths tabulated in figure 8.20. These dimensions apply to RT Duriod 5880 microstrip board with 0.254mm dielectric thickness.

Line Impedance In Ohms	Electrical Line Length	Line Width In mm.	Line Length In mm.
50 Ohms	90 Degrees	0.76 mm	18.67 mm
50 Ohms	360 Degrees	0.76 mm	74.67 mm
50 Ohms	180 Degrees	0.76 mm	37.33 mm
70.7 Ohms	90 Degrees	0.43 mm	19.01 mm

Figure 8.20. Microstrip line lengths and widths

The nodal model given in figure 8.19 was used with the TOUCHSTONE package. A listing is included in Appendix D. The theoretical response of the power splitter produced by TOUCHSTONE is shown in figure 8.21.

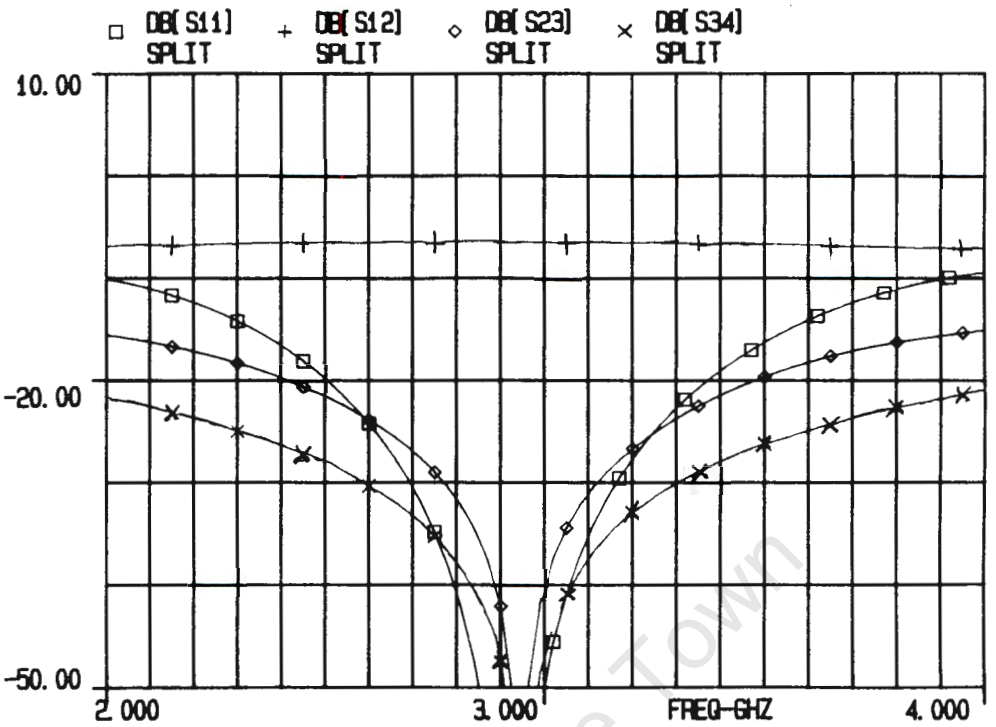

Figure 8.21. Response of power splitter

The performance of the actual device was good with each port having an insertion loss of 6.3dB. The return loss S_{11} was measured to be 34dB at 3.03GHz. The 100ohm chip resistors were epoxy bonded to the board. A foil layout is given in Appendix D.

8.2.2.3. Results

Cylindrical chalk samples of diameter 1cm were examined in the cavity. Sample lengths from 1cm to 3cm were studied. The system performed well for dry samples which had a much lower dielectric constant than wet samples. The results shown in figure 8.22 are for 2cm long dry chalk samples in various orientations. These data were obtained by

static measurement with the samples held in position by means of expanded polystyrene foam. Refer to figure 8.15 for an explanation of the different planes and E-field orientations.

	CHANGE IN FREQUENCY	CHANGE IN Q FACTOR	CHANGE IN FREQUENCY	CHANGE IN Q FACTOR	CHANGE IN FREQUENCY	CHANGE IN Q FACTOR
PLANE 1	46.8 MHz	836.5	25.9 MHz	559.1	26.1 MHz	559.1
PLANE 2	24.3 MHz	417.3	48.2 MHz	613.9	24.5 MHz	359.3
PLANE 3	25.5 MHz	534.4	26.1 MHz	529.5	50.3 MHz	743.1
	Sample aligned with Emax in Plane 1.		Sample aligned with Emax in Plane 2.		Sample aligned with Emax in Plane 3.	

Figure 8.22. Results for 2cm dry chalk samples

It can be seen from figure 8.22 that the greatest change in resonant frequency shift occurs when the sample is aligned with the E-field. This is consistent for the three different sample orientations shown. The same information about the sample is provided for each of the three sample orientations, provided that all three planes are monitored. The change in Q factor appeared to be less consistent. This could have been due to experimental inaccuracy caused by the samples not being positioned accurately enough.

The cylindrical samples have a much higher dielectric constant when the water content is increased. The cavity gave poor results when analysing these wet samples, even with short 1cm long samples. It was found that multiple resonant peaks would appear at the output of each plane.

When these peaks were closely examined it was found that there was an interaction between the different planes.

Each individual plane appeared to function correctly but extra resonant peaks corresponding to the other planes were visible. For example, if a sample were aligned with the E-field maxima in plane 2 then this plane would experience the greatest resonant frequency shift and the greatest change in Q factor. This was correctly observed. However, a resonant peak at the resonant frequency observed for planes 1 or 3 would also be observed on the output of plane 2. This extra peak was of greater amplitude than the correct peak for plane 2 due to the lesser E-field interaction in the other planes (1 and 3). Now, using electrical detection mechanisms, it is not possible to correctly identify the correct peak for each plane.

The abovementioned problem was clearly serious and a cure had to be effected. This problem could have been due to the interaction of the similar H field patterns for the three different planes.

The problem was one of isolating the correct resonant peaks. A solution appeared to be to separate the different resonant peaks. The resonant frequencies of the three different planes were shifted apart by approximately 70MHz each by changing the cavity dimensions. This resulted in a rectangular parallelopiped simultaneously excited in three orthogonal planes. This will eliminate the polarisation coupling from the excited plane to the other two planes as the

coupled planes will not be resonant at the same time as the excited plane and can, therefore, not support a cavity mode.

The existing cavity was modified as shown in figure 8.23.

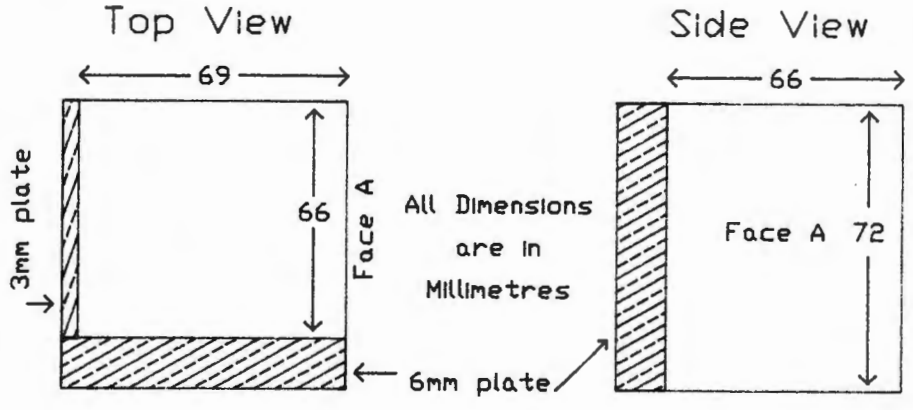

Figure 8.23. Modified cavity dimensions

Copper plates were fixed into the cavity to reduce its internal dimensions. The new resonant frequencies in each plane can be calculated using a standard formula [28]. The measured resonant frequencies do, however, differ from the calculated values for a number of reasons. Some of the walls are thicker than the original cavity walls. This means that some of the iris holes are effectively thicker than others. No iris hole was thicker than 2mm but the thicker walls had to be recessed to facilitate this (this could be viewed as a composite iris of varied thickness). The effect of iris thickness has been documented by Marcuvitz [29].

Tests with the new modified cavity indicated that it performed well. The results with the dry chalk samples were similar to those for the original cavity for all lengths of sample from 1cm to 3cm. Tests were performed using various lengths of wet chalk samples. The new cavity performed well and no interpeak interference was observed. If any signal interference did occur it was well off the resonant frequency being examined and was very low level.

The results shown in figure 8.24 were for a 2cm wet chalk sample aligned with the E-field maxima of plane 2. The samples were angled at 45^{o} as shown.

PLANE	CHANGE IN FREQUENCY 1	CHANGE IN FREQUENCY 2
1	63.0	70.8
2	88.9	80.6
3	47.0	47.0

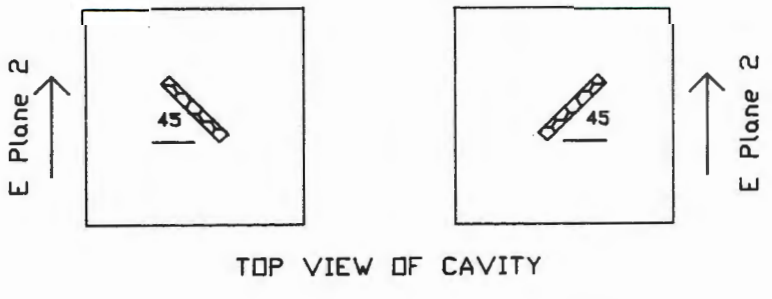

Figure 8.24. 2cm Wet chalk in new cavity

These results clearly indicate that the greatest frequency shift occurs in the plane in which the sample is aligned with the E-field.

Experiments were then performed with rectangular samples of apple of varied size and mass. If a linear correlation of sample mass versus frequency shift were possible then this cavity structure could be used in on-line applications for processing irregular shaped samples. A lower operating frequency would be used to process the larger samples but the concept and principle remain identical.

A plot of sample mass versus frequency shift is shown in figure 8.25. These data were obtained using 32mm long rectangular shaped samples. The other two sample dimensions were varied to obtain samples of different mass. The cavity outputs were recorded for different orientations of the samples. The cavity output with the greatest observed frequency shift was selected and plotted in figure 8.25. The other two cavity outputs were ignored. It can be seen that there is good correlation between maximum frequency shift and sample mass.

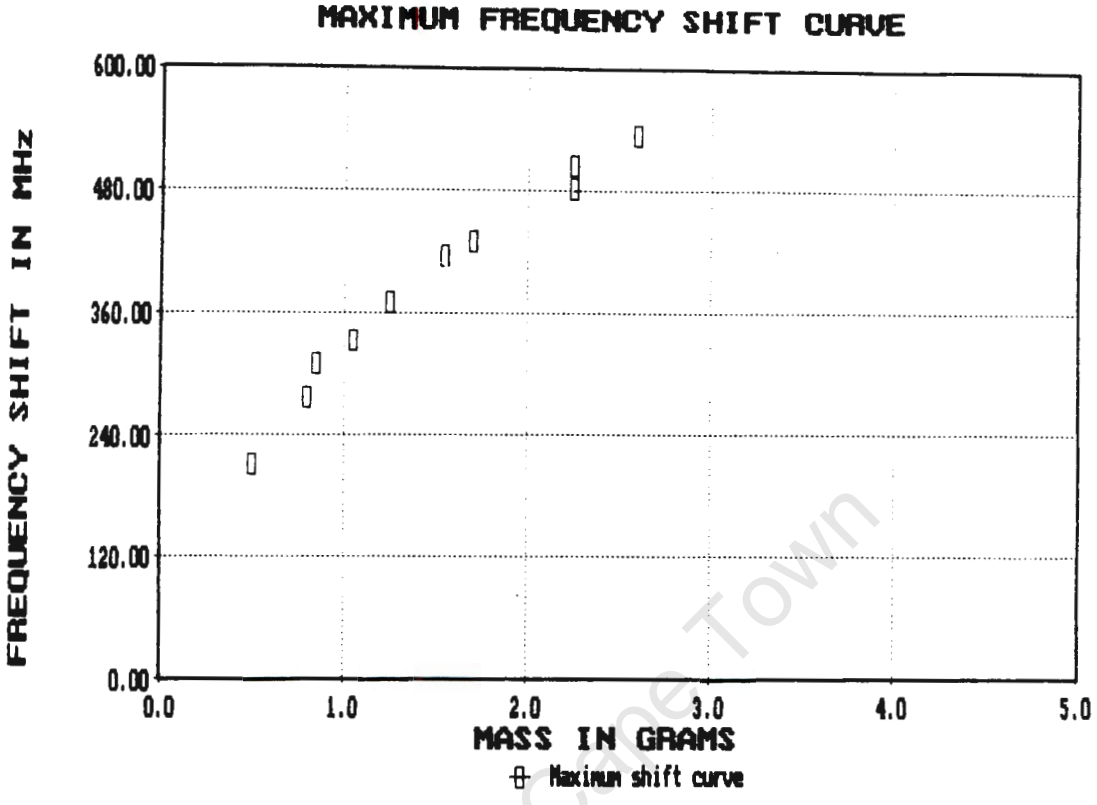

Figure 8.25. Plot of sample mass versus maximum frequency shift

This curve, however, discards information from two of the three cavity outputs. Improved accuracy can be obtained by using the information from all three cavity outputs. Preliminary tests were performed using a single plane of polarisation. Dielectric rods of equal diameter but different lengths were studied in the cavity.

Plots of sample length versus frequency shift and sample mass versus frequency shift are shown in figure 8.26 and figure 8.27.

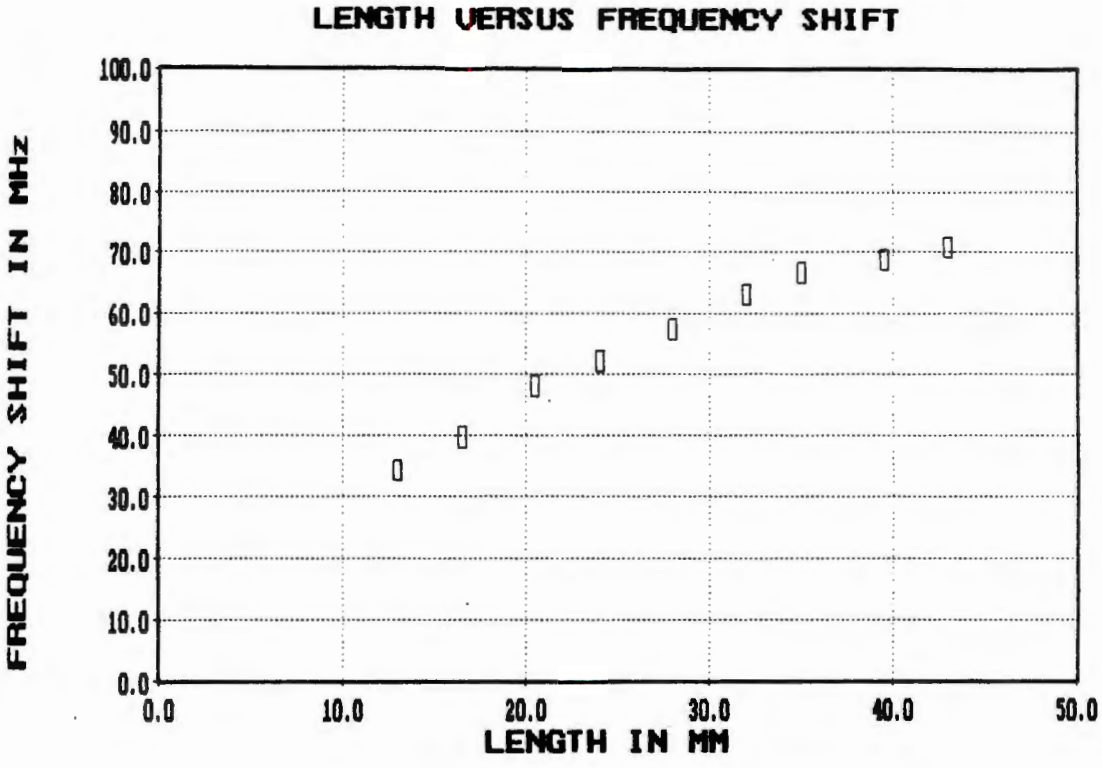

Figure 8.26. Sample length versus frequency shift

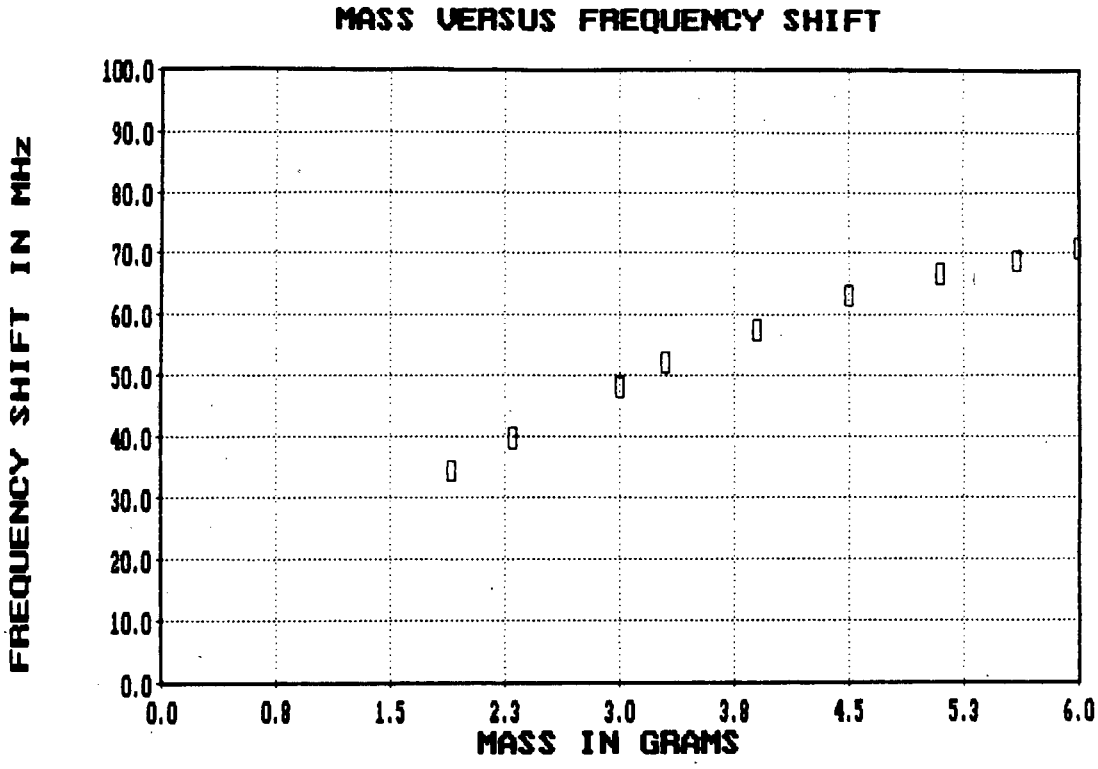

Figure 8.27. Sample mass versus frequency shift

It can be seen from these plots that there is a linear relationship between sample mass and frequency shift and between sample length and frequency shift. Although some nonlinearity occurs at the upper end of these curves, they are linear over the ranges being considered. The longest sample used for figure 8.25 was 32mm and the sample mass did not exceed 2.6g.

Pythagoras' theorem can be used to determine the length of a sample, as shown in figure 8.28, by calculating the square root of the sum of the squares of the components in orthogonal planes. This argument is also valid for three orthogonal planes.

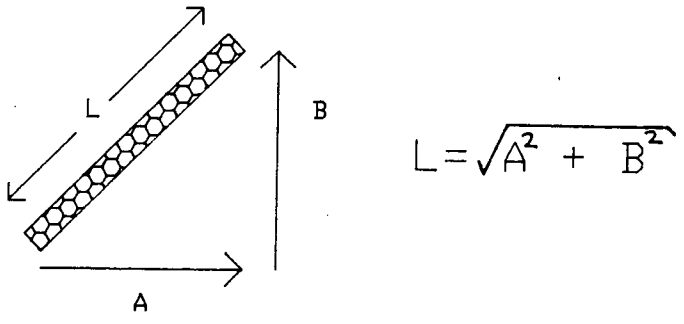

Figure 8.28. Pythagoras theorem for two orthogonal planes

There are three orthogonal and independent planes of polarisation in the resonant cavity under consideration. In the light of the above information, the square root of the sum of the squares of the three cavity outputs should provide useful information regarding the mass of a sample.

The data for figure 8.25 was used again but the information from all three cavity outputs was combined as suggested above. This curve is shown in figure 8.29. It can be seen that the linearity of the curve has improved when compared with figure 8.25.

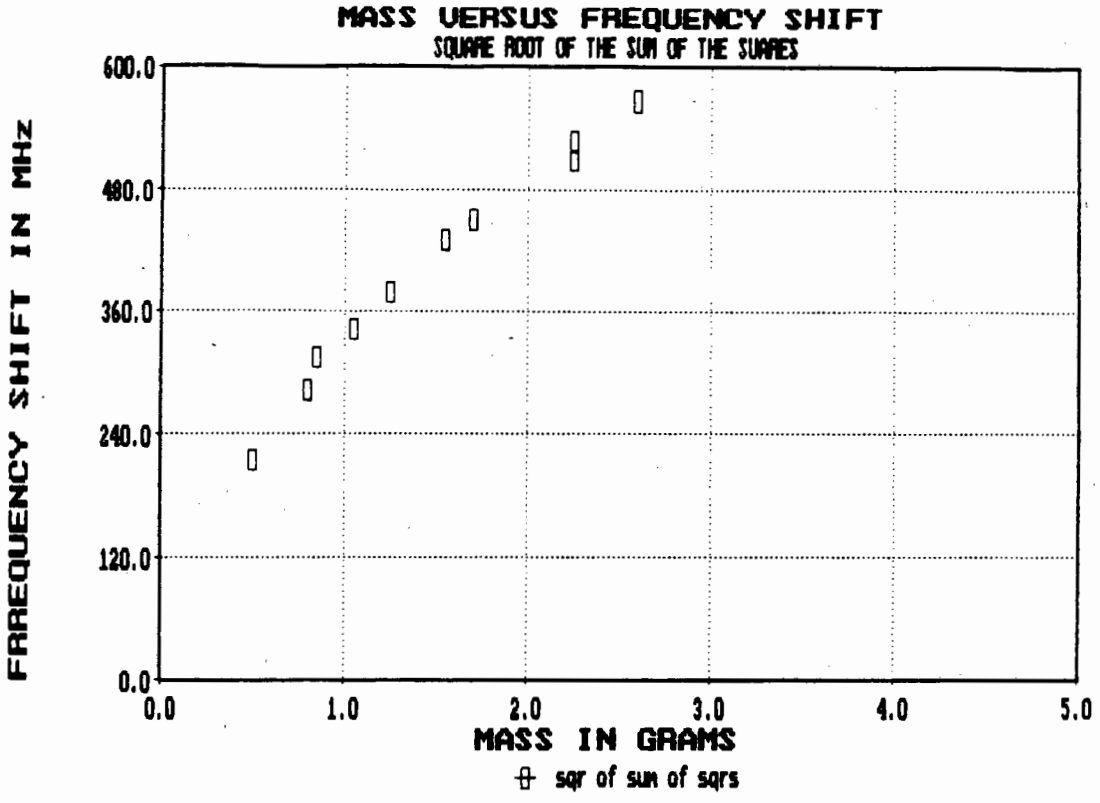

Figure 8.29. Plot of the square root of the sum of the squares of the cavity outputs versus mass.

The effect of widely varied sample shape was examined. Rectangular samples of lengths ranging from 10mm to 35mm were considered. The other two sample dimensions were also varied to obtain samples of different mass. The cavity output with the greatest change in resonant frequency was plotted in figure 8.30. It can be seen that the correlation between sample mass and maximum frequency shift is much poorer than with the previous data. This is due to the greatly differing sample dimensions in that two samples with very different geometries can have the same mass.

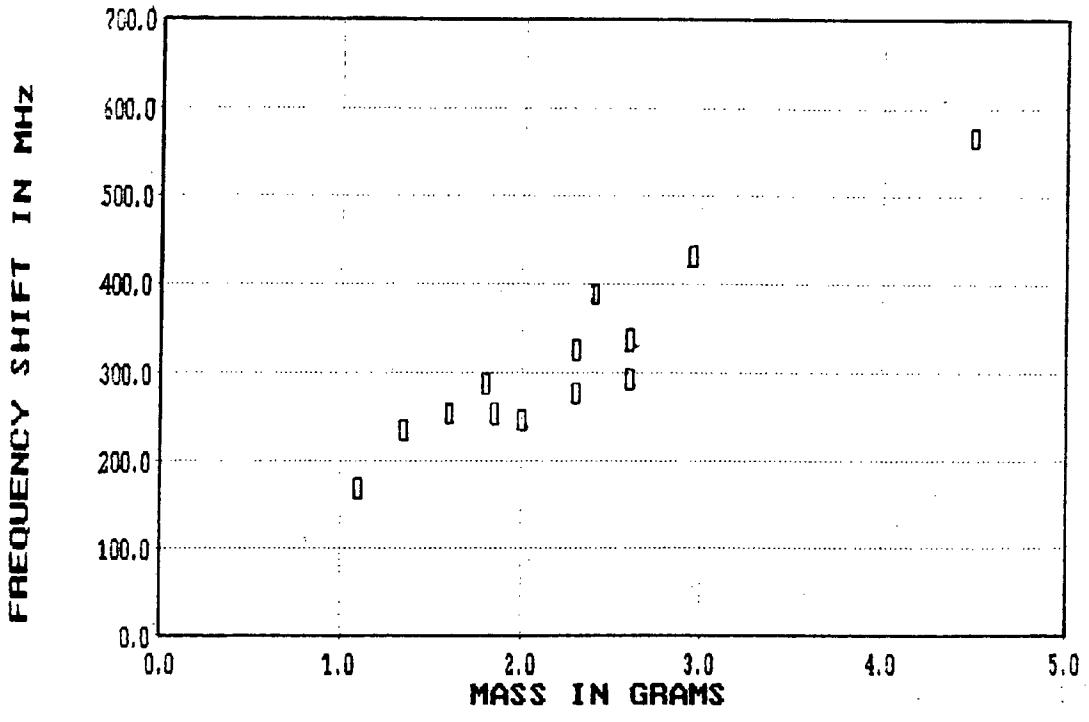

Figure 8.30. Plot of sample mass versus maximum frequency shift

When all three cavity outputs are considered, the linearity of the curve is again improved. The square root of the sum of the squares of the cavity outputs is plotted in figure 8.31.

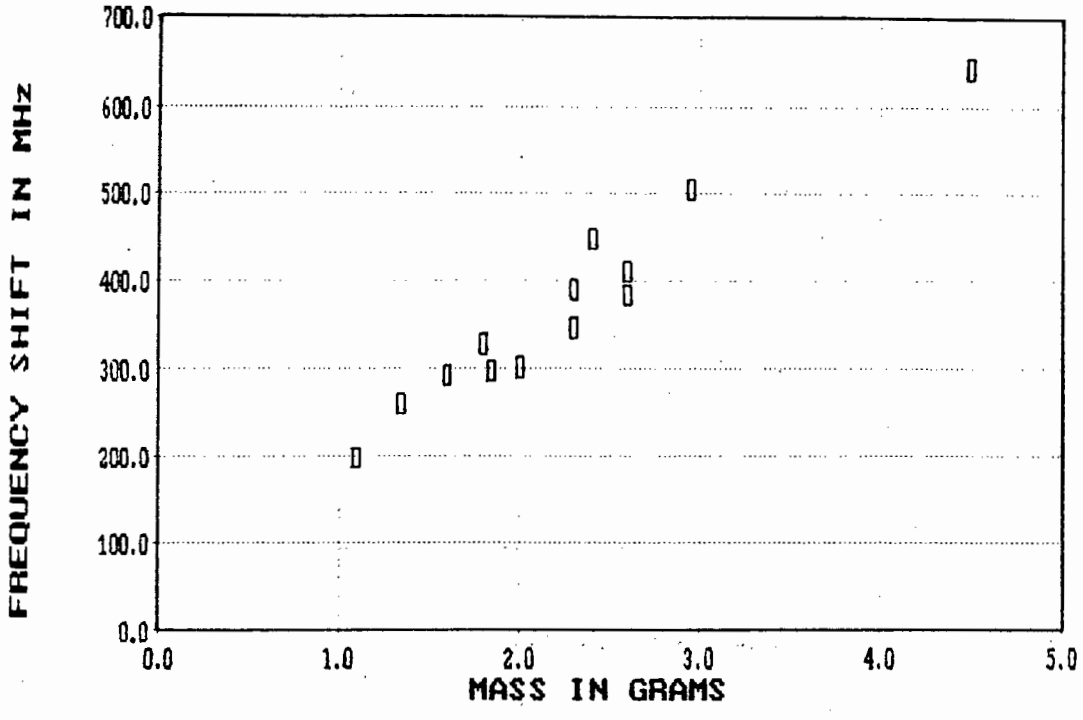

Figure 8.31. Sample mass versus the square root of the sum of the squares of the cavity outputs

The plot shown in figure 8.31 represents samples with a size variation of 3.5 to 1. For applications where a high degree of accuracy is required, the samples would have to be so screened to control their dimensional variation. There is a trade off between the accuracy of mass measurement and the sample dimensions. This can be seen by comparing figure 8.29 and figure 8.31. there is a better correlation between the sample mass and frequency shift when the samples are closely sized. This resonant cavity was, however, able to provide useful data for samples with a size variation of 3.5 to 1.

A viable resonant structure for on-line processing of irregular shaped dielectric samples has been devised, constructed and tested [30,31]. This structure, simultaneously excited in three different planes, allows correct analysis of the sample by providing information from three independent planes of polarisation.

8.3. LIST OF REFERENCES

[1] MULLER, W., KRAMER, C., KRUEGER, J., "Calculation of 2- or 3-dimensional linear or nonlinear fields by the CAD-program PROFI", IEEE vol. MA 6-19, no 6, Dec 1983, pp 2670-2673.

[2] KOSHIBA, M., HAYATA, M., SUZUKI, M., "Improved Finite-Element Formulation in Terms of the Magnetic Field Vector for Dielectric Waveguides", IEEE vol. MTT-33, no 3, March 1985, pp 227-233.

[3] KOSHIBA, M., HAYATA, K., SUZUKI, M., "Finite-Element Formulation in Terms of the Electric-Field Vector for Electromagnetic Waveguide Problems", IEEE vol. MTT-33, no 10, Dec 1985, pp 900-905.

[4] SILVESTER, P., "A General High-Order Finite-Element Waveguide Analysis Program", IEEE vol. MTT-17, no 4, April 1969, pp 204-209.

[5] TORTSHANOFF, T., "Survey of numerical methods in field calculations", IEEE vol. MAG-20, no 5, Sept 1984, pp 1912-1917.

[6] ENGLISH, W.J., "Vector Variational Solutions of Inhomogeneously Loaded Cylindrical Waveguide Structures", IEEE vol. MTT-19, no 1, Jan 1971, pp 9-18.

[7] HORNSBY, J.S. GOPINATH, A., "Numerical Analysis of a Dielectric-Loaded Waveguide with a Microstrip Line-Finite-Difference Methods", IEEE vol. MTT-17, no 9, Sept 1969, pp 684-690.

[8] MARTINELLI, M., ROLLA, P.A., TOMBARI, E., "A Method for Dynamic Dielectric Measurements at Microwave

Frequencies : Applications to Polymerization Process Studies", IEEE vol. IM-34, no 3, Sept 1985, pp 417-421.

[9] CSENDES, Z.J., SILVESTER, P., "Numerical Solution of Dielectric Loaded Waveguides : I-Finite-Element Analysis", IEEE vol. MTT-18, no 12, Dec 1970, pp 1124-1131.

[10] THOMAS, D.T., "Functional Approximation for Solving Boundary Value Problems by Computer", IEEE vol. MTT-17, no 8, Aug 1969, pp 447-454.

[11] BARLOW, H.E.M., EFFEMEY, H.G., "Propagation characteristics of low-loss tubular waveguides",

[12] AGDUR, B., ENANDER, B., "Resonances of a Microwave Cavity Partially Filled with a Plasma", J. of Applied Physics, vol. 33, no 2, Feb 1962, pp 575-581.

[13] HORNER, F., TAYLOR, T.A., DUNSMUIR, R., LAMB, J., JACKSON, W., "Resonance methods of dielectric measurement at centimetre wavelengths", Proc.Inst.Elec.Eng.(London), vol. 93, pt. III, pp 53-68, 1946.

[14] SAITO, S., KUROKAWA, K., "A Precision Resonance Method for Measuring Dielectric Properties of Low-Loss Solid Materials in the Microwave Region", Proc. IRE, Jan 1956, pp 35-42.

[15] SPROULL, R.L., LINDER, E.G., "Resonant-Cavity Measurements", Proc. IRE, May 1946, pp 305-312.

[16] MARTINELLI, M., ROLLA,P.A., TOMBARI, E., "A Method for Dielectric Loss Measurements by a Microwave Cavity in

Fixed Resonance Condition", IEEE vol. MTT-33, no 9, Sept 1985, pp 779-783.

[17] LI, S., AKYEL, C., BOSISIO, R.G., "Precise Calculations and Measurements on the Complex Dielectric Constant of Lossy Materials using TM_{010} Cavity Perturbation Techniques", IEEE vol. MTT-29, no 10, Oct 1981, pp 1041-1047.

[18] MARGINEDA, J., MARTIN, E.F., QUINTILLAN, M., "Ambiguity Elimination in the Measurement of Permittivity with TE_{011} Cylindrical Cavities", IEEE vol. IM-30, no 1, March 1981, pp 71-73.

[19] LI, S., BOSISIO, R.G., "Composite Hole Conditions on Complex Permittivity Measurements using Microwave Cavity Perturbation Techniques", IEEE MTT-30, no 1, Jan 1982, pp 100-103.

[20] ESTIN, A.J., BUSSEY, H.E., "Errors in Dielectric Measurements Due to a Sample Insertion Hole in a Cavity", IRE Trans. on Microwave Theory and Tech., Nov 1960, pp 650-653.

[21] MONTGOMERY, C.G.,"Techniques of Microwave Measurement", MIT Radiation Laboratory Series, vol.11 , p 297.

[22] TOKUMITZU, Y., SAITO, T., OKUBO, N., KANEKO, Y., "A 6-GHz 80-W GaAs FET Amplifier with a TM-Mode Cavity Power Combiner", IEEE vol. MTT-32, no 3, March 1984, pp 301-308.

[23] DYDYK, M., "Efficient Power Combining", IEEE vol. MTT-28, no 7, July 1980, pp 750-760.

[24] COHN S.B., "A Class of Broadband Three-Port TEM-Mode Hybrids", IEEE vol. MTT-16, no 2, Feb 1968, pp 110-116.

[25] WILKINSON, E.J., "An N-Way Hybrid Power Divider", IRE Trans. Microwave Theory Tech., vol. 13, no 1, Jan 1965.

[26] HARVEY, A.F., "Microwave Engineering", Academic Press Inc(London)Ltd, 1963, pg 216.

[27] CURRIE, M.R., "The Utilization of Degenerate Modes in a Spherical Cavity", J. of Applied Physucs, vol. 24, no 8, Aug 1953, pp 998-1003.

[28] MONTGOMERY, C.G., "Techniques of Microwave Measurement", MIT Radiation Laboratory Series, vol.11 , p 295.

[29] MARCUVITZ, N., "Waveguide Handbook", MIT Radiation Laboratory Series, vol. 10, pg 408.

[30] MERCER, S., DOWNING, B.J.,"On line fruit weighing using resonant cavity techniques.",Joint IEEE & SAIEE Symposium on Antennas and Propagation and Microwave Theory and Techniques,24 August 1990.

[31] MERCER, S., DOWNING, B.J.,"A cavity system for online processing of irregularly shaped samples.",Electronics Letter - in print.

CHAPTER 9

9.0 CONCLUDING REMARKS

The use of microwave signal transmission measurements has been shown to be a viable method of on-line sample discrimination. A number of different methods of signal propagation and application were investigated.

The microwave heating method was shown to be impractical in applications such as on-line ore sorting due to it's high power requirements. The microwave signal reflection method was found to be suitable for the study of a continuous product stream. The method did not appear viable for use with discrete samples due to problems with signal scattering. The concept of passing a product through an overmoded waveguide was shown to be impractical due to signal propagation around the sample.

Microwave signal attenuation between two antennae was shown to be successful in a previously unsolved ore sorting problem of separating dimendiferous kimberlite from barren gabbro. A detectable difference in signal attenuation was found between the two rock types. The use of reduced aperture antennae for discrimination of small samples was investigated. Resonant patch antennae and dielectrically loaded antennae were, however, shown to have poor performance.

A study of different types of resonant structure was undertaken to measure, on-line, the complex dielectric constant. Rectangular waveguide was shown to be more suitable than coaxial or stripline structures for dielectric examination. The electric field in the rectangular waveguide structure is constrained such that a dielectric sample must pass through it's maxima. Possible field distortions in the TEM structures (coaxial and stripline

structures) make them less attractive for the purpose of sample analysis.

A linearly polarised rectangular waveguide cavity was found to be successful in the analysis of regular shaped objects. Problems were, however, encountered with irregular shaped samples in that different results were obtained for different sample orientations. This led to the investigation of structures with two independent planes of polarisation.

A TE_{11} cylindrical cavity was found to be unsuitable for analysis of irregular shaped objects that were dropped through it. Signal polarisation twisting was shown to occur in this structure. An attempt was made to establish circular polarisation in this cavity but this was found to be impractical due to problems with poorly matched launchers.

A study of a TM_{011} cylindrical cavity indicated that this structure offered an improvement over the linearly polarised rectangular waveguide cavity due to it's radially symmetric electric field distribution. This cavity was shown to offer orientation independence in two planes. In an attempt to completely categorise a sample, the concept of multiple planes of polarisation was extended to three independent planes.

Spherical cavity structures were deemed unsuitable due to the high degree of degeneracy in their field distributions. The use of a resonant cube was then investigated. This was linearly polarised but simultaneously excited in three different planes. The results were promising but problems with ambiguity were encountered due to the three very close resonant frequencies.

A rectangular parallelopiped was used to eliminate the ambiguity problem. The three different planes of polarisation had different resonant frequencies. It was shown that sample length and mass were directly proportional to resonant frequency shift in the cavity. Using this information and Pythagoras' theorem, the three separate cavity outputs were combined.

The square root of the sum of the squares of the cavity outputs was plotted. The results indicated that the effect of the orientation of an irregular shaped sample was significantly reduced by using this method. A structure had been developed to improve the accuracy of results by reducing the effect of sample orientation in the measuring cavity.

APPENDIX A

An approximate calculation of the power requirements of an on line microwave rock heating plant.

This calculation is based on the work of M.A. Aldera [1]. It was found by experimentation that the temperature of a 230g kimberlite sample was raised by 50°C after a one minute exposure to an incident power of 500W at a frequency of 2.45GHz.

From elementary Physics:

$$\Delta H = mc\Delta T$$

where ΔH = the change in the samples heat content in Joules.

m = the mass of the samples in grams.

c = the specific heat capacity of the sample.

Now if t is the time period of heating then

$$\Delta H/\Delta t[\text{watts}] = mc\Delta T/\Delta t$$

where $\Delta H/\Delta t$ = the power required in Watts to heat the sample by a given temperature ΔT in a given time.

The specific heat capacity "c" lies within the range 0 to 1. A value of c = 0.5 is assumed for this calculation.

The power required to heat a 230g kimberlite sample by 30°C in 1 minute is therefore:

$$P_i = \Delta H/\Delta t = 230 * 0.5 * 50/60 = 95.8W$$

A transmission line equivalent circuit of the rock heating process is indicated in figure A1.1.

$$P_t = 0.5 * \Delta T_k * 10^6 \ (1 - |\rho|^2)$$

Assuming that the rocks are transported at a rate of 15 tons/minute, (0.25 tons/second) and the required rise in the temperature of kimberlite is $10^{o}C$ to effect reliable rock differentiation then

$$P_t = 0.5 * 0.25 * 10^7 / 0.19$$
$$= 6.58MW$$
$$= \text{required microwave power}$$

This calculation may yield a pessimistic result due to the approximate nature of the data used but serves to indicate that an excessive amount of microwave power would be required to raise the temperature of the desired tonnage of ore by a mere $10^{o}C$.

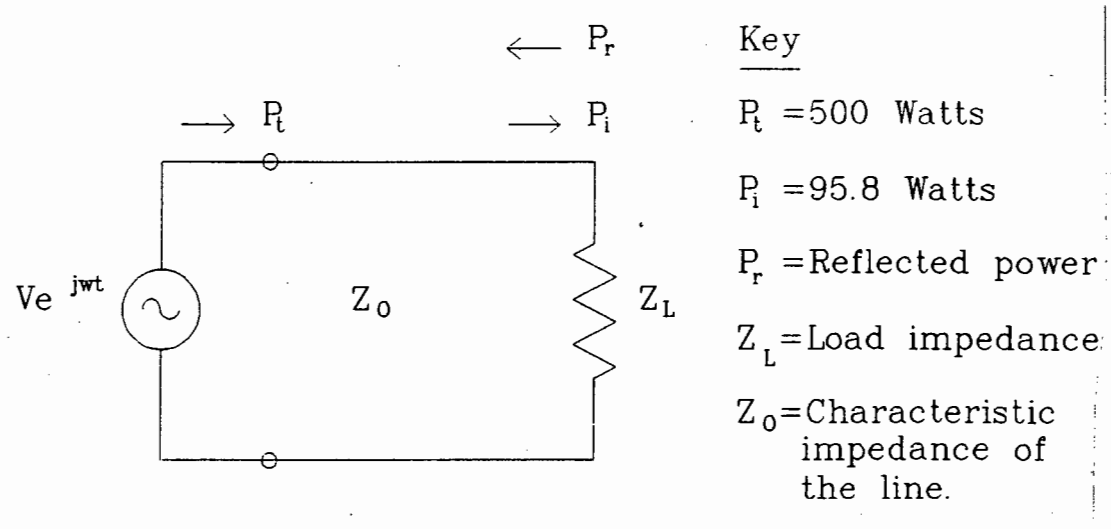

Figure A1.1. Transmission Line Equivalent Circuit.

Since $Z_L = Z_0$, a certain amount of signal reflection takes place at the rock/air interface. The power absorbed by the rock, P_i, is given by

$P_i = (1- |\rho|^2)P_t$ where ρ is the reflection coefficient of the rock.

Substituting known values of P_i and P_t we find

$$1 - |\rho|^2 = 0.19$$

indicating that 19% of the transmitted power is absorbed in the rock (Z_L) whilst 81% of the transmitted power is reflected.

If rocks are transported on a conveyor belt at a rate of x tons/second and the required change in the temperature of kimberlite is $T_k[^oC]$ then

$$P_i = (1 - |\rho|^2)P_t = m_k c_k \Delta T_k / \Delta t$$

therefore

$$P_t = 0.5*\Delta T_k*10^6/(1- |S|^2)$$

Assuming that the rocks are transported at a rate of 15 tons/minute, (0.25 tons/second) and the required rise in the temperature of kimberlite is 10=^{o}C to effect reliable rock differentiation then

$$P_t = 0.5*0.25*10^7/0.19$$
$$= 6.58MW$$
$$= \text{required microwave power}$$

This calculation may yield a pessimistic result due to the approximate nature of the data used but serves to indicate that an excessive amount of microwave power would be required to raise the temperature of the desired tonnage of ore by 10^{o}C.

REFERENCE

[1] ALDERA. M.A., "A 10GHz Rock Differentiation System", Undergraduate thesis project, UCT, 1986.

APPENDIX B: **Design criteria for waveguide antennae and rectanguiar to square waveguide transformers.**

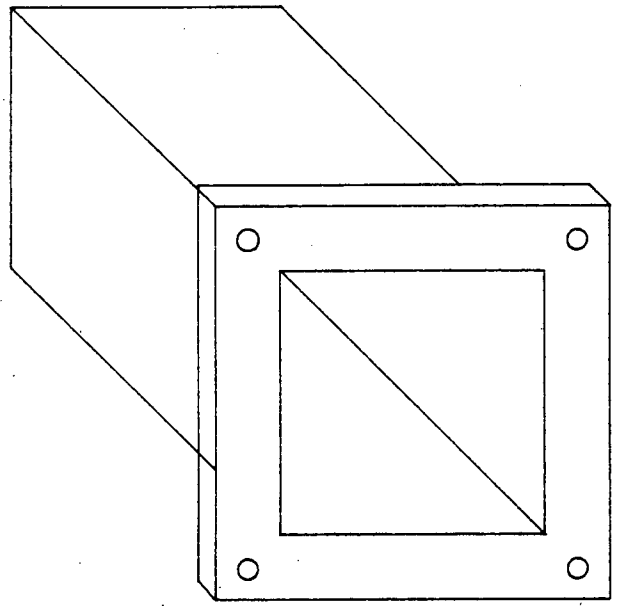

All dimensions in mm.

	A	B	C	D	X	Y	L	Hole diameter
X band	16.3	15.5	41.3	20.6	22.9	17.3	50.8	4.3
J band	12.1	12.6	33.3	16.7	15.8	11.9	50.8	4.7
K band	8.1	8.5	22.2	11.1	10.7	8.2	50.8	2.9

Square waveguide antennae.

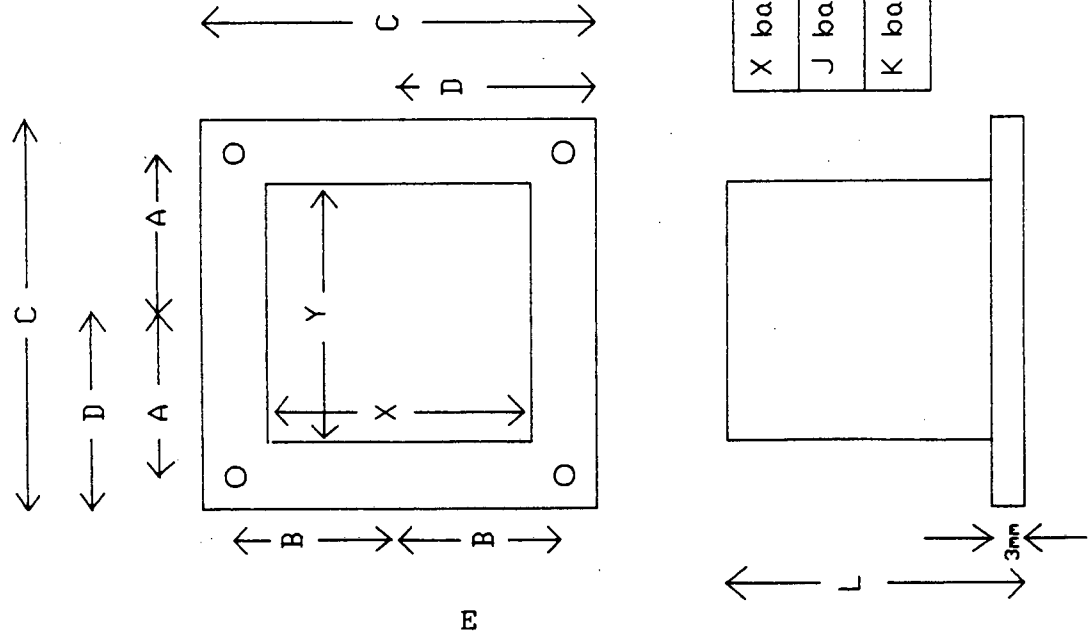

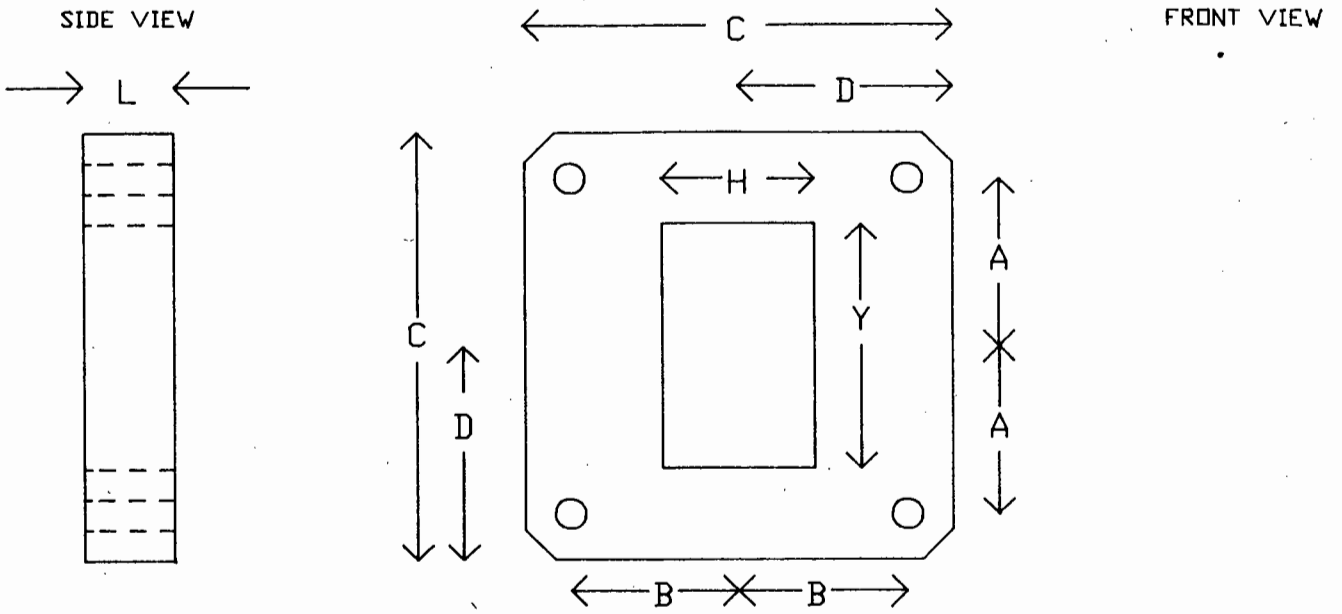

	A	B	C	D	L	H	Y	HOLE DIAMETER
K BAND	8.1	8.5	22.2	11.1	4.1	5.9	10.7	2.9

ALL DIMENSIONS IN mm

RECTANGULAR TO SQUARE WAVEGUIDE TRANSFORMER

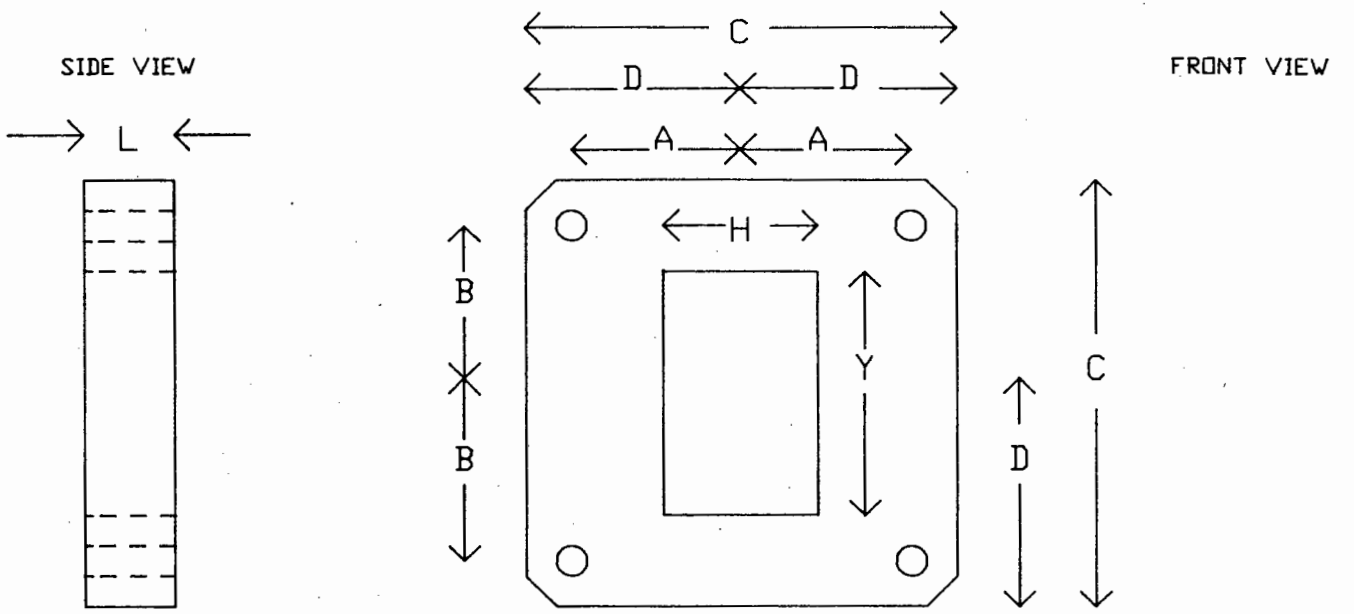

	A	B	C	D	L	H	Y	HOLE DIAMETER
X BAND	16.3	15.5	41.3	20.6	9.9	13.2	22.9	4.3
J BAND	12.1	12.6	33.3	16.7	6.3	9.7	15.8	3.7

ALL DIMENSIONS IN mm

RECTANGULAR TO SQUARE WAVEGUIDE TRANSFORMERS

APPENDIX C: Printed Circuit Board foil patterns

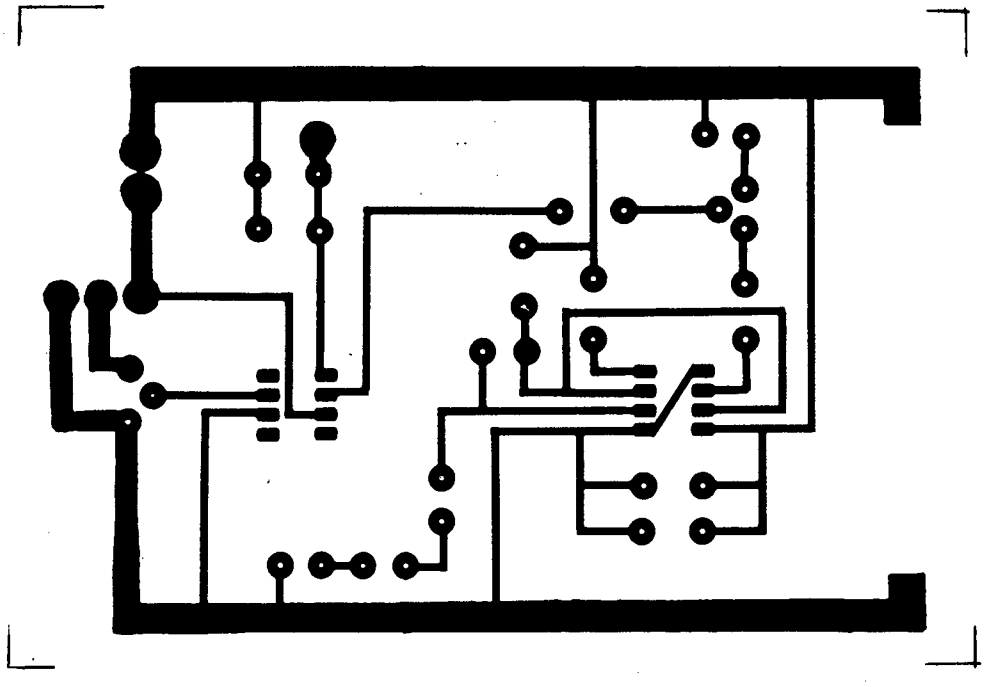

Transmitter printed circuit board foil pattern.

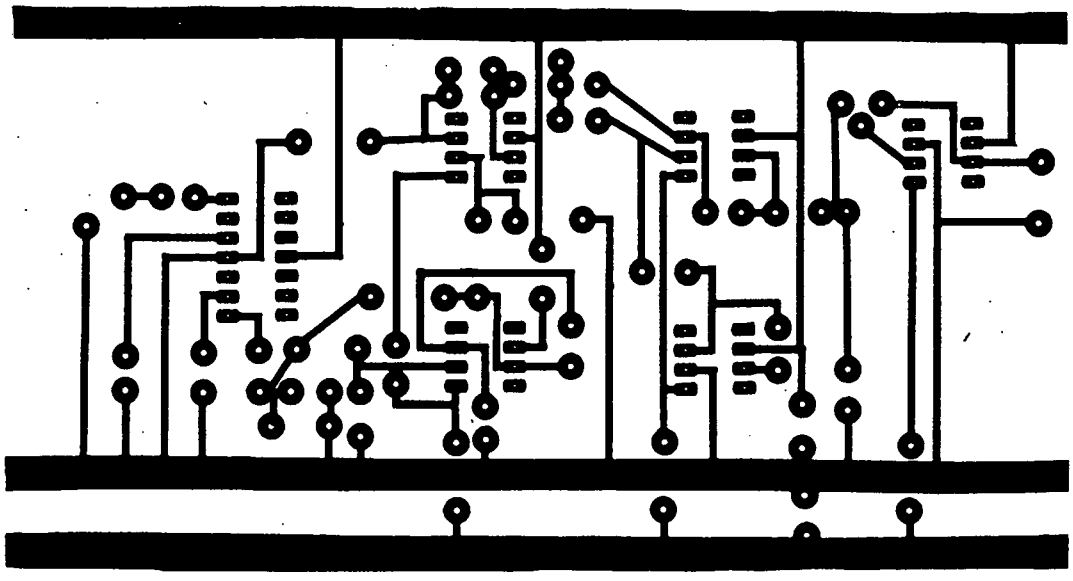

Receiver printed board foil pattern.

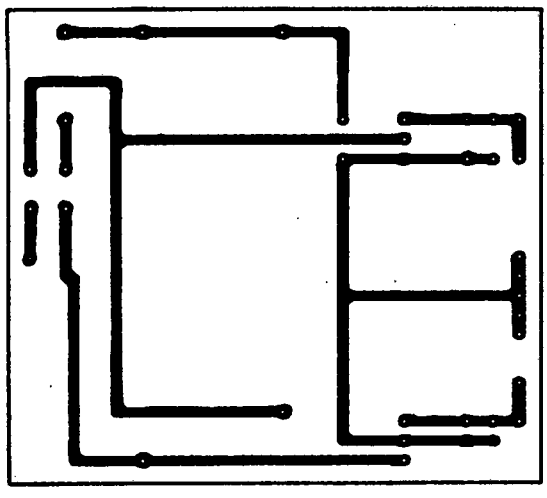

Transmitter and receiver power supply printed circuit board foil pattern.

APPENDIX D: Wilkinson couplers - Touchstone program listings and microstrip foil layout.

```
DIM
  FREQ GHZ
  RES OH
  IND NH
  CAP PF
  LNG MM
  TIME PS
  COND /OH
  ANG DEG

CKT
   MSUB  ER=2.2  H=0.2548  T=0.01778  RHO=0.84  RGH=0.00
   MLIN  1  2   W=0.76  L=109.78              !50 OHM INPUT
   MLIN  2  3   W=0.43  L=27.95               !1ST QW SPLIT ELEMENT
   MLIN  2  4   W=0.43  L=27.95               !2ND QW SPLIT ELEMENT
   RES   3  4   R=100                         !RES. ACROSS PORTS 2 & 3
   MLIN  3  5   W=0.76  L=109.78              !50 OHM OUTPUT SECTION
   MLIN  4  6   W=0.76  L=137.23
   DEF3P  1  5  6  SPLIT

OUT
  SPLIT  DB[S11]  GR1
  SPLIT  DB[S12]  GR1
  SPLIT  DB[S13]  GR1
  SPLIT  DB[S23]  GR1
FREQ
  SWEEP  1  3  .01

GRID
  RANGE  1  3  .25
  GR1  -10  10  1
```

Touchstone nodal model for the two way Wilkinson power splitter.

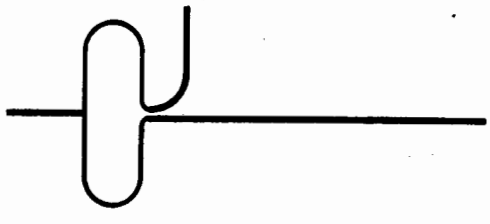

Microstrip (RT Duroid 5880) foil pattern for the two way Wilkinson power splitter.

```
DIM
  FREQ GHZ
  RES OH
  IND NH
  CAP PF
  LNG MM
  TIME PS
  COND /OH
  ANG DEG

CKT
   MSUB  ER=2.2  H=0.2548  T=0.01778  RHO=0.84  RGH=0.00
   MLIN  1  2   W=0.76  L=74.67                  !50 OHM INPUT
   MLIN  2  3   W=0.43  L=19.01                  !1ST QW SPLIT ELEMENT
   MLIN  2  5   W=0.43  L=19.01                  !2ND QW SPLIT ELEMENT
   MLIN  3  4   W=0.76  L=37.33                  !50 OHM LINE
   RES   3  5   R=100                            !ISOLATION RESISTOR
   MLIN  5  6   W=0.76  L=37.33                  !50 OHM LINE
   MLIN  4  7   W=0.43  L=19.01                  !3RD QW SPLIT ELEMENT
   MLIN  4  8   W=0.43  L=19.01                  !4TH QW SPLIT ELEMENT
   RES   7  8   R=100                            !ISOLATION RESISTOR
   MLIN  6  9   W=0.43  L=19.01                  !5TH QW SPLIT ELEMENT
   MLIN  6  10  W=0.43  L=19.01                  !6TH QW SPLIT ELEMENT
   RES   9  10  R=100                            !ISOLATION RESISTOR
   MLIN  7  11  W=0.76  L=74.67                  !50 OHM OUTPUT - PORT 2
   MLIN  8  12  W=0.76  L=74.67                  !50 OHM OUTPUT - PORT 3
   MLIN  9  13  W=0.76  L=74.67                  !50 OHM OUTPUT - PORT 4
   MLIN  10  14  W=0.76  L=74.67                 !50 OHM OUTPUT - PORT 5
   DEF5P 1  11  12  13  14  SPLIT                !DEVICE DEFINITION

OUT
  SPLIT  DB[S11]  GR1
  SPLIT  DB[S12]  GR1
  SPLIT  DB[S23]  GR1
  SPLIT  DB[S34]  GR1

FREQ
  SWEEP  2  4  .03

GRID
  RANGE  2  4  .1
  GR1    -50 10 10
```

Touchstone nodal model for the four way Wilkinson power splitter.

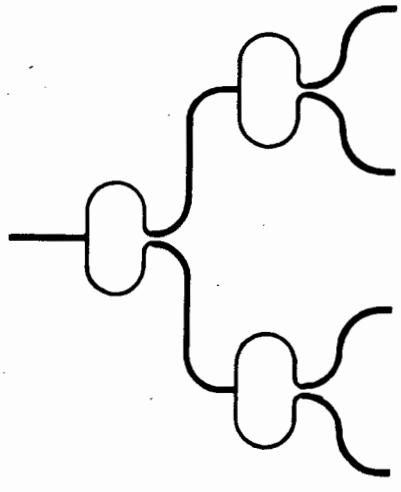

Microstrip (RT Duroid 5880) foil pattern for the four way Wilkinson power splitter.